Bearing capacity of shallow foundations on simulated lunar soil
by Danmei Gui

A thesis submitted in partial fulfillment of the requirements for the degree of Master of Science in Civil Engineering
Montana State University

Abstract:
Construction of an outpost on the lunar surface requires a thorough investigation of lunar regolith bearing capacity. A series of centrifuge bearing capacity experiments and conventional triaxial compression experiments were performed using a lunar soil simulant, MLS-1, in order to examine the appropriateness of using conventional bearing capacity solutions on lunar regolith.

The preliminary testing programs were designed and conducted to assess the plane strain conditions and the effects of the container walls and bottom on test results. A reasonable minimum depth of soil was determined which prevented effects from the container bottom and a rational configuration of the test footings designed to ensure a plane strain condition was obtained by assessment of the test results. In addition, the bearing capacity values of surface footings and embedded footings on MLS-1 were tested.

In order to obtain accurate bearing capacity predictions, evaluation of shear strength parameters is important. Two different analytical approaches, nonlinear tangent analysis and nonlinear secant analysis, were used to obtain the shear strength parameters of MLS-1. These approaches require the determination of mean normal stress level in the soil. A proposed expression for evaluation of the mean normal stress as a function of friction angle is presented. The shear strength parameters of MLS-1 corresponding to Meyerhofs, Vesic's, and Chen's methods are obtained using this expression. The bearing capacity of MLS-1 was predicted by the aforementioned methods. The bearing capacity values from the experiments and these analytical approaches are compared.

The analysis shows that, for the particular soil property of MLS-1, directly using the conventional approaches to evaluate ultimate bearing capacity cannot give a satisfactory explanation of the experimental results, especially for the problems with embedded footings.

BEARING CAPACITY OF SHALLOW FOUNDATIONS ON SIMULATED LUNAR SOIL

BY

DANMEI GUI

A thesis submitted in partial fulfillment
of the requirements for the degree

of

Master of Science

in

Civil Engineering

MONTANA STATE UNIVERSITY
Bozeman, Montana

March 1995

APPROVAL

of a thesis submitted by

DANMEI GUI

This thesis has been read by each member of the thesis committee and has been found to be satisfactory regarding content, English usage, format, citations, bibliographic style, and consistency, and is ready for submission to the College of Graduate Studies.

15 March, 1995
Date

Chairperson, Graduate Committee

Approved for the Major Department

15 March 1995
Date

Head, Major Department

Approved for the College of Graduate Studies

4/26/95
Date

Graduate Dean

STATEMENT OF PERMISSION TO USE

In presenting this thesis in partial fulfillment of the requirements for a master's degree at Montana State University, I agree that the Library shall make it available to borrowers under rules of the Library.

If I have indicated my intention to copyright this thesis by including a copyright notice page, copying is allowable for scholarly purposes, consistent with "fair use" as prescribed in the U.S. Copyright law. Requests for permission for extended quotation from or reproduction of this thesis in whole or in parts may be granted only by the copyright holder.

Signature [illegible]

Date March 27, 1995

ACKNOWLEDGEMENTS

The author gratefully acknowledges the financial support provided by the NSF EPSCoR MONTS program, by NASA EPSCoR through the Montana Space Grant Consortium Program, and the Engineering Experiment Station at Montana State University.

The author expresses appreciation to Dr. Steven W. Perkins for his guidance and support leading to the completion of this thesis. The author also extends her appreciation to the professors of the Department of Civil Engineering for their guidance in the academic progress of this student.

The author would like to express her appreciation to Dr. Hon - Yim Ko and Dr. Stein Sture of the University of Colorado, Boulder for their advice during the experimental portion of this research. Gratitude is also extended to the staff and the graduate students at the University of Colorado, Boulder for their kind help during the experimental program.

TABLE OF CONTENTS

TABLE OF CONTENTS (Continued)

LIST OF TABLES

LIST OF FIGURES

LIST OF FIGURES (Continued)

LIST OF FIGURES (Continued)

LIST OF FIGURES (Continued)

LIST OF FIGURES (Continued)

LIST OF FIGURES (Continued)

ABSTRACT

Construction of an outpost on the lunar surface requires a thorough investigation of lunar regolith bearing capacity. A series of centrifuge bearing capacity experiments and conventional triaxial compression experiments were performed using a lunar soil simulant, MLS-1, in order to examine the appropriateness of using conventional bearing capacity solutions on lunar regolith.

The preliminary testing programs were designed and conducted to assess the plane strain conditions and the effects of the container walls and bottom on test results. A reasonable minimum depth of soil was determined which prevented effects from the container bottom and a rational configuration of the test footings designed to ensure a plane strain condition was obtained by assessment of the test results. In addition, the bearing capacity values of surface footings and embedded footings on MLS-1 were tested.

In order to obtain accurate bearing capacity predictions, evaluation of shear strength parameters is important. Two different analytical approaches, nonlinear tangent analysis and nonlinear secant analysis, were used to obtain the shear strength parameters of MLS-1. These approaches require the determination of mean normal stress level in the soil. A proposed expression for evaluation of the mean normal stress as a function of friction angle is presented. The shear strength parameters of MLS-1 corresponding to Meyerhof's, Vesic's, and Chen's methods are obtained using this expression. The bearing capacity of MLS-1 was predicted by the aforementioned methods. The bearing capacity values from the experiments and these analytical approaches are compared.

The analysis shows that, for the particular soil property of MLS-1, directly using the conventional approaches to evaluate ultimate bearing capacity cannot give a satisfactory explanation of the experimental results, especially for the problems with embedded footings.

CHAPTER ONE

INTRODUCTION

Background and Problem

Among the proposals for future U.S. space program missions, one is returning to the moon to establish a permanent outpost. This moon base would include radio and optical telescopes which, along with other base facilities, must be placed on the lunar soil. The construction of lunar bases will be conceptually similar in many ways to the construction of terrestrial facilities. Extraterrestrial engineering requires, however, different approaches both in terms of technology and in philosophy. The major philosophical difference will be the approach to the "exactness" of our designs. It may be said that commonplace terrestrial civil structures are relatively inexact, in that large factors of safety are incorporated to insure successful operation, resulting in excessive use of materials and workmanship. Lunar facilities will require the incorporation of load and resistance factors that are clearly defined and do not result in excessive factors of safety. This in turn requires an accurate understanding of the mechanics of these structures and their interaction with the lunar environment. Hence, the extraterrestrial engineer must employ new technological tools in such a way that an accurate picture of the functional ability of constructed lunar facilities emerges prior to construction itself.

Basic geotechnical engineering properties of lunar regolith became available through the Apollo lunar landings. The lunar regolith has been defined as a stratum of debris of relatively low cohesion that overlies a more coherent substratum. The composite regolith mass is described as a fine silty sand with nearly 40% characterized as silt with particle size smaller than 100 micrometers. Various estimates have been made of the cohesion and the friction angle of the regolith. These estimates have relied on the observation and analysis of the interaction of loaded surfaces with the native regolith. It was found that the cohesion ranges from nearly zero to 4 *kPa* with the friction angle ranging from approximately 40° to 60°. The low values of friction angle and cohesion pertain to loose regolith (regolith with low relative density) and the high values to very dense regolith (regolith with a high relative density). Dry terrestrial sands commonly do not possess any cohesion. Even though the cohesion is relatively small, it plays an important role in the engineering solution of many soil mechanics problems.

Since working with real lunar regolith is difficult from the standpoint of availability, a simulant has been developed which matches the more significant engineering properties of lunar regolith. This soil is known as Minnesota Lunar Simulant (MLS-1) and is described by Weiblen and Gordon (1989). Perkins (1991) has performed an extensive series of laboratory strength and deformation experiments to characterize the stress-strain properties of MLS-1. In general, it was found that the frictional characteristics of real lunar regolith could be closely matched. It was difficult to match the cohesion levels observed for lunar regolith. This was due, in part, to the absence of aggregated particles and the absence of electrostatic attractive forces between soil particles.

The construction of structures on the lunar surface, like the construction of terrestrial structures, requires a thorough investigation of stability behavior of the lunar soil such as its bearing capacity. Conventional analysis of stability problems in soil mechanics relies typically upon the soil's frictional and cohesive strength parameters. Bearing capacity solutions, used to establish the ultimate load carrying capacity of shallow foundations, are expressed in terms of bearing capacity factors which are expressed as analytical functions of the friction angle. These solutions have been verified only for soil of relatively modest friction angles (less than 50°). These bearing capacity factors, and the resulting ultimate bearing capacity of the foundation, are quite sensitive to small changes in the friction angle for friction angles exceeding 50°.

Friction angles for lunar regolith and MLS-1 range from 41° to 60° (Perkins, 1991). Most bearing capacity factor charts stop at $\phi=40^{\circ}$ and never go beyond $\phi=50^{\circ}$, however. Since the assumed modes of failure for soils with very high friction angles have not been investigated, it is difficult to comment on the appropriateness of the formulation of the bearing capacity, particularly the term N_{γ}. Perkins (1991) conducted finite element analyses of a surface footing bearing on dense MLS-1. The material model was calibrated from conventional laboratory strength versus deformation experiments using dense MLS-1, where the peak friction angle was as great as 60°. It was found that conventional bearing capacity theory overpredicted the peak bearing pressure as compared to that determined from the finite element analyses. The results indicated the need for further study and analysis of bearing capacity theory in general, before applying this theory to the design and construction of lunar base facilities.

Experimental model tests have a very significant meaning in the evaluation of existing theories used for bearing capacity problems. Three different types of model tests, full-scale model tests, small-scale model tests under 1-*g* environment and centrifuge small-scale model tests, have been performed by various researchers on different soils. Experimental difficulties and expense tend to prohibit full scale testing and only a few full scale tests have been reported in the literature in the last few decades. Small-scale 1-*g* model tests do not satisfy most similitude requirements for dimensional analysis, and these small-scale tests are believed to result in a significant discrepancy between the experimental results and extrapolated field behavior.

An importance in determining the bearing capacity of strip footings is the assumption of plane strain inherent in most theoretical approaches. When performing footing tests, the maintenance, as closely as possible, of plane strain conditions is important so that the experiments will be carried out under the same conditions as assumed in the theories. Many researchers have tried to create a condition of plane strain in different ways.

To the author's knowledge, one disadvantage, in many previous bearing capacity experiments, is that sample containers were too small to allow the entire failure plane to develop. The rigidity of containers certainly influences test results. The basic theoretical assumption of a complete failure plane in failed soil could be violated due to the above problems.

An accurate prediction of the bearing capacity of a soil largely depends on the analysis method used for the shear strength obtained from conventional triaxial tests. In most cases, a linear Mohr-Coulomb strength criterion is widely used to describe shear strength. For many soils, a linear Mohr-Coulomb strength criterion is an approximation of the actual non-linear shape of the failure envelope. This curvature should be taken into account if more realistic bearing capacity solutions are to be expected. As a consequence, the friction angle, ϕ, depends upon normal stress in a material of a given density. Conventional bearing capacity solutions, however, rely upon the use of constant friction angle and cohesion. Since the results obtained by conventional triaxial compression tests for MLS-1 provided a nonlinear relation between the shear strength parameters and normal stress, normal stress then has to be determined first in order to obtain some estimate of a linear friction angle and cohesion.

In determining a soil's normal stress state the physical characteristics of the footing must be considered in addition to the soil's mechanical properties. Various assumptions have been made by researchers in order to simplify the determination of the normal stress state. Meyerhof (1948) suggested taking the mean normal stress to be one tenth the applied average ultimate bearing capacity for friction angles in the range of 45° to 46°. This is thought, however, to be limited and arbitrary.

Scope of Work

The objective of this thesis is to examine existing and improved methods for the design of foundations and for the analysis of bearing capacity using simulated lunar regolith, MLS-1, compacted in a very dense state and possessing very high friction angles. Load versus displacement experiments were performed on models of footings tested in an elevated gravity fields. The results are compared to predictions using conventional analysis methods, a numerical analysis method and the limit plasticity method.

The previous section introduced the background of the research and defined the problems to be addressed in this thesis. The tasks that need to be accomplished to solve the various issues were outlined in general terms. This section defines how the solution can be reached in more specific terms and provides a description of the contents of the remaining Chapters to this thesis.

As indicated in the previous section, full-scale model tests are usually impractical due to expense, while 1-*g* small-scale model tests cannot achieve adequate similarity requirements because of reduced dimensions. In order to satisfy similitude requirements, centrifuge small-scale model tests were designed to test the bearing capacity of shallow foundations on MLS-1. In general, the similitude requirements state that a model scaled down from prototype dimensions by a factor of n must be tested in a gravity field whose magnitude is increased from the prototype gravity field by the same factor n. This is easily accomplished in a geotechnical centrifuge and has been shown to produce valid results for terrestrial applications. The experimental work undertaken in this thesis has two major advantages over the previous studies: (1) plane strain conditions were examined effectively from a preliminary testing program and plane strain conditions were modeled properly in the bearing capacity experiments. (2) A reasonable preliminary testing program was designed and conducted to evaluate the effects of the container boundary on the test results, so that the effects were prevented from influencing the experimental results.

In order to model plane strain conditions in the centrifuge experiments, the footing feature was designed to provide as well as to evaluate plane strain conditions. The composite footing was constructed of five segments, where the three interior segments each had a length equal to its width B, and the two end segments could be interchanged with various strip footings of length varying from $1B$ to $3B$. The conditions required to achieve plane strain can be assessed from the experimental results through variation of the footing lengths for the same g-level and sample.

In order to avoid the influence of the container boundaries, the test program was designed to test different depths of soil under the same g level and the same footing dimension. By the assessment of these test results, a minimum height of the sample could be obtained to prevent the influence of the container boundaries on test results.

As mentioned in the above section, evaluation of shear strength analysis parameters is very important in order to obtain accurate bearing capacity predictions, especially for high friction soils. In this thesis, two different analytical approaches, nonlinear tangent analysis and nonlinear secant analysis, were used to obtain the shear strength of MLS-1.

Using the tangent analysis method, the friction angle, ϕ, can be obtained by taking the slope of tangent of the failure envelop, and the cohesion, c, can be obtained by the intersection of the tangent line with the shear stress axis. Using the secant analysis, where the cohesion is assumed to be zero, a straight line can be drawn from the origin to a point on the failure curve and the secant friction angle can be obtained from the slope of the straight line. The curvature of the failure envelop was taken into account in both the analytical methods.

In order to obtain linear values of friction angle and cohesion, a general function for determining an average normal stress state corresponding to soil properties and footing physical conditions was produced. The slip-line method was used to determine ultimate bearing capacity and mean normal stress in a soil, and the ratio of average mean normal stress to ultimate bearing capacity was obtained to be a function of friction angle.

The next chapter of this thesis begins with a succinct presentation of principles of modeling. This section will describe the similarity laws of modeling, and the principles of conventional small-scale model tests, and centrifuge model tests are presented. The content in this section constitutes the theoretical supporting structure for the centrifuge experiment methodology used to study the bearing capacity problems on MLS-1. The previous experimental work related to the bearing capacity problem will be reviewed in this chapter, which includes full-scale model tests, small-scale model tests as well as centrifuge model tests. The theoretical approaches applied to the analysis of bearing capacity problems such as limit analysis, slip-line, and limit plasticity will also be reviewed in light of this thesis. The impacts of centrifuge model tests will be discussed for a further understanding of centrifuge model tests.

Chapter three presents the experimental work for the bearing capacity research of shallow foundations on MLS-1. This chapter is concerned with the philosophy of the testing program, the techniques of the sample preparation, the experimental procedure, as well as the assessment of plane strain conditions and boundary effects of the container. The properties of MLS-1 used in this study will be described in this chapter where the failure criterion of the material was derived from CTC results. Detailed results of CTC tests and bearing capacity experiments are given in Appendix A and Appendix B, respectively.

Chapter four presents a comparison of analytical results predicted from existing theories and methods such as Meyerhof, Vesic, Chen and the slip-line method with the experimental results. From these predictions, conclusions will be made regarding the suitability of these analysis methods for lunar applications. In order to analyze the experimental results adequately, two analysis approaches ("tangent" and "secant" analyses) to obtain shear strength parameters of the soil will be discussed first, and the shear strengths obtained from these two approaches will be presented in the first section of this chapter. The numerical solution for slip-line method will be presented and the bearing capacity values obtained from this method will be compared with the experimental results as well as aforementioned predictions. The detailed solution of the slip-line method is presented in Appendix C, and the computer program for the slip-line method will be presented in Appendix D.

CHAPTER TWO

LITERATURE REVIEW

Introduction

The literature review in this chapter consists of three sections: principles of soil-structure interaction modeling, experimental approaches to bearing capacity problems, and analytical approaches to bearing capacity problems. In the first section, the similarity laws of modeling are succinctly discussed, and the principles of conventional small-scale model tests, and centrifuge model tests are presented. The content in this section constitutes the theoretical supporting structure for the centrifuge experiment methodology used to study the bearing capacity problems on the simulated lunar soil (MLS-1). The second section introduces the issues of experimental approaches to bearing capacity problems, which include three approaches of full-scale model tests, small-scale model tests as well as centrifugal small-scale model tests. Several issues impacting centrifuge model tests are discussed in this section. The remaining section is a presentation of issues related to theoretical approaches to the bearing capacity problems, which form the theoretical backbone for the analysis techniques in later chapters. These issues include the limit equilibrium analytical method, the slip-line method, and the method of limit analysis applied to bearing capacity studies.

Principles of Soil - Structure Interaction Modeling

Soil engineering problems such as stability of slopes, earth pressure, bearing capacity etc., are usually solved by using theories based on a set of simplifying assumptions, which may not be valid in all conditions and may lead to erroneous conclusions. Prior to the construction of an important structure, it is desirable to conduct a large scale field test in order to validate that behavior of the footing matches the predictions if the analytical technique used. The cost, however, and time it requires and the difficulty in controlling the test conditions reduce the value of the field test for research purposes. On the contrary, laboratory reduced scale model tests have two advantages compared with full scale or field experiments: (1) they allow study of the behavior of structures under different conditions; and (2) they are relatively rapid, inexpensive and easy to operate.

The development of models for geotechnical analysis includes the following steps: (1) choice of materials satisfying laws of similitude; (2) construction of the model; and (3) application of the loadings and observation of the model. The following sections will present a discussion of the similarity laws and the principles of conventional small-scale model tests as well as centrifuge model tests.

Principles of Modeling - Similarity

The rational study of all model tests must be based upon considerations of the requirements for achieving adequate similarity between the field prototype and the model. The equality of stresses between a model and the prototype built of the same materials is crucial to the maintenance of any reasonable similarity in models of particulate assemblies such as soil. In order to demonstrate the principle of similarity, consider a small element of volume *V* contained within a larger body of a granular medium (Roscoe, 1968). The entire body is saturated with a pore fluid which is flowing through the skeleton. Considering the volume as two distinct phases (solid and liquid), as shown in Figure 1(a), the local value of the porosity, i.e. ratio of voids to total volume, is *k* for the element, and the unit weight of the solid material is γ_s. The forces on the solid phase of the element are (1) the self-weight of the solid $\gamma_s(1-k)V$ acting vertically downwards, (2) the upward thrust of the fluid displaced by the grain $\gamma_f(1-k)V$, where γ_f is the unit weight of the fluid, (3) the net resultant $\sigma'_{ij}S$ of the effective stresses acting on the boundary surface of

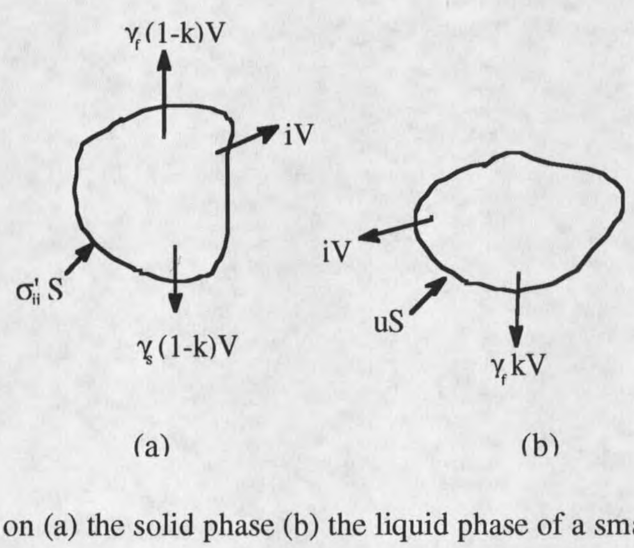

Figure 1. Forces on (a) the solid phase (b) the liquid phase of a small element of soil

the element, and (4) the seepage force iV due to the hydraulic gradient causing fluid flow through the element, where i is the seepage force per unit volume

The forces on the fluid phase within the element are shown in Figure 1(b), and are (1) the seepage force iV in the opposite direction to that in Figure 1(a), (2) the self-weight of the fluid $\gamma_f kV$ vertically downwards, and (3) the net resultant uS of the pore-water pressure on the boundary of the element.

Assume that two such elements are homologous in the prototype and in the model, and that the medium used in the prototype has a unique stress-strain curve which is not necessarily linear, but is independent of time. Let the linear length scale ratio between prototype and model be h (where h >1). There is $V_p=h^3V_m$ for the two elements where the subscripts p and m refer to prototype and model, respectively. In addition, assume that the medium used in the model has a similar stress-strain curve as the prototype material obeying the same restrictions but in which all stresses are scaled down by the ratio $1/\alpha$ and all strains by the ratio $1/\beta$. This condition is illustrated in Fig.2 (Rocha, 1957). With these assumptions it is now possible to develop the condition of similarity if data from the model are to be used to predict the behavior of the prototype.

For similarity all stresses, including pore-water pressure, must be to the scale and consequently all forces to the scale $h^2\alpha$ Scaling the self-weight of the solid phases then requires that:

$$\frac{\gamma_{sp}(1-k_p)V_p}{\gamma_{sm}(1-k_m)V_m} = h^2\alpha \qquad (1)$$

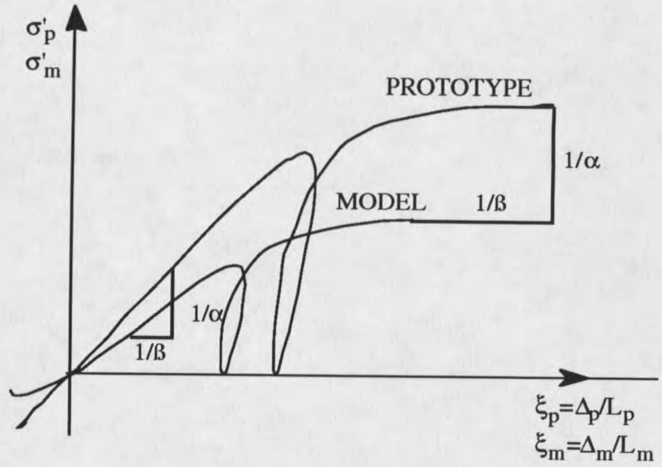

Figure 2. Similarity of stress -strain curves for model and prototype (Rocha,1957)

If $\gamma_{sp} = n_s\gamma_{sm}$ is used, where n_s is the scale factor for the unit weights of the solid materials, this requirement in equation (1) becomes:

$$\alpha = hn_s \frac{1-k_p}{1-k_m} \tag{2}$$

where the length scale has been applied to the volume terms. Likewise, scaling the uplift force due to the liquid phase $\gamma_f(1\text{-}k)V$ requires that:

$$\alpha = hn_f \frac{1-k_p}{1-k_m} \tag{3}$$

and scaling the self-weight of the liquid phase $\gamma_f kV$ requires that:

$$\alpha = hn_f \frac{k_p}{k_m} \tag{4}$$

From the equations (3) and (4), it is evident that:

$$k_m = k_p \tag{5}$$

Inserting the condition $k_m = k_p$ in equations (4) and (5) then requires that $n_s = n_f$. The bulk unit weight of a saturated medium is given by $\gamma = k\,\gamma_f + (1-k)\,\gamma_s$ and if n, the scale factor for the bulk unit weight, is defined by $\gamma_f = n\,\gamma_m$, then, provided $k_m = k_p$ and $n_s = n_f$, it follows that

$$n = n_s = n_f \tag{6}$$

If equations (5) and (6) are satisfied, the following equation can be written:

$$\alpha = hn \tag{7}$$

Equations (5), (6) and (7) specify the conditions that the materials must satisfy for similarity to prevail if all effects of migration of the pore water are ignored, provided that the initial assumptions regarding their stress-strain behavior are satisfied. The quantities listed in Table 2.1 should then scale as shown.

For most modeling applications, the length scale will range from 10 to perhaps 100. The minimum value of the unit weight scale for fluids is approximately 0.7. From equation (7) it is then seen that the stress scale must range from 7 to 70 for most applications. This requires the fabrication of a soil which is quite weak, and thereby difficult to handle. To avoid this problem, and any accompanying difficulties with the fabrication of such a soil, it is convenient to use a model soil such as that $\alpha = 1$. This then requires that:

$$h = \frac{1}{n} \tag{8}$$

This indicates that it is necessary to increase the soil and fluid unit weight by the reduction in the length scale. The quantities given in table 1 then reduce to:

$$L_p = nL_m;\ F_p = \frac{F_m}{n^2};\ \sigma_p = \sigma_m;\ \varepsilon_p = \varepsilon_m;\ \gamma_p = n\gamma_m;\ k_p = k_m \qquad (9)$$

For bearing capacity problems of shallow foundations, it is usually considered that, under a plane strain condition, nine independent quantities might influence load versus deflection curve for the foundation which are:

γ	(N/m^3)	the unit weight of soil
B	(m)	the width of a footing
D	(m)	the initial embedment of the footing
e		the void ratio of the soil
ϕ		the internal friction angle of the soil
c	(N/m^2)	the cohesion of the soil
σ_g	(N/m^2)	the crushing strength of the grain material
E_g	(N/m^2)	the coefficient of elasticity of the grain material
d_g	(m)	the average grain size

The quantities entering into the problem contain two basic units, length and force. In dimensional analysis the quantities and B are chosen to represent the basic units and the peak load P_p of the footing can be expressed in dimensionless form as a function of seven independent dimensionless parameters in the following way (Ovesen, 1979):

$$\frac{P_p}{\gamma B} = F\left(e, \phi, \frac{c}{\gamma B}, \frac{\sigma_g}{\gamma B}, \frac{E}{gb}, \frac{d_g}{\gamma B}, \frac{D/n}{B/n}\right) \qquad (10)$$

Table 1 Similarity requirements of modeling:

Quantity	**Scale Factor**	**Relationship**
Length	$1/h$	$L_p = L_m/h$
Force	$h^2\alpha$	$F_p = h^2\alpha F_m$
Stress	$1/\alpha$	$\sigma_p = \sigma_m/\alpha$
Strain	$1/\beta$	$\epsilon_p = \epsilon_m/\beta$
Unit Weight (Fluid, Solid)	n	$\gamma_p = n\gamma_m$
Porosity	1	$k_p = k_m$

Table 2 Similarity requirements for conventional model and centrifuge model

No.	**Prototype**	**Conventional Model**		**Centrifuge Model**	
	gravity: *g*	gravity: *g*		gravity: *ng*	
1	e	e	similar	e	similar
2	ϕ	ϕ	similar	ϕ	similar
3	$\frac{c}{\gamma B}$	$\frac{c}{(\gamma B/n)}$	not similar	$\frac{c}{(\gamma nB/n)}$	similar
4	$\frac{\sigma_g}{\gamma B}$	$\frac{\sigma_g}{(\gamma B/n)}$	not similar	$\frac{\sigma_g}{(\gamma nB/n)}$	similar
5	$\frac{E_g}{\gamma B}$	$\frac{E_g}{(\gamma B/n)}$	not similar	$\frac{E_g}{(\gamma nB/n)}$	similar
6	$\frac{d_g}{\gamma B}$	$\frac{d_g}{(B/n)}$	not similar	$\frac{d_g}{(B/n)}$	not similar
7	$\frac{D}{B}$	$\frac{D/n}{B/n}$	similar	$\frac{D/n}{B/n}$	similar

In order to obtain complete similarity, model tests for bearing capacity problems must be designed in such a way that the seven independent dimensionless parameters attain the same values for the model and for the prototype. The model and the prototype are then said to be completely similar. Table 2 (Ovesen, 1979) shows the similarity behavior of the dimensional analysis on the conventional small-scale tests and on the centrifuge model tests.

The Conventional Small-Scale Model Tests

For the conventional small-scale model tests, usually, the same soils are used in both model and prototype. In this type of model test, the unit weight of a model soil is identical to that of the prototype soil, whereas the linear length scale ratio h is always greater than unity. So the stress scale factor in equation (7) is not unity. Consequently, the stresses in the model and in the prototype do not satisfy the similarity requirements.

Since the self weight stresses present in soils largely control material behavior, not meeting this requirement of similarity has a significant impact on comparisons of the model to the prototype.

The Centrifuge Model Tests

The laws of similitude require that $\gamma_p = n\,\gamma_m$ where $n = 1/h$. Recognizing that the unit weight of a material can be expressed as

$$\gamma = \rho g \tag{11}$$

this requirement can then be restated as:

$$\rho_p g_p = \frac{1}{h} \rho_m g_m \tag{12}$$

If we use the same soil in the model as that in the prototype equation (12) reduces to:

$$g_m = h g_p \tag{13}$$

This condition can be easily accomplished in a geotechnical centrifuge.

Ovesen (1979) examined the dimensional analysis of similarity requirements on centrifugal model tests. It was shown that five of six similarity requirements are fulfilled in the centrifugal models (table 2). The centrifugal model tests only deviate from the prototype in that the similarity requirement concerning the grain size of the soil is not fulfilled due to the fact that the prototype material is used in the model. In order to investigate grain-size effects, some researchers conducted centrifugal model tests using different grain sizes. This will be discussed in next section. In addition to the problem of grain size scaling in centrifugal model tests, other problems, such as scale effects and variation of gravity level across the heights of samples and across the model containers, are also considered to influence the test results. Their influences on the tests results will be discussed later.

Experimental Approaches to the Bearing Capacity Problem

Improvements in the understanding of the bearing capacity problem of soils depends upon the simultaneous advances in theoretical and experimental work. Experimental model tests have a very significant meaning for the evaluation of existing prediction techniques. Conventional model tests and centrifuge model tests have been widely applied to the study of bearing capacity problems by investigating the shape of the rupture surface and examining the results obtained as the failure is reached in the soil. A brief description of the bearing capacity experiments preformed by some investigators using different approaches will be presented in this section.

Full-Scale Model Tests

Muhs (1965a) presented results of full-scale tests with rectangular footings on sands. Deformations of the ground surface at various points away from the footing were recorded by using vertical glass tubes filled with colored water. As a result, he found a progressive rupture phenomenon accompanying the sand failure in the tests. He showed a diagram regarding the deformation of the sand under a vertical pressure with the test time, and indicated that the sand reached failure at the time the settlement changed to a heave movement. He mentioned that the displacement before the soil fails will induce a change of porosity which is believed to influence the original shear strength of soil. Therefore, the general equations of bearing capacity based on a constant shear strength do not meet the real conditions when the phenomenon of progressive rupture exists. Additionally, he showed that a larger settlement occurred corresponding to a large foundation than that corresponding to a small foundation.

At the same time, Muhs (1965b) presented experimental data reflecting vertical and horizontal stress distributions beneath full-scale concrete footings. He introduced a specific gauge for measuring the horizontal stress in the tests. From the test results, he stated that, under relatively low pressure, the distributions of normal stress are smaller in the middle part of the footings than in the outer parts, while the distributions under higher pressure change over to full unsymmetrical parabolic forms when the failure loads are reached. The friction angle between the footing base and the soil was calculated by dividing the corresponding value of horizontal stress to normal stress and a much higher friction was found at the side where the failure took place. Therefore, Muhs suggested that during failure the friction at the base of a footing should amount to about 0.6 of the possible maximum value.

Muhs (1965c) performed another group of experiments for the purpose of determining the bearing capacity factors of shallow foundations according to different failure loads. The diagrams of the failure loads versus the parameter m (m is the ratio of the footing length to width) were presented in the paper, for the tests of surface footings and embedded footings. He indicated that, for surface footings, the bearing capacity increases with higher values of m and it approaches a limiting value for $m \rightarrow \infty$, but for the embedded footing, the failure loads decrease with increasing values of m. He explained that the bearing capacity of a square footing is much higher than that of a long slender footing with the same width, provided that footings are embedded into the bearing stratum. He concluded that the bearing capacities of single square footings are greater than those of strip footings with the same width.

Milovic(1965) conducted a series of field tests and compared the results of ultimate bearing capacities obtained from the field tests with the calculated values of some researchers. He stated that, for cohesionless soils, the test results of the ultimate bearing capacity agree well with the solution of Balla (1962), while for cohesive material, the most reliable results are given by the Brinch Hansen theory (1952).

Small-Scale Model Tests

De Beer (1965) performed small-scale model tests on cohesionless sands. By comparing the results with the full-scale tests which were conducted by Muhs (1965a), he found that there exists a discrepancy in the predictions of the bearing capacity results between the small-scale tests and the full-scale tests. He showed that, experimentally, for dense sands, the relative settlement at rupture increases with the increase in footing width, but much lower than would be expected by extrapolating the results of the small model tests. The N_γ values of the larger footings are smaller than that of smaller footings. The variation of the relative settlement at rupture indicates that there exist some scale effects in the progressive rupture phenomenon which cannot be reduced to scale. These scale effects are a consequence of the influence of the mean normal stress, and larger footings will have a larger progressive failure effect compared to smaller footings since settlement is larger for larger footing.

De Beer (1970) performed another extensive series of tests on small footings in order to determine, experimentally, the values of the shape factors in formula of ultimate bearing capacity of shallow foundations. He deduced the shape factors s_q and s_γ from the experimental results for both non-overburden and overburden cases. Furthermore, he compared the experimental values of N_γ and N_q with some theoretical solutions such as

Terzaghi's (1943), Meyerhof's (1963), Brinch Hansen's (1961), and indicated that at a high relative density the experimental curve of N_γ has the tendency to give higher values than all the compared theoretical solutions. Also, at low densities the experimental values of $N_\gamma/2$ tend to become larger than the theoretical values. For the values of N_q in his report, the experimental values gradually tend to become the Terzaghi's value if the adjusted shear strength (ϕ'=2/3) proposed by Terzaghi for local shear is taken into account.

Jumikis (1965) performed small-scale tests for studying the shape of the rupture surface in dry sands. He showed some experiments in which the rupture plane occurred on both sides of the footing or on only one side of the footing. The rupture surfaces were mathematically and graphically analyzed. The study revealed that the failure surface in the test sands coincides remarkably well with the arc of a logarithmic spiral having the general equation:

$$r = r_o e^{\omega \tan\phi} \tag{14}$$

where r is the radius vector, r_0 is a segment on the polar axis from the pole of the spiral cut off by the spiral at $\omega = 0$, e is the base of natural logarithms, and ω is the angle between r_0 and r.

Chummar (1972) demonstrated some small-scale experimental work regarding failure mechanisms and ultimate bearing capacity of dense sands. He found that there is some difference between the observed failure shape and those assumed by existing theories, with a much smaller failure surface being observed in the tests. From these observations, he deduced a failure surface which fits in closely with Balla's (1962) mechanism, but the plane surface at the tail end makes an angle of 45^{o} with the horizontal which is different from the assumed value of $(45^{o}-\phi/2)$ in all existing theories. Additionally, he stated that the theories of Terzaghi (1943), Meryerhof (1955) and Brinch Hansen (1961) overestimated bearing capacities in the high ranges of friction angle ϕ, while Lundgren and Mortensen (1953) underestimated bearing capacities in all ranges of ϕ with the comparative study.

Ko and Davidson (1973) performed a series of small-scale bearing capacity tests providing for the condition of plane strain for both smooth and rough footings. Smooth glass or sandpaper were employed for simulating a smooth footing base or a rough footing base in the tests, respectively, and a plane strain condition was simulated by constructing a glass sided soil box where lateral deformation could be prevented. However, the author didn't mention if any shear stress occurred between the container wall and the soil. If the shear stress existed the validity of the plane strain condition might be suspected. The experimental results showed that there exists about a 10% difference of ultimate bearing capacities between the smooth and rough footing tests. As a main purpose of the tests, they compared the bearing capacity results of the rough and smooth footing bases with the exact solution predicted by Sokolovskiî (1963) and the approximate solutions of Terzaghi (1943), Brinch Hansen (1961) and Coquot-Kerisel (1948). Consequently, the solution predicted by Sokolovskiî (1963) was thought to be the best prediction of the ultimate bearing capacity for smooth footings and slightly underestimated the values for the rough footings. Also, the author stated that the predictions of Terzaghi (1943) overestimated the actual bearing capacity value if a plane strain angle of friction is used.

Centrifuge Small-Scale Model Tests

Ovesen (1975) conducted experiments regarding the application of centrifugal model tests on bearing capacity problems of surface footings. Two series of tests were conducted. The first series consisted of tests on model footings whose size was varied. The centrifuge acceleration level was also varied for each test such that the combination of the model footing size and the acceleration level represented the same prototype footing size for each model. The corrected bearing capacities obtained from this series of tests agreed remarkably well with each other. The second series of tests had a constant diameter of model footings but subjected to a varying acceleration ng so that the models represented prototypes of different sizes. Consequently, the results showed a nonlinear relationship between the bearing capacities and acceleration field ng. The author explained that the internal friction angle ϕ of the sample is not a constant for various acceleration fields but a function of stress level reflected by ng, and the highest value of ϕ was found for the lowest stress level. Ovesen also presented some other test results conducted by Mikasa et.al (1973) and Cherkasov et. al. (1970) which obtained the same conclusions.

Kimura et. al.(1985) introduced their research activities of centrifuge modeling tests which focused on bearing capacities of shallow foundations on dense sands. They conducted a series of experiments to explain De Beer's scale effect and to investigate the effects of roughness of a footing base, anisotropy in dense sands, the embedment of footings as well as the effect of slopes near footings. They stated that De Beer's scale effect of footings can be reasonably explained by the progressive failure, and the assumption of constant shearing strain in existing bearing capacity theories cannot be accepted due to the progressive failure. With respect to the effect of roughness of a footing base, the authors stated that the experimental observations are consistent with the analytical result of Chen (1975), who pointed out that, provided the footing has a certain depth of embedment, a single wedge failure mechanism proposed by Prandtl gives a more critical upper bound calculation than Hill's two symmetrical wedge failure mechanism regardless of roughness of the footing base. However, one problem was that a very small soil container was used in the author's experimental activities. As a result, the container was too small to allow the shear strain to completely develop. Theoretically, it would influence the value of shear stress and the results of the bearing capacities obtained from the tests.

Pu and Ko (1988) performed centrifuge model tests to determine the ultimate bearing capacity of shallow foundations in sands. Failure mode and effects of footing size, shape and depth of burial were investigated for diverse densities of a granular soil. Bearing capacity factors N_q and N_γ as well as shape factors ζ_q and ζ_γ were derived based on the test data. A comparison of these factors was made with the existing predictions. Analytically, they indicated that the definition of ultimate bearing capacities not only depends on the peak bearing pressures, but also depends on the relation to footing penetrations which were required to reach the capacity. They demonstrated the experimental data which reflects effect of soil densities and footing embedments.

Aiban (1991) performed a group of centrifuge model tests for the research of bearing capacities of shallow foundations. He studied the effects of load eccentricity, inclination as well as initial embedment on bearing capacities of shallow footings on dense sands. An improved experimental method was conducted in the tests for ensuring a plane strain condition with testing three adjacent footings along a line and having the same width. Also, the failure surfaces of the failed samples were monitored by trimming. He showed a good agreement of the ultimate bearing capacities between the experimental and theoretical values proposed by Vesic (1975), Meyerhof (1963) and Hansen (1970), among the three theoretical values, Meyerhof's (1963) solution gave the best agreement with the experimental results. He proved that using the shearing strength from the conventional triaxial test will underestimate the bearing capacity of shallow foundations. In the paper, the author didn't mention the boundary effects of the soil container used in the experiments.

Issues Impacting Centrifuge Model Tests

Although the concept of centrifuge model testing for bearing capacity problems is relatively simple and the stress similarity can be established between a model and the prototype, some problems still exist when the centrifuge is used in model experiments. Among them, the influence of the variation of the gravity level across the model container, influence of particle size of model soils as well as scale effects are considered as the most important problems.

The problem of variation of the gravity level comes from the structure of the centrifuge. In the centrifuge, the acceleration acts in the radial direction and the magnitude depends on the radial distance from the center of rotation. Hence, a variable gravity level will be produced across a sample height due to the different rotation radii. This variation of the gravity level causes a discrepancy of bearing capacities between centrifuge model and the prototype under a constant level. In order to evaluate the influence of this effect, Yamaguchi et. al. (1976) calculated the bearing capacities for a centrifugal model in which the acceleration increases in the radial direction in proportion of the distance from the center of rotation and a prototype in which the uniform acceleration works perpendicularly to the surface. The results showed that the difference in bearing capacities does not exceed more than 5%.

The second problem is the problem of scaling the particle grain size between the model and the prototype soil. When a model is subjected to an acceleration of ng, the size of each particle in the model scales up n times of its original size. In order to study the effect on the bearing capacity, some experiments were conducted by several investigators, one of whom Yamaguchi et al. (1977) found that, experimentally, bearing capacities show no difference even though the quite different average particle sizes were used. Fuglsang and Ovesen (1988) compiled the experimental results reported by some investigators concerning grain sizes on bearing capacities of foundations. They concluded that the effect of grain size on bearing capacity exists only if the ratio of the model footing width to the average grain size is less than 30. This conclusion also was supported by Christensen and Bagge (1977) who presented the test results of minor particle size effects when the ratio of model size to the average grain size is about 15. However, theoretically, the effect due to model particle size exists and it violates the deformation similarity of the centrifuge model in the dimensional analysis.

Scale effect of footings on bearing capacities in centrifuge model tests was investigated by Yamaguchi (1977) and Ovesen (1979). Yamaguchi presented a diagram (Fig.3) showing that N_q generally decreases with the increase of the parameter B_N/E_q (where B_N denotes the prototype width, E_q donates the Young's Modules of the testing sands). He called this phenomenon a scale effect and explained that the increase in the shearing strains along the slip line with the increase of a footing width gives rise to the scale effect. Ovesen presented test results showing the deformation at peak load is somewhat dependent on the diameter of the circular tested model for the same prototype size.

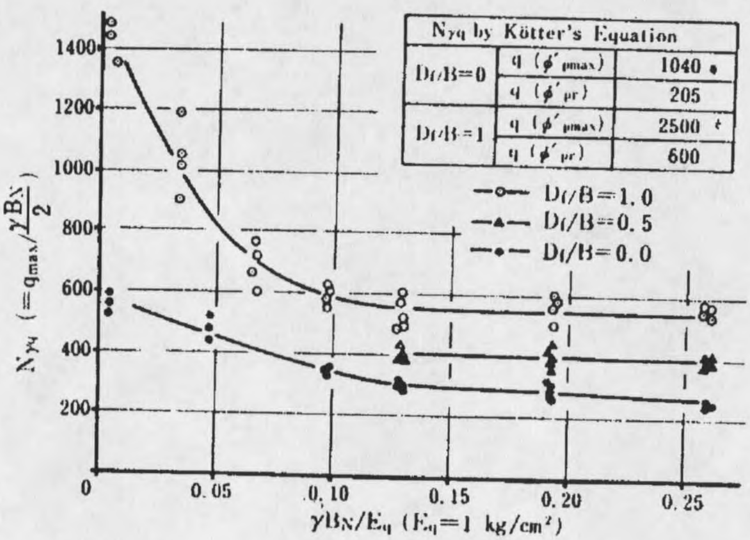

Figure 3. Relationship between $N_{\gamma q}$ and $\gamma B_n/E_q$ for Toyoura sand (Yamaguchi, 1977)

In addition, centrifugal model tests assume that the self-weight forces are perpendicular to the axis of rotation of the centrifugal model, whereas in the prototype gravity forces are virtually parallel. This self-weight force, in a centrifugal model, creases a resultant force having an orientation of θ with respect to the direction of the acceleration force. Theoretically, this resultant force will affect experimental results of bearing capacity in the centrifugal model, and the influence will become insignificant as the

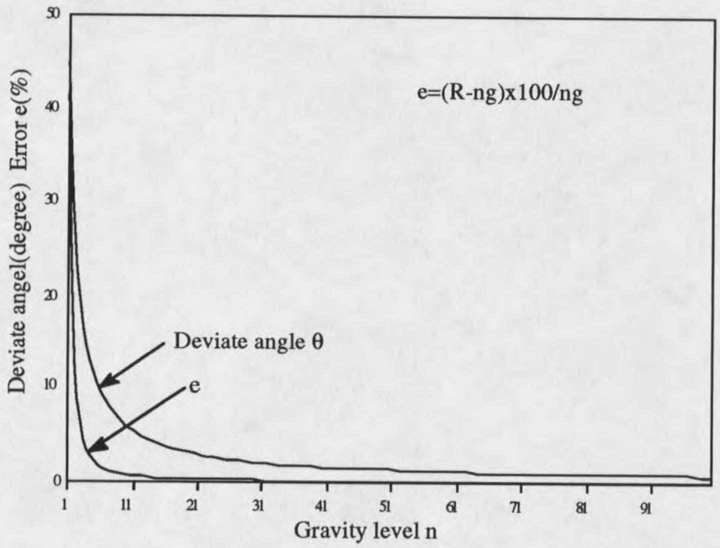

Figure 4. The effect of self-weight on bearing capacity in centrifugal model

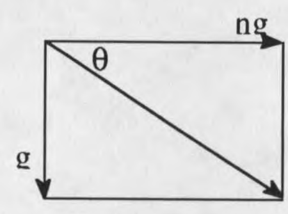

Figure 5. The direction of the resultant force.

gravity level is high. Clearly, it can be seen from Fig.4 that, when acceleration level n increases from 1 to 10, the deviate angle decreases sharply and the error e tends to zero.

Analytical Approaches to the Bearing Capacity Problem

The performance of a foundation is evaluated by its stability. This stability depends upon the safety of the soil under the footing against its failure in shear as well as the possibility for excessive vertical deformation. Therefore, the design of foundations must satisfy two main requirements simultaneously: (1) complete bearing capacity failure of the foundation must be avoided with an adequate factor of safety, (2) the total and relative settlement of the foundation must be kept within the limits that can be tolerated by the superstructure.

Since the first formula for the computation of the bearing capacity problem was initiated by Rankine (1857), the study of this subject has been developed by various researchers using the limit equilibrium method, the slip-line method or the method of characteristics, and the method of limit analysis. Traditionally, the limit equilibrium method has been used to obtain approximate solutions for problems of stability in soil mechanics. The method is based upon an analysis of static stress conditions for the ultimate plastic failure of soils with the assumption of various simple failure surfaces. In this method, it is also necessary to make sufficient assumptions regarding the stress distribution along the failure surface so that an overall equation of equilibrium can be formulated in terms of stress resultants. Therefore, this approach makes it possible to solve various problems by statics but typically gives no consideration of the soil kinematics, and the equilibrium conditions are only satisfied in a limited sense (i.e. the differential equations of stress equilibrium are not necessarily satisfied).

The so-called slip-line method or method of characteristics is a solution procedure based on more sound principles of mechanics. The solution is developed by writing the differential equations of equilibrium for stress for idealized conditions of plane strain or axi-symmetry. A failure criterion is then substituted into the equations of stress equilibrium. For soils, the Mohr-Coulomb criterion is widely used to describe conditions at failure. With the consideration of certain boundary conditions, the stresses which occur in the soil at the instant of impending plastic flow can be investigated by solving this set of differential equations using the method of characteristics and appropriate finite-differential numerical schemes. The method is typically confined to homogeneous and isotropic soils. However, at least two weaknesses are believed to exist in the slip-line method, one of which is the neglect of a more realistic stress-strain relationship for soils, the other is that only a part of the soil mass near a footing is assumed to be in the state of plastic equilibrium. The solution consists of constructing a slip-line field in the region, which satisfies all the stress boundary conditions that directly concern the region, as well as the equilibrium and yield conditions at every point inside the region. The stress field so obtained has been termed a partial stress field. The stress distribution outside this partial stress region is not defined.

In contrast to slip-line and limit equilibrium methods, the method of limit analysis considers the stress-strain relationship of the soil within the context of energy principles.

The basic theorems of limit analysis give upper and lower bounds on the collapse load. For the upper bound theorem, collapse loads are determined by equating the external rate of work to the internal rate of dissipation in an assumed deformation mode. This assumed deformation mode is made to satisfy the velocity boundary conditions as well as strain and velocity compatibility conditions, and thereby is a kinematically admissible solution. Rigorous proofs demonstrate that the collapse load is an upper bound to the exact solution. For the lower bound theorem, loads are determined from an assumed stress distribution which satisfies the equilibrium equations and stress boundary conditions while the failure criterion is not exceeded for all points within the region. It can be proved that these loads represent a lower bound to the exact collapse load. In this approach, an assumption of perfectly plastic behavior of soils is made so that the behavior of strain softening or hardening is ignored. Typically the condition of normality (associated flow) is used to develop conditions of compatibility. The following sections briefly outline the historical developments of the aforementioned analytical approaches used to develop bearing capacity solutions.

The Limit Equilibrium Method

Limit equilibrium, which is also called plastic equilibrium, deals with the stresses in the soil mass at failure. The basic concept of limit equilibrium consists of writing equations of overall force or moment equilibrium and the condition of yield or failure.

Consider all possible combinations of stresses which can be applied to an element of a homogeneous, isotropic soil. The state of stress in this element can be represented by a circle of stress on Mohr's diagram as shown in Fig.6. If none of the stress circles in the soil mass touches the failure envelope *O'R*, the deposit is in a state of elastic equilibrium, and satisfies the following inequality:

$$|\tau_n| < \sigma_n \tan\phi + c \tag{15}$$

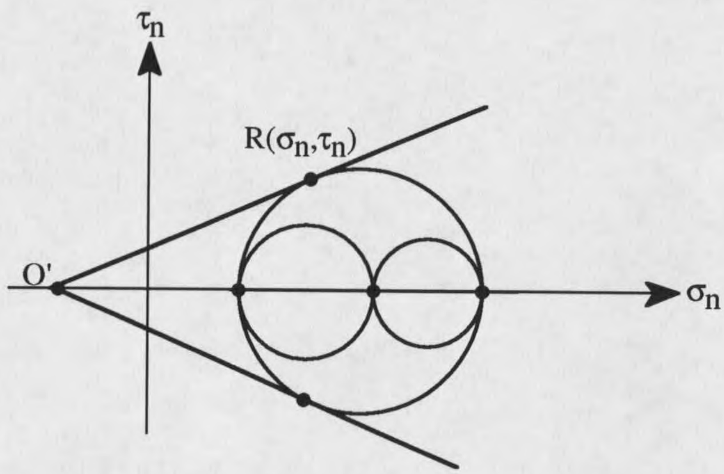

Figure 6. Mohr's circle and plastic equilibrium

If the Mohr's circles touch the failure envelope, an infinitesimal increase of the stress difference produces a steady increase of the corresponding strain, and this phenomenon constitutes plastic flow. The flow is preceded by a state of limit equilibrium. When the element is in the state of limit equilibrium, the following equation should be satisfied:

$$|\tau_n| = \sigma_n \tan\phi + c \tag{16}$$

This equation is defined as the Mohr-Coulomb failure criterion and is widely used in solving soil mechanics problems.

The study of the bearing capacity problem of soils using the limit equilibrium concept is based on the work of Prandtl (1920). Prandtl studied the penetration process of a rigid punch into another softer, homogenous, isotropic material from the viewpoint of limit equilibrium. A two-dimensional penetration problem was analyzed in which a vertical punch of width $2b$ was applied to the horizontal surface of an infinitely extending body according to Fig.7. The punch represented a surface strip loading with a infinite length perpendicular to the drawing plane. The contact surface between the punch and the softer material is assumed to be smooth. According to his study, when a uniform vertical pressure is applied to a softer material, the triangle ABC in Fig.7 is pushed downward into the material and the sectors ACD and BCE are pushed outward so that the triangles ADF and BEG were forced to move to the side and upwards. The outer edge lines CD and CE of the sectors ACD and BEC are logarithmic spirals with the poles of these spirals at points A and B, respectively. The stream lines of the plastic displacement are illustrated in the right-hand part of Fig.7.

In his analysis, Prandtl considered the plastic equilibrium of the plastic sectors. From Mohr's stress theory, and using Airy's stress function, Prandtl obtained an analytical expression for the ultimate bearing capacity of the soft material which is:

$$\sigma_u = \frac{c}{\tan\phi} \left[\tan^2\left(\frac{\pi}{4}+\frac{\phi}{2}\right) e^{\tan\phi - 1} \right] \tag{17}$$

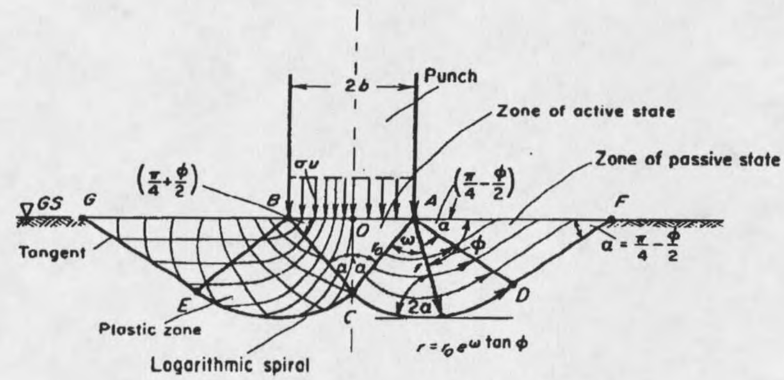

Figure 7. Prandtl failure mechanism (Jumikis, 1984)

where c and ϕ are the cohesion and the frictional angle of the material, respectively. Extending equation (17) to include a surcharge, it can be written as:

$$q_{ult} = cN_c + qN_q \tag{18}$$

where

$$N_q = e^{\pi \tan\phi} \tan^2(45^\circ + \frac{\phi}{2})$$

$$N_c = (N_q - 1)\cot\phi$$

These equations then became the bearing capacity factors adopted by Meyerhof (1963), Hansen (1970) and Vesic (1975).

Prandtl's theory of plastic failure in a system where a vertical punch is applied on a horizontal surface of a metal can be applied for calculating bearing capacity of soil. In such a case, Prandtl's theory is based on an analysis of the stress condition for the ultimate plastic failure of the soil. However, there exist some problems with Prandtl's solution if it is applied directly to the soil:

∘ Prandtl's theory is only applicable to an infinite strip foundation while not to axis-symmetric foundations.

∘ Prandtl's formula of ultimate bearing capacity is only applicable to frictional, cohesive soil ($\phi - c$) and to a pure cohesive soil (c). However, for cohesionless soil ($c = 0$, $\phi > 0$), Prandtl's formula gives that the ultimate bearing capacity of an ideal, frictional sand at its ground surface is zero, which is in contradiction to common observations in reality. The contradiction originates mainly from the assumption that soil wedge directly underneath the base of the footing is weightless.

∘ When$\phi = 0$, the original Prandtl's formula transforms into an indeterminate quantity.

∘ Prandtl's theory does not account for the shearing resistance developed along the slip lines extending above the footing base for buried foundations.

∘ Prandtl's formula also does not consider the effects of inclined loads and eccentric loads.

Based on Prandtl's theory of plastic failure, Terzaghi (1943) presented a modified solution which incorporates a failure mechanism as illustrated in Fig.8. He described two shear failure modes--general shear failure and local shear failure. The concept of general shear failure is characterized as a failure pattern where the failure of soil by plastic flow is very small and the footing does not sink into the ground until a state of plastic equilibrium has been reached. The relation between load and settlement is shown by the solid curve C_1 in Fig.9. For local shear failure, the concept was defined that, if the mechanical properties of soil are such that the plastic flow is proceeded by a strain, the approach to the general shear failure is associated with a rapidly increasing settlement and the relation of load and settlement is approximately as indicated in Fig.9 by the dash curve C_2. Meanwhile, he defined a shallow foundation as one whose depth of embedment is less than or equal to the width of the foundation. In Terzaghi's ultimate bearing capacity analysis, the following additional assumptions were made:

•The base of the foundation is rough so that only vertical displacement can occur.

•The line elements AC and BC are straight lines and form an angle with the horizontal, which is in contrast to Prandtl's mechanism.

•The condition of general shear failure was assumed to govern the solution of bearing capacity of shallow foundation.

•The shearing resistance of the soil above the level of the footing base is neglected.

Terzaghi developed an expression for the critical load, Q_u, a load per unit length of the footing, of a rough strip foundation for the general case of soil with cohesion c, surcharge q and unit weight γ as well as friction angle ϕ. The equation is:

$$Q_u = Q_c + Q_q + Q_\gamma \tag{19}$$

From equation (19), the ultimate bearing pressure, or capacity, was given as:

$$q_u = \frac{Q_u}{B} = cN_c + \gamma DN_q + \frac{1}{2}\gamma BN_\gamma \tag{20}$$

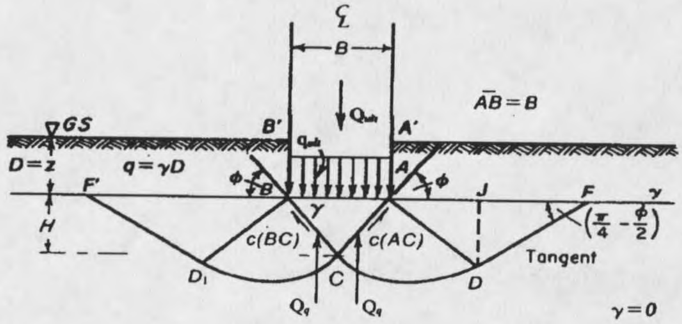

Figure 8. Terzaghi's failure mechanism (Terzaghi, 1943)

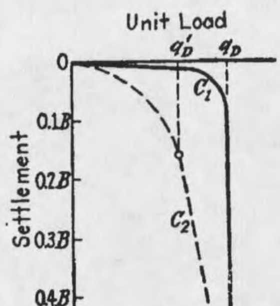

Figure 9. Different shear failure curve

where the so-called bearing capacity factors were expressed as:

$$N_c = \cot\phi\left[\frac{a_\theta}{2\cos^2(45^\circ + \frac{\phi}{2})} - 1\right] \tag{21}$$

$$N_q = \frac{a_\theta}{2\cos^2(45^\circ + \frac{\phi}{2})} \tag{22}$$

$$N_\gamma = \frac{1}{2}\tan\phi\left(\frac{K_p}{\cos^2\phi} - 1\right) \tag{23}$$

$$a_\theta = e^{(\frac{3}{2}\pi - \frac{\phi}{2})\tan\phi}$$

where K_p is the coefficient of passive pressure.

In the case of a local shear failure condition, because of a large compressibility of the soil, Terzaghi recommended the cohesion and friction factors be reduced by $c' = 2/3\ c$ and $\tan\phi' = 2/3 \tan\phi$.

Meyerhof (1963), Hansen(1970) and Vesic(1975) have published a series of papers with the contents of ultimate bearing capacity problems. Their work constituted a modern outlook in the field of approximate bearing capacity solution of shallow foundations, incorporating all major contributions to the subject, along with the appropriate numerical values of bearing capacity factors and coefficients. General formulas of bearing capacity for shallow foundations and the bearing capacity factors were generated by the investigators. Table 3 lists the general equations and bearing capacity factors produced by Meyerhof (1963), Hansen(1970) and Vesic(1975). It can be seen from table 3 that they all proposed the same equations for the bearing capacity factors N_c and N_q as those of Prandtl and Reisner (1929), but the formulas of N_γ are different due to the different assumptions and experiments built by them.

In Meyerhof's analysis (1963), he made use of a failure mechanism as shown in Fig.10. The expression for N_γ was obtained according to his previous theoretical analysis (1951, 1953), combining with the experimental observation. Meyerhof's work (1963) also included equations which account for the effects of footing shape and depth and the effect of load inclination. The shape factors obtained are partly theoretical and partly semi-empirical factors. He proposed expressions of depth factors which reflect approximate failure surface in many test results. He pointed out that, while the proposed bearing

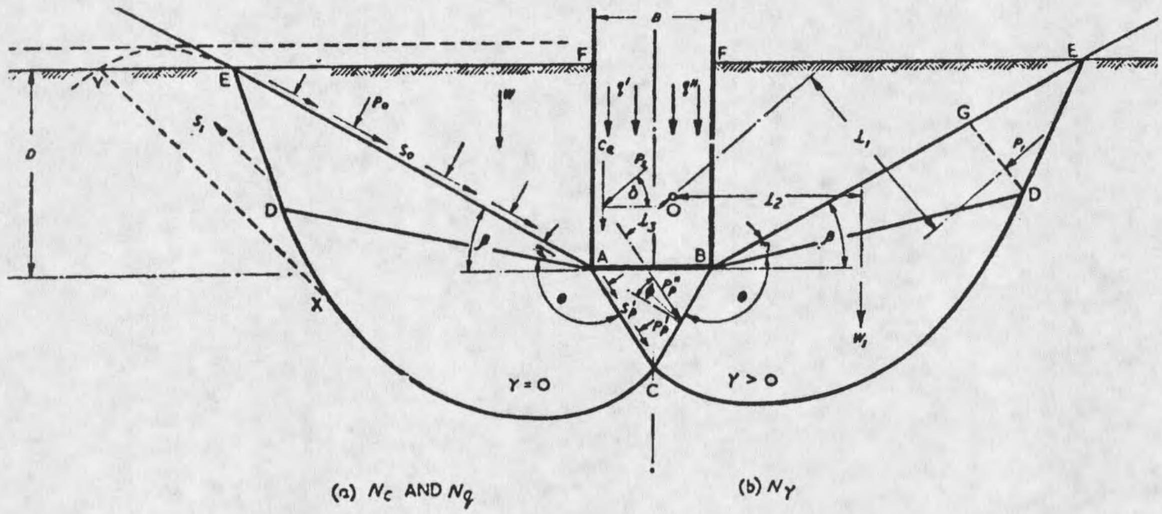

Figure 10. Meyerhof's failure mechanism (Meyerhof, 1951)

capacity factors in table 4 neglect the shearing resistance of the soil above a foundation base, the corresponding increase of the bearing capacity can be estimated from the depth factors. Meyerhof (1963) also indicated that bearing capacities of inclined foundations decrease with greater inclinations of foundations, especially for cohesionless soils.

From table 3, it can be readily seen that the general bearing capacity equation proposed by Hansen (1970) is a further extension of Meyerhof's work. Hansen's shape, depth and other factors making up the general bearing capacity equation represent revisions and extensions from his earlier proposals in 1957 and 1961. These extensions include a factor for a footing being tilted from the horizontal and for the possibility of a footing being on a slope. It can be noted that, in Hansen's formula, the depth factors implicitly allow any depth of foundation and thus can be used for both shallow footings and deep foundations.

Vesic's procedure (1973, 1975) is quite similar to the Hansen method. Essential differences in his solution are in using different expressions for N_γ (Table 3) and a variation on some of Hansen's factors. In Vesic's N_γ equation, N_γ value varies sharply with friction angle ϕ of soils. With respect to the soil failure pattern, he pointed out that the radial zone is bounded by a curve and this curve depends upon the friction angle ϕ and the ratio of $\gamma B/q$, where q is the uniformly distributed surcharge at a footing base, $q = \gamma D$. For a weightless, cohesionless material, a logarithmic spiral will result, while a circle will be generated in the case of cohesive materials. In the real case when a soil has weight, the curve lies between a logarithmic spiral and a circle.

Another important effect which Vesic emphasized is the influence of soil compressibility. He stated that the failure mode depended on the relative compressibility of the soil and geometrical and loading conditions, which includes soil density, embedment and size of the footing as well as soil layering. He utilized cavity expansion theory to derive equations for compressibility factors which depend on the friction angle ϕ, the size of the footing as well as the critical rigidity index I_r. Meanwhile, he adopted Terzaghi's formula for accounting for a reduction factor of shearing strength parameters in the case of local failure mode, and proposed to use $0.67 + D_r - 0.75 D_r^2$ instead of 0.67 in Terzaghi's formula when D_r is less than 0.67. Vesic also stated that a foundation's roughness has little effect on the bearing capacity as long as the external loads remain vertical which is in contrast with the theory of Meyerhof (1963).

Table 3 Bearing capacity equations by several researchers

Terzaghi:

$$q_{ult} = cN_c s_c + qN_q + 0.5\gamma B N_\gamma s_\gamma$$

$$N_q = \frac{a}{2\cos^2(45+\phi/2)}$$

$$a = e^{(0.75\pi-\phi/2)\tan\phi}$$

$$N_c = (N_q-1)\cot\phi$$

$$N_\gamma = \frac{\tan\phi}{2}\left(\frac{K_{p\gamma}}{\cos^2\phi}-1\right)$$

$$K_{p\gamma} = \frac{1+\sin\phi}{1-\sin\phi}$$

For:	strip	round	square
s_c =	1.0	1.3	1.3
s_γ =	1.0	0.6	0.8

Meyerhof: (see Table 2.4 for shape, depth, and inclination factors)

Vertical load: $q_{ult} = cN_c s_c d_c + qN_q s_q d_q + 0.5\gamma B N_\gamma s_\gamma d_\gamma$

Inclined load: $q_{ult} = cN_c d_c i_c + qN_q d_q i_q + 0.5\gamma B N_\gamma d_\gamma i_\gamma$

$$N_q = e^{\pi\tan\phi}\tan^2\left(45+\frac{\phi}{2}\right)$$

$$N_c = (N_q - 1)\cot\phi$$

$$N_\gamma = (N_q - 1)\tan(1.4\phi)$$

Hansen (see Table 2.5 for shape, depth, and other factors)

General: $q_{ult} = cN_c s_c d_c i_c g_c b_c + qN_q s_q d_q i_q g_q b_q + 0.5\gamma B N_\gamma s_\gamma d_\gamma i_\gamma g_\gamma b_\gamma$

when $\phi = 0$

use $q_{ult} = 5.14 s_u(1+s_c'+d_c'-i_c'-b_c'-g_c')+q$

$$N_\gamma = 1.5(N_q -1)\tan\phi$$

Vesic (see Table 2.5 for shape, depth, and other factors)

Use Hansen's N_q and N_c equations above

$$N_\gamma = 2(N_q +1)\tan\phi$$

Table 4 Shape, depth, and inclination factors for the Meyerhof bearing capacity equation of Table 3

Factors	Value	For
Shap	$s_c = 1 + 0.2K_p\frac{B}{L}$	Any ϕ
	$s_q = s_\gamma = 1+0.1K_p\frac{B}{L}$	$\phi > 10^o$
	$s_q = s_\gamma = 1$	$\phi = 0$
Depth:	$d_c = 1 + 0.2\sqrt{K_p}\frac{D}{B}$	Any ϕ
	$d_q = d_\gamma = 1 + 0.1\sqrt{K_p}\frac{D}{B}$	$\phi > 10^o$
	$d_q = d_\gamma = 1$	$\phi = 0$
Inclination:	$i_c = i_q = (1 - \frac{\theta^o}{90^o})^2$	Any ϕ
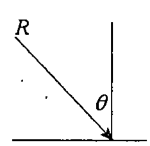	$i_\gamma = (1 - \frac{\theta^o}{90^o})^2$	$\phi > 0$
	$i_\gamma = 0$	$\phi = 0$

Where $K_p = \tan2(45 + \phi/2)$

θ = angle of resultant measured from vertical without a sign

B, L, D = footing width, length, and depth respectivelly

Table 5: Shape, depth, inclined factors and other factors for Hansen and Vesic equations (factors for both unless subscripted)

Shape factors	Depth factors	Inclination factors	Ground factors (base on slope)
$s'_c=0.2\frac{B}{L}$ $s_c+1+\frac{N_q B}{N_c L}$ $s_c=1$ *for strip*	$d'_c=0.4k$ $d_c=1+0.4k$	$i'_{c(H)}=0.5-0.5\sqrt{1-\frac{H}{A_f c_a}}$ $i_{c(V)}=1-\frac{mH}{a_f c_a N_c}$ $i_c=i_q-\frac{1-i_q}{N_{q1}}$ (Hansen;Vesic)	$g'=\frac{\beta^o}{147^o}$ *for Vesic use* $N_\gamma=2\sin\beta$ *for* $\phi=0$ $g_c=1-\frac{\beta^o}{147^o}$ $g_{q(H)}=g_{\gamma(H)}=(1-0.5\tan\beta)^5$
$s_q=1+\frac{B}{L}\tan\phi$	$d_q=1+2\tan\phi(1-\sin\phi)\,k$	$i_{q(H)}=(1-0.5\frac{H}{V+A_f c_a\cot\phi})^5$	$g_{q(V)}=g_{\gamma(V)}=(1-0.5\tan\beta)^2$
	$d_\gamma=1.00$ for all ϕ	$i_{q(V)}=(1-\frac{H}{V+A_f c_a\cot\phi})^m$	**Base factors (tilted base)**
$s_\gamma=1-0.4\frac{B}{L}$	$k=\frac{D}{B}$ *for* $\frac{D}{B}\leq1$ $k=\tan^{-1}\frac{D}{B}$ *for* $\frac{D}{B}>1$ (*rad*)		$b'_c=\frac{\eta^o}{147^o}$ $b_c=1-\frac{\eta^o}{147^o}$
(see notes below)		$i_{\gamma(H)}=(1-0.7\frac{h}{V=A_f c_a\cot\phi})^5$ $(\eta=0)$ $i_{\gamma(H)}=(1-\frac{(0.7-\eta^o/450)H}{V}+A_f c_a\cot\phi)^5$ $i_{\gamma(V)}=(1-\frac{H}{V+A_f c_a\cot\phi})^{m+1}$	$b_{q(H)}=\exp(-2\eta\tan\phi)$ $b_{q(H)}=\exp(-2.7\eta\tan\phi)$ $b_{q(v)}=b_{\gamma(V)}=(1-\gamma\tan\phi)^2$
		$m=m_B=\frac{2+B/L}{1+B/L}$ $m=m_L=\frac{2+L/B}{1+L/B}$ *Note:* $i_q, i_\gamma>0$	*Notes:* $\beta+\eta\leq90^o$ $\beta\leq\phi$

Where A_f=effective footing area $B'\times L'$
c_a=adhesion to base=cohesion or a reduced value
D=depth of footing in ground (used with B and not B')
e_B,e_L=eccentricity of load with respect to center of footing area
H=horizontal component of footing load with $H\leq V\tan\delta+c_a A_f$
V=total vertical load on footing
β=slope of ground away from base with downward=(+)
δ=friction angle between base and soil usually $\delta=\phi$ for concrete on soil
η=tilt angle of base from horizontal with(+)upward as usual case

General: 1.Do not use s_i in combination with i_i
2.Can use s_i in combination with d_i ,g_i ,and b_i.
3.For $L/B\leq2$ use ϕ_{tr}
For $L/B>2$ use $\phi_{ps}=\phi_{tr}-17$
For $\phi\leq34$ use $\phi_{ps}=\phi_{tr}$

The Slip - Line Method

The slip-line method or the method of characteristics is in essence an exact solution of limit equilibrium of soils. If we consider a two-dimensional element of soil stressed to failure under principal stresses σ_1' and σ_3' we note that the direction of the major principal stressσ_1' with the vertical z axis and the pole of the Mohr's circle at P (Fig.11a, b) is denoted by the angle η. We locate the plane α and β in Fig.11(a) on which the stresses are those at A and B in Fig.11(b), and the stresses σ_1' and σ_3' are subjected to the Mohr-Coulomb's failure criterion under the condition of plastic equilibrium. The α andβ lines in Fig.11(a) represent planes upon which failure occurs, and are typically referred to as slip lines.

Clearly, there will be similar slip-lines at every point for which the Mohr's circle touches the failure envelop, and thus we can construct families of and lines throughout a region of soil experiencing failure. For a two-dimensional material element, the equations of stress equilibrium are:

$$\frac{\partial \sigma_x}{\partial x} + \frac{\partial \tau_{xz}}{\partial z} = 0 \tag{24}$$

$$\frac{\partial \sigma_x}{\partial z} + \frac{\partial \tau_{xz}}{\partial x} = \gamma \tag{25}$$

The Mohr-Coulomb failure criterion, expressed in a plane-strain formulation, is used to provide expressions for σ_x, σ_z and τ_{xz} in terms of the angle η. The expressions can be inserted into the stress equilibrium equations. This set of two partial differential equations can be solved using the method of characteristics, yielding two ordinary differential equations subject to the conditions of the characteristic lines:

$$\frac{dx}{dz} = \tan\left(\eta \pm \left(45 - \frac{\phi}{2}\right)\right) \tag{26}$$

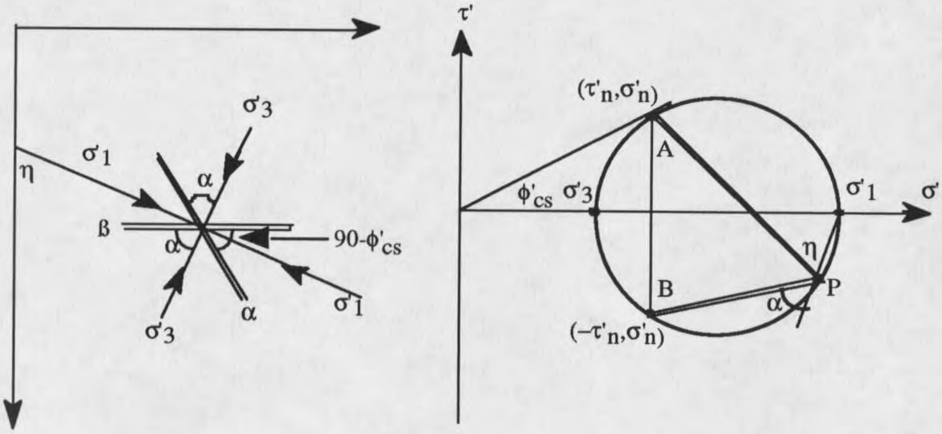

(a) (b)

Figure 11. Stress characteristics of drain loading

It is noted that the characteristic lines correspond to the directions of the α and β slip lines, meaning that the two ordinary differential equations are satisfied along planes of plastic collapse. These equations can then be solved using finite-difference schemes subject to certain boundary conditions.

Sokolovskiî (1965) presented a book which is devoted to the theory of slip line solutions for a granular medium. He presented the equations of limit equilibrium and investigated the transformation forms of these equations into the canonical coordinate system. Furthermore, the problem of mechanical similarity was studied and effective methods of numerical integration were suggested in the book. The limit equations of smooth shallow foundations were studied and the derivation of the required solutions was reduced to combine the boundary conditions for the canonical system.

A theoretical analysis of axially symmetric plastic deformation in soils was given by Cox et. al. (1961) using the method of characteristics. The study was made of quasi-static stress and velocity fields occurring in deformed ideal soils under axially symmetric conditions. Cox et. al. (1961) specialized the general field equations to various plastic regimes, where the stress and velocity fields are hyperbolic with coincident families of characteristics. The stress field is statically determinate under appropriate boundary conditions. In addition, the applications of the study to certain problems were illustrated with regard to soil mechanical testing and foundation engineering.

Cox (1962) presented another paper where the numerical results of average bearing capacity of smooth footings were shown as a function of dimesionless soil weight parameter G ($G = \gamma B/2c$) and internal friction angle ϕ. He computed the values of mean yield point pressures for indentation by a punch and by a die with a range of internal friction angles between 0^o and 40^o as well as a range of soil weight parameter G from 10^2 to 10. He indicated that, for a given frictional soil, the yield point pressure increases markedly as the size of the indenter increases. He also stated that the ratio of footing width to the corresponding width of slip plane decreases as G increases, provided that ϕ is not zero.

Graham (1968) developed a solution for cohesionless material using the slip-line method. Based on Sokolovskiĩ's numerical method, he gave an improved numerical procedure with regard to the iterations of the mean stress σ, $\sigma = (\sigma_1 + \sigma_3)/2$, and of the inclination angle η of the major principle stress to the vertical direction instead of only iterations on η. The paper also presented the applications of the improved method to non-homogeneous slopes and to deep strip footings.

Graham and Stuart (1971) described the effects of footing scale and boundary conditions (e.g. surcharge and roughness of footing base) using the slip-line method. They plotted contours of the friction angle ϕ for different footing widths. The results show that the value of ϕ decreases as the footing width increases. Therefore, they stated that the usual assumption for constant internal friction angle is a major simplification of the real soil behavior. They compared the bearing capacity values obtained from the numerical method with small scale and full scale experiments and stated that the results from the small scale experiments agree with the theoretical values.

Graham and Hovan (1985) introduced a critical state model to the solution of stress characteristic method for determining the bearing capacity of a strip footing on sand. The solution allows for the inclusion of the effects of different stress levels, placement densities and soil compressibility. A linear relationship between $\log(N_\gamma)$ and log (footing width) was obtained and the increasingly ductile behavior of the soil was observed as footing width increases. The authors also showed the variation of mobilized ϕ in the failure zone for different size footings, which is a decrease of 10° between the edge of the passive zone and the center point of the footing. However, there is approximately a 6° decrease in ϕ between geometrically similar points when comparing footings with different widths. They also stated that the trend of the results agrees with available data from laboratory and field tests.

Pope (1975) presented a bearing capacity chart for 2-*D* partially rough foundations using the method of characteristics. He compared the chart with the solution obtained by Terzaghi and indicated that the superposition procedure overestimates the bearing capacity of footings as compared to his solution.

Ko and Scott (1973) presented a solution and a series of charts for the bearing capacity of a smooth strip foundation by the slip-line solution. Comparison with Terzaghi's superposition method, they indicated that the bearing capacity calculated from Terzaghi's method is always greater than those obtained by means of the plasticity method. The reason for the large values using the superposition method, the writers explained, is that the value of N_γ in all superposition formulas is obtained from an approximate analysis of internal friction angles in soil. They pointed out that a lower bearing capacity will be predicted if the frictional angle in triaxial compression conditions is used than that in plane strain condition.

The Method of Limit Analysis (Limit Plasticity)

In contrast to the limit equilibrium and slip-line methods, the method of limit plastic analysis predicts an upper and lower bound to the true collapse load of a foundation. By ignoring the equilibrium condition we may calculate an upper bound to the collapse load so that if a structure is loaded to this value it must collapse. Similarly, by ignoring the compatibility conditions we can calculate a lower bound to the collapse load so that if the structure is loaded to this value it cannot collapse. The true collapse load must lie between these bounds. Thus, by using the method of limit analysis, we calculate upper and lower bounds for the true collapse load instead of a specific collapse load.

The theorems of upper bound and lower bound were first defined by Drucker and Prager (1952). The definition of the two theorems made it possible to establish the solution of limit analysis for collapse loads on soil mass. For the upper bound, the theorem was stated as: *collapse must occur if for any compatible flow pattern, considered as plastic only, the rate at which the external forces do work on the body equals or exceeds the rate of internal dissipation.* Therefore, according to the definition, Chen (1975) explained that the conditions required to establish such an upper-bound solution are essentially as follows:

- A valid mechanism of collapse must be assumed which satisfies the mechanical boundary conditions.
- The expenditure of energy by the external loads (including soil weights) due to the small displacement defined by the assumed mechanism must be calculated.
- The internal dissipation of energy by the plasticity deformed regions which is associated with the mechanism must be calculated.
- The most critical; or least upper-bound solution corresponding to a particular layout of the assumed mechanism must be obtained via the work equation.

If we consider a structure which collapses when subjected to a set of external loads F_c, we seek an upper bound set of the external loads F_u which give rise to a set of internal stresses σ_u. These are associated with a set of boundary displacements δW_u and a set of internal strain increments $\delta \varepsilon_u$ which make up a compatible mechanism of collapse. From the statement of the upper bound theorem, loads F_u must cause collapse if:

$$\sum F_u \delta W_u = \int_v \sigma_u \delta \varepsilon_u dv \qquad (27)$$

where the term on the left is the increment of work done by the external loads and the term on the right is the increment of work done by the internal stresses.

Ducker and Prager (1952) also defined the lower bound theorem which was stated as: *collapse will not occur if any state of stress can be formed which satisfies the equations of equilibrium and the boundary conditions of stress for which f < k everywhere (f represents a yield function and k is a positive constant at each point of the material).* So the conditions required to establish such a lower bound solution are as follow (Chen, 1975):

- A complete stress distribution or stress field must be found everywhere satisfying the differential equations of equilibrium.
- The stress field at the boundary must satisfy the stress boundary conditions
- The stress field must nowhere violate the yield condition

For a proof of the lower bound theorem, consider a lower bound set of external loads F_l which are in equilibrium with internal stresses σ which do not exceed the failure criterion. For the true collapse conditions the virtual work equation becomes a real work equation:

$$\sum F_l \delta W_l = \int_v \sigma_l \delta \varepsilon_l dv \qquad (28)$$

Therefore, the real external forces F_c of a structure should be:

$$F_l < F_c < F_u \qquad (29)$$

Shield et. al. (1953) applied limit analysis to obtain upper and lower bounds of the punch pressure for punch-indentation problems. The analysis assumed Tresca's yield criterion of constant maximum shearing stress k during plastic deformation. Two-dimensional flat punch and three-dimensional flat square and rectangular punch problems were analyzed according to the Hill mechanism and the Prandtl mechanism of velocity fields, respectively. The results showed that, in the case of two-dimensional punch, the pressure lies between the upper bound value $(2+\pi)k$ and lower bound $5k$, and in the case of three-dimensional punch, the upper bound lies in the range of $5.71k$ and $(2+\pi)k$, where $5.71k$ corresponds to a square punch and $(2+\pi)k$ corresponds to a very long rectangular punch. The lower bound for a three-dimensional punch is $5k$ for any rectangular punch.

Chen (1973, 1975) presented various solutions for the bearing capacity problems by means of the limit analysis method. In his analysis, the soil was assumed to be an isotropic, homogeneous and rigid-perfectly plastic material which obeys the Mohr-Coulomb's yield condition and the associated flow rule. Two different failure mechanisms of plastic materials--Hill Mechanism (Fig.12) and Prandtl mechanism were used for the analyses (Fig.13). From Fig.12(a), it can be seen that Hill mechanism is symmetric about the axis of the footing, and the mechanism of the left-hand plastic flow regions in Fig.12(a) consists of a rigid triangular wedge, AOC, with base angles $\pi/4 + \phi/2$, a logspiral shear zone, ACD, of central angle $\pi/2$, and a wedge, ADE, with base angle $\pi/4 - \phi/2$. Fig.12(b) shows the compatible velocity diagram for the Hill mechanism and Fig.12(d) shows the displaced position of the Hill mechanism which would result if the footing moved with the downward velocity V_p for a short period of time.

The Prandtl mechanism shown in Fig.13(a) consists of a triangular wedge *ABC*, with base angles $\pi/4 + \phi/2$, moving downwards as a rigid body with the velocity of the footing V_p, a logspiral shear zone, *ACD*, of central angle $\pi/2$, and a rigid wedge, *ADE*, with base angle $\pi/4 - \phi/2$. Fig.13(c) shows the displaced position of the Prandtl mechanism which would result if the footing moved with the downwards velocity V_p for a short period of time. Chen (1975) developed two different methods to predict bearing capacity of shallow foundations, which one makes use of the three components of Terzaghi's equation, the new expressions for N_γ values were developed corresponding to the two distinct failure mechanisms. In this method, the bearing capacity factors N_c and N_q were the same as those used by Meyerhof (1963), and the N_γ expression corresponding to the Hill mechanism was developed as:

$$N_\gamma = \frac{1}{4}\tan\xi[\tan\xi\exp(\frac{3\pi}{2}\tan\phi) - 1]$$

$$+ \frac{3\sin\phi\cos\phi}{4(1+8\sin^2\phi)(1-\sin\phi)}([\tan\xi - \frac{\cot\phi}{3}]$$

$$*\exp(\frac{3\pi}{2}\tan\phi) + \tan\xi\frac{\cot\phi}{3} + 1) \qquad (30)$$

$$\xi = \frac{\pi}{4} + \frac{\phi}{2}$$

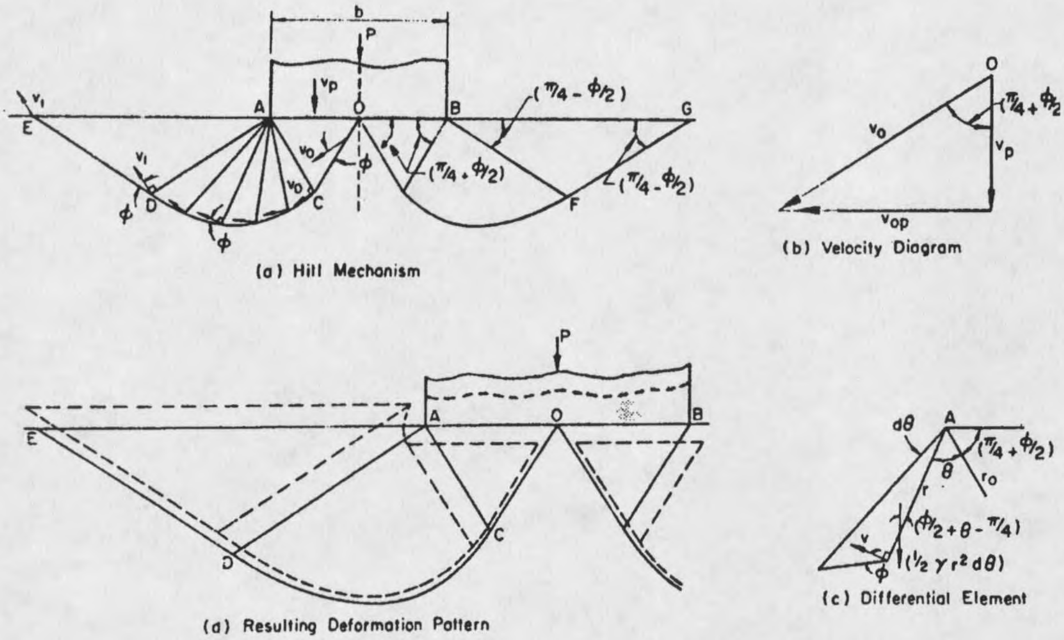

Figure 12. Bearing capacity calculation based on Hill mechanism

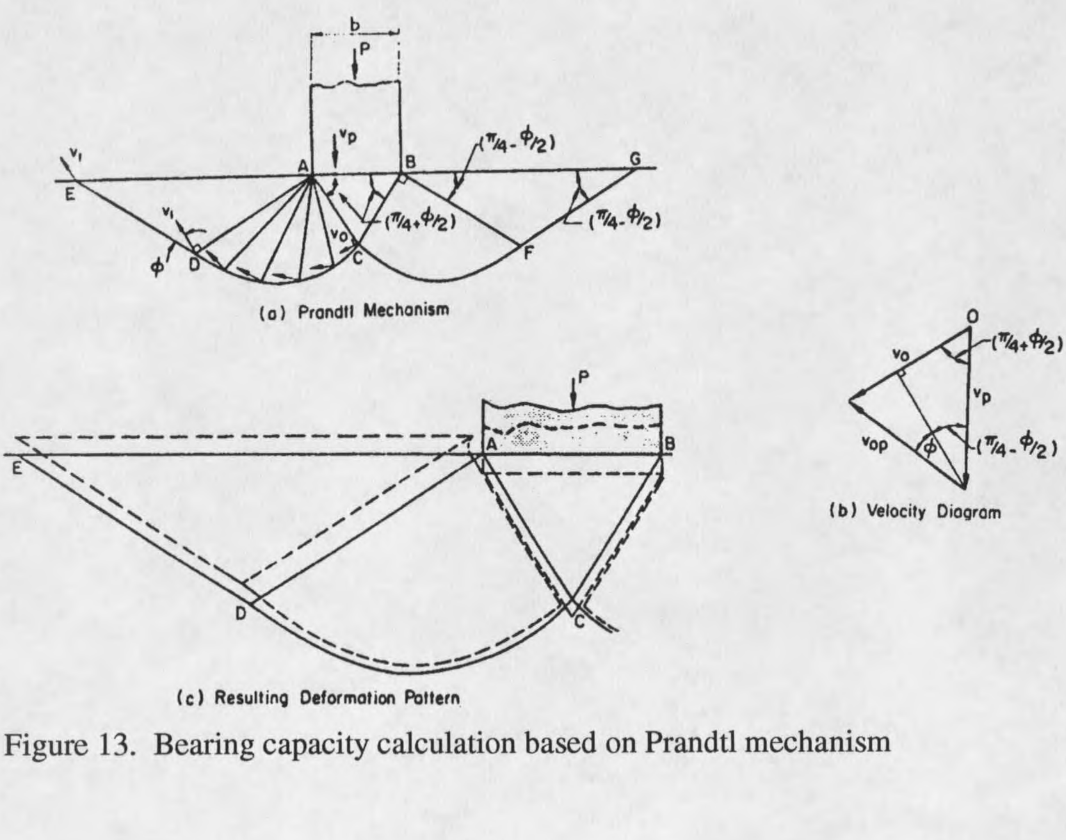

Figure 13. Bearing capacity calculation based on Prandtl mechanism

Corresponding to the Prandtl mechanism, N_γ is two times the value obtained from the expression above.

The second method Chen developed is that only two components are used in bearing capacity equation, where the first component represents the effect produced by cohesion, and the second component represents the effects of surcharge and self-weight of the soil. For this case, the new expressions of N_c and N_γ are developed for a strip footing with an initial embedment. Corresponding to the Hill mechanism, the expressions of N_c and N_γ are:

$$N_c(\xi,\eta,\zeta) = \frac{\sin\xi\cos\phi + \sin\zeta \text{abs}[\cos(\xi+\zeta-\phi)]}{\sin(\zeta+\xi)\sin(\zeta-\phi)}$$

$$+\frac{\alpha\sin\eta\sin\zeta\exp[2(\pi+\beta-\eta-\xi)\tan\phi}{\cos(\phi+\eta)\sin(\zeta+\xi)\sin(\zeta-\phi)}$$

$$+\frac{\alpha\sin\zeta(\exp[2(\pi+\beta-\eta-\xi)\tan\phi]-1)}{\sin(\zeta+\xi)\sin\phi\sin(\zeta-\phi)} \tag{31}$$

$$N_\gamma(\xi,\eta,\zeta) = \frac{-0.5\sin\zeta\sin\xi}{\sin(\zeta+\xi)} + \frac{0.5\alpha\sin^2\zeta}{\sin^2(\zeta+\xi)\cos\phi\sin(\zeta-\phi)(1+9\tan^2\phi)}$$

$$\cdot\{3\tan\phi\cos(\beta-\eta)+\sin(\beta-\eta)]\exp[3(\pi+\beta-\eta-\xi)\tan\phi]+3\tan\phi\cos\xi+\sin\xi\}$$

$$+\frac{\alpha\sin\zeta\sin\eta\cos(\beta-\eta)\exp[2(\pi+\beta-\eta-\xi)\tan\phi]}{\sin(\zeta+\xi)\cos\phi\sin(\zeta-\phi)\sin\beta}(D/B)$$

$$+\frac{2\alpha\cos(\beta-\eta)\exp[(\pi+\beta-\eta-\xi)\tan\phi]}{\tan\beta\cos\phi\sin(\zeta-\phi)}\left(\frac{D}{B}\right)^2 \tag{32}$$

where $\alpha = \sin(\xi+\zeta-2\phi)$ if $-0.5\pi+\xi+\zeta-\phi > 0$, otherwise $\alpha = \sin(\xi+\zeta)$. β is related to the ratio of (D/B), the values ξ, ζ and η determine the position of the critical mechanism. The corresponding governing equation for β is:

$$\sin\beta\exp(\beta\tan\phi) = \frac{2(D/B)\sin(\zeta+\xi)\cos(\phi+\eta)}{\sin\zeta\cos\phi\exp[(\pi-\eta-\xi)\tan\phi]}$$

For a surface footing, the value η is expressed as: $\eta = 45^{\circ} - \phi/2$, and the values of the parameters ξ and ζ are found to satisfy the condition: $\xi + \zeta = 90^{\circ} + \phi$.

By using the Prandtl mechanism, N_c and N_γ are developed as:

$$N_c(\xi,\eta) = \cot\phi\left[\frac{\cos\eta\cos(\xi-\phi)\exp\{2(\pi+\beta-\xi-\eta)\tan\phi\}}{\cos\xi\cos(\eta+\phi)} - 1\right] \tag{33}$$

$$N_\gamma(\xi,\eta) = -\frac{\tan\xi}{2}+\frac{0.5\cos(\xi-\phi)}{\cos^2\xi\cos\phi(1+9\tan^2\phi)}$$

$$\cdot\{[3\tan\phi\cos(\beta-\eta)+\sin(\beta-\eta)]\exp[3(\pi+\beta-\eta-\xi)\tan\phi]+3\tan\phi\cos\xi+\sin\xi\}$$

$$+\frac{\cos(\xi-\phi)\sin\eta\cos(\beta-\eta)\exp[2(\pi+\beta-\eta-\xi)\tan\phi]}{\cos\xi\cos\phi\sin\beta}\left(\frac{D}{B}\right)$$

$$+\frac{2\cos(\xi-\phi)\cos(\beta-\eta)\exp[(\pi+\beta-\eta-\xi)\tan\phi]}{\cos\phi\tan\beta}\left(\frac{D}{B}\right)^2 \qquad (34)$$

As was the case for the Hill mechanism, the value β is related to D/B. The values of η and ξ determine the critical position of the failure mechanism, and by the transcendental equation:

$$\sin\beta\exp(\beta\tan\phi) = \frac{2(D/B)\cos\xi\cos(\phi+\eta)}{\cos\phi\exp[(\pi-\eta-\xi)\tan\phi]}$$

For a surface footing, the value of η can be determined by the same equation as the Hill mechanism, ξ may be approximated by using the following approximated equations:

$\xi = 45^{o} + \phi/2 \quad$ if $G \leq 0.1$

$\xi = \phi + 15^{o} \quad$ if $G > 0.1$

Since the kinematically admissible velocity field used in the Prandtl mechanism is such that no slip occurs between the footing and the soil, the equation (33) and (34) are applicable to either a rough or a smooth footing.

Chen analyzed the methods of limit equilibrium and slip-line with the concept of limit plasticity and pointed out the main limitations of both methods. He stated that, although the limit equilibrium technique utilizes the basic philosophy of the upper-bound theorem of limit analysis, the solution may not be an upper bound, and also, he related that the superposition method suggested by Terzaghi (1943) violates the soil behavior which in the plastic range is nonlinear so that the superposition does not hold for general soil bearing capacity. Chen remarked that the bearing capacities computed using the Hill mechanism are rigorous upper bounds only for perfectly smooth footings, while bearing capacities computed with the alternate mechanism are true upper bounds for any arbitrary base friction.

A new method of limit analysis for plane problems in soil mechanics was developed by Lysmer (1970), which is a general computer method for lower bound analysis of plane stability problems. The main aim of this method is to find good statically admissible stress fields involving arbitrary geometry and stress boundary conditions. Finite element theory was used to build element equilibrium and equilibrium at interfaces of elements as well as to generate the external boundary conditions and no-yield condition. The author applied the new method to solve several simple earth problems and bearing capacity problems. He showed that the results compare favorably with known solutions to these problems.

CHAPTER THREE

EXPERIMENTAL WORK

Introduction

The purpose of this chapter is to present the experimental work related to the bearing capacity of a lunar soil simulant, MLS-1. Centrifuge small-scale modeling tests were conducted by using the 400g-ton centrifuge machine at the University of Colorado at Boulder. The concept of using a centrifuge for model-scale experiments was presented in chapter two. The philosophy of the testing program which directs the bearing capacity experiments is presented. The experimental methods used to create a plane strain condition, to evaluate the boundary effects of the container as well as to obtain a uniform sample density are also described. A total of 30 bearing capacity experiments were performed in an increased gravity environment. The main variable included in the testing program was the centrifuge acceleration level and footing embedment. The experimental results are presented in the last section of this chapter.

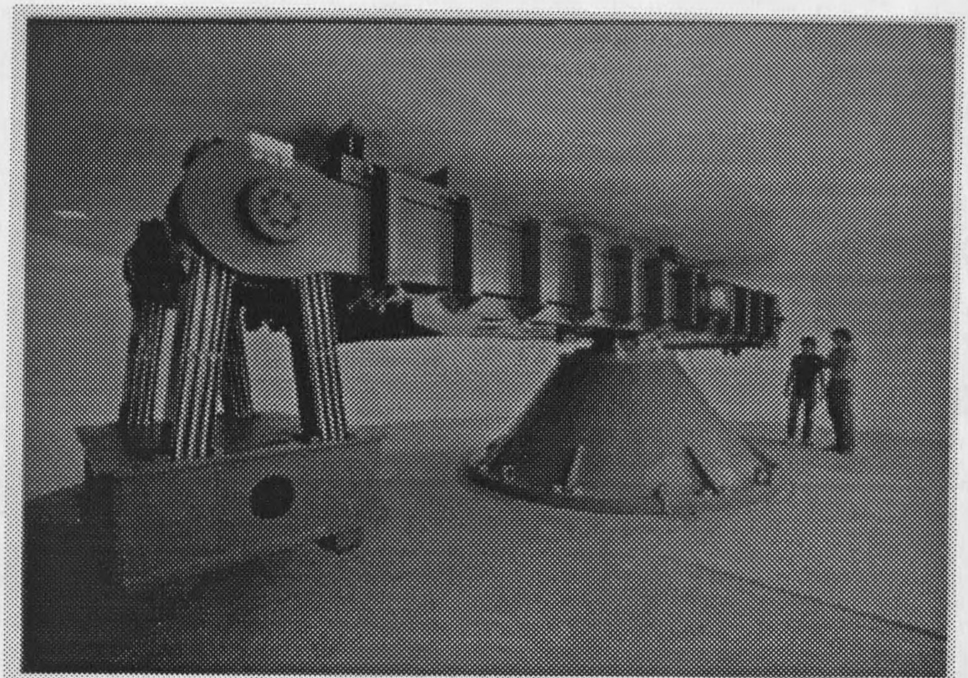

Figure 14 The 400g - ton centrifuge at University of Colorado, Boulder.

The 400g-ton Centrifuge Facility at the University of Colorado

The model footing experiments were conducted in the 400g-ton centrifuge located at the University of Colorado, Boulder. The centrifuge has an unsymmetrical rotor arm, with a swing platform on one end of the arm to carry the testing payload and a fixed counterweight compartment on the other (Fig.14). In the fully extended position, the top of the swing platform is at radius of 5.94 *m* and the platform can carry testing loads as large as 1.22 *m* by 1.22 *m* by 0.91 *m* and with a mass of 2,000 *kg*. A 684 *kw* electrical motor drives the centrifuge through a right-angle gearbox with a 6 to 1 speed reduction. It is capable of accelerating the testing sample to a maximum of 200g in 6 *mm*.

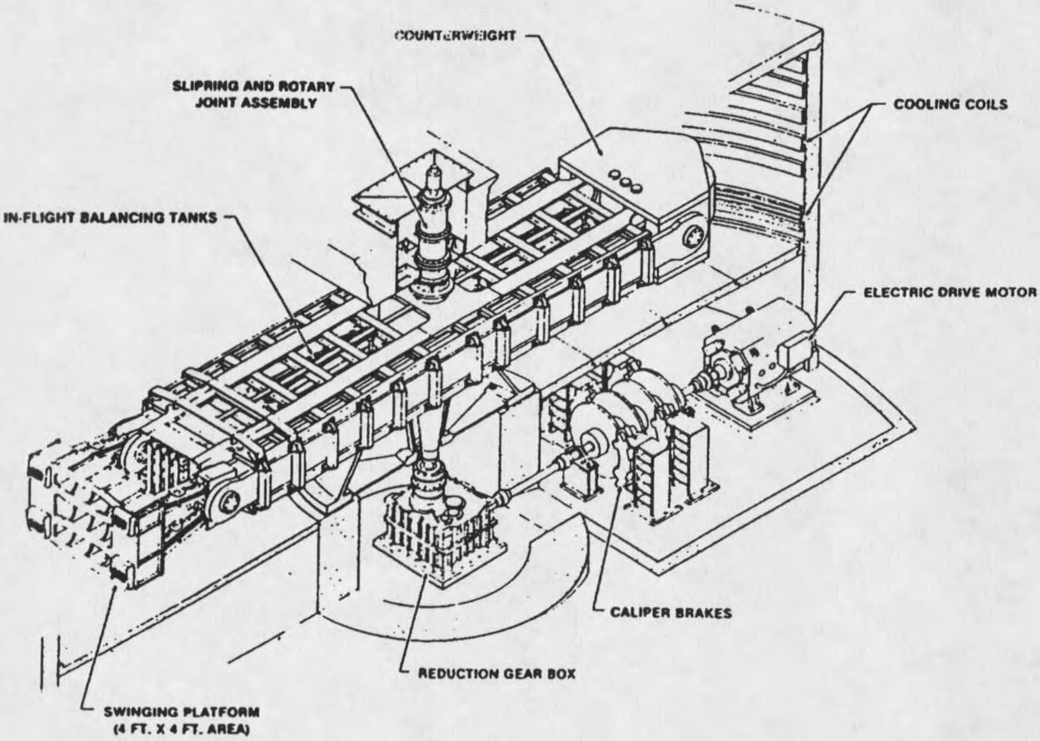

Figure 15 Schematics of the 400g - ton centrifuge (Ko, 1990)

The operation of the centrifuge is controlled automatically by using two computers. One computer is a programmable logic controller which regulates the operations of the drive motor and the brake. The second is used to receive the signals from the various transducers monitoring the parameters of performance of the entire system. Data acquisition can be obtained by using transducers and a 64-channel digital data acquisition system is available for a variety of transducers.

The centrifuge operates in a completely enclosed underground chamber which is accessible through a hatch in the ceiling when the centrifuge is stationary. Fig.15 shows the centrifuge with the swing basket in the in - flight position.

Philosophy of Testing Program

As described in Chapter 2, conventional analyses of bearing capacity problems in soils typically rely upon the use of two main properties-- friction angle and cohesive strength. Bearing capacity solutions, used to establish the ultimate load carrying capacity of shallow foundations, are formulated in terms of bearing capacity factors which are expressed as analytical functions of the friction angle. These solutions have been verified only for soils of relatively modest friction angles (less than 50°), while most bearing capacity factor charts stop at $\phi = 40^{\circ}$ and never go beyond $\phi = 50^{\circ}$. Also, these bearing capacity factors or the resulting ultimate bearing capacities of shallow foundations are quite sensitive to small changes in the friction angle for friction angles exceeding 50°. However, the friction angles of the lunar regolith and MLS-1 range from 41° to 60° (Perkins, 1991). In order to examine the viability of the conventional bearing capacity solutions for lunar regolith, Perkins (1991) conducted finite element analysis of a surface footing bearing on MLS-1 and found that conventional bearing capacity theory overpredicted the peak bearing pressure of MLS-1 soil as seen in the finite element analysis. For further study and analysis of the conventional bearing capacity solution applied to lunar regolith, centrifugal model footing tests were conducted. The research undertaken here was designed to satisfy the following requirements:

(1) Plane strain condition

(2) No influence of the sample container wall and bottom on the experimental results

(3) Reasonable loading system

(4) Uniform soil density

One important assumption in determining the bearing capacity of a strip footing is a plane strain condition inherent in all conventional solutions. The angle of internal friction as determined under an axially symmetric triaxial compression stress state, ϕ_t, is known to be several degrees less than that determined under plane strain conditions, ϕ_p, for low confining pressure. Bishop (1957) proved that the angle of internal friction in plane strain compression tests is roughly 10 percent greater than in triaxial compression tests, and the friction angles ϕ_r for rectangular foundations are roughly given by:

$$\phi_r = \left(1.1 - 0.1\frac{B}{L}\right)\phi_t \tag{35}$$

Therefore, when conducting footing tests, the maintenance, as closely as possible, of plane strain conditions is important in that the experiments will be carried out under the same conditions as assumed in the theories. This allows related methods of calculating bearing capacities to be verified for materials containing elevated levels of frictions. In our centrifugal tests, the footing feature was designed for the purpose of simulating the plane strain condition, and a proper testing program was conducted for the assessment of the condition of plane strain, which details will be described in the section of results.

The influence of the sample container boundaries on the experimental results is another important factor. To the author's knowledge, one disadvantage in many previous bearing capacity experiments is that sample containers were designed too small to allow a whole failure plane extending in containers. As a result, the rigidity of the containers certainly influences the test results. This violates the basic theoretical assumption of a complete failure plane in soil. In order to avoid this problem, a series of tests were also conducted to assess the influence from the container bottom and walls, and a minimum sample depth and a minimum sample surface size were found to avoid these influences. These results will be described in the section of results.

Material Properties

The lunar soil simulant, MLS-1, was used exclusively for the centrifuge bearing capacity experiments described in this thesis. Laboratory experiments were performed by a few investigators on this material to characterize its behavior. Perkins (1991) performed an extensive series of laboratory strength and deformation experiments on MLS-1, and has shown that this material matches the more significant engineering properties of real lunar regolith.

The bulk mineralogy of MLS-1 is described by Weiblen and Gorden (1988) and has been shown to match that of Apollo 11 sample 10084. Specific gravity of MLS-1 was measured to be approximately 3.2 (Perkins, 1991), falling within the range of values reported for lunar regolith, namely 2.9 to 3.2 (Carrier et. al. 1991). The mass unit weight used in the bearing capacity experiments was 2.2 g/cm^3. The crushing process used to produce this simulant results in highly angular particles that are comparable in shape to lunar regolith. The soil has been processed further by sieving the material into its respective particle sizes and recombining it in such proportions as to fall within the band of grain size distributions reported for the Apollo and Lunar missions. This gradation classifies the material as a silty sand with nearly 40% passing the #200 sieve. The grain size distribution for recombined MLS-1 is shown in Fig.16.

Conventional triaxial compression experiments have been performed on MLS-1 soil to obtain the soil strength parameters. The samples were prepared to a density 2.2 g/cm^3 and tested at seven levels of confining pressures of approximately 750, 600, 500, 350, 200, 150 and 50 *kPa*. The results of all conventional triaxial tests will be given in Appendix A. The peak strength measures and the residual strength measures are plotted on a p -q stress space in Fig.17, where $p = (\sigma_1+2\sigma_3)/3$ and $q = (\sigma_1 - \sigma_3)$. On this figure possible peak strength envelope and residual strength envelop are shown. The description of the two failure surface follow the form of the yield function proposed by Sture et al.(1989), and the parameters of the yield function corresponding to the peak strength could be found to match the CTC results which is:

$$F = q(1 + q)^{0.0332} - 2.61(p + 0.1) = 0 \tag{36}$$

and the parameters of the yield function corresponding to the residual strength is:

$$F = q(1 + q)^{0.00056} - 1.81p = 0 \tag{37}$$

The material shear strength parameters (c, ϕ) can be obtained from the functions

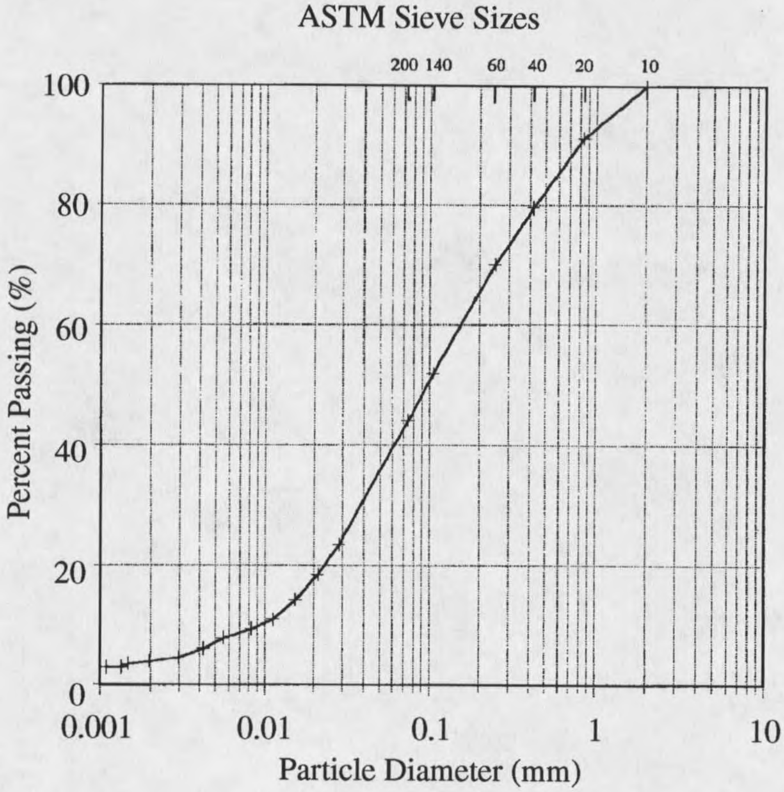

Figure 16 The grain size distribution for MLS - 1

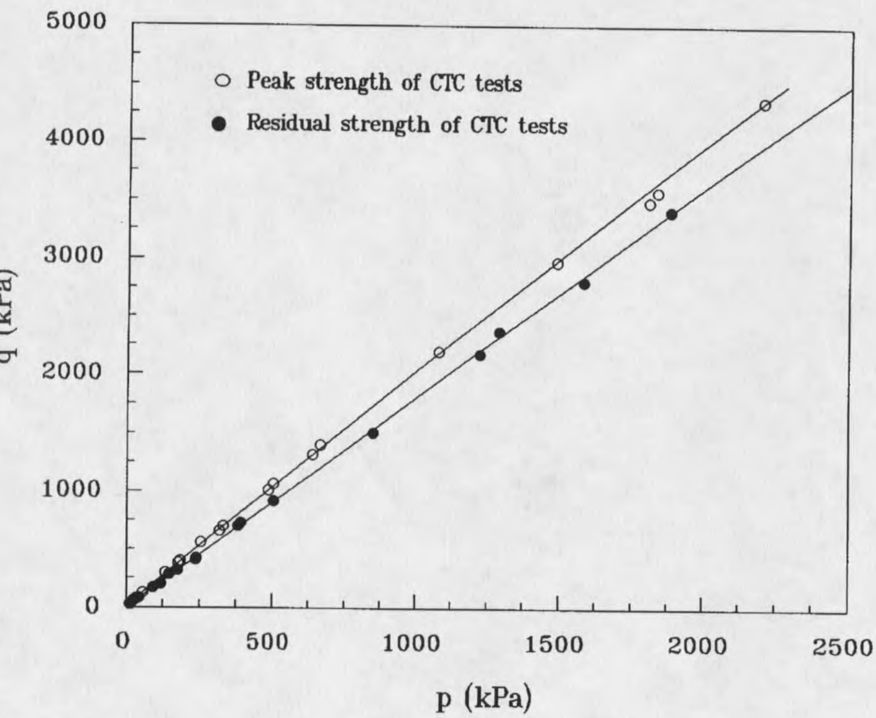

Figure 17 The *p* -*q* stress space of MLS - 1

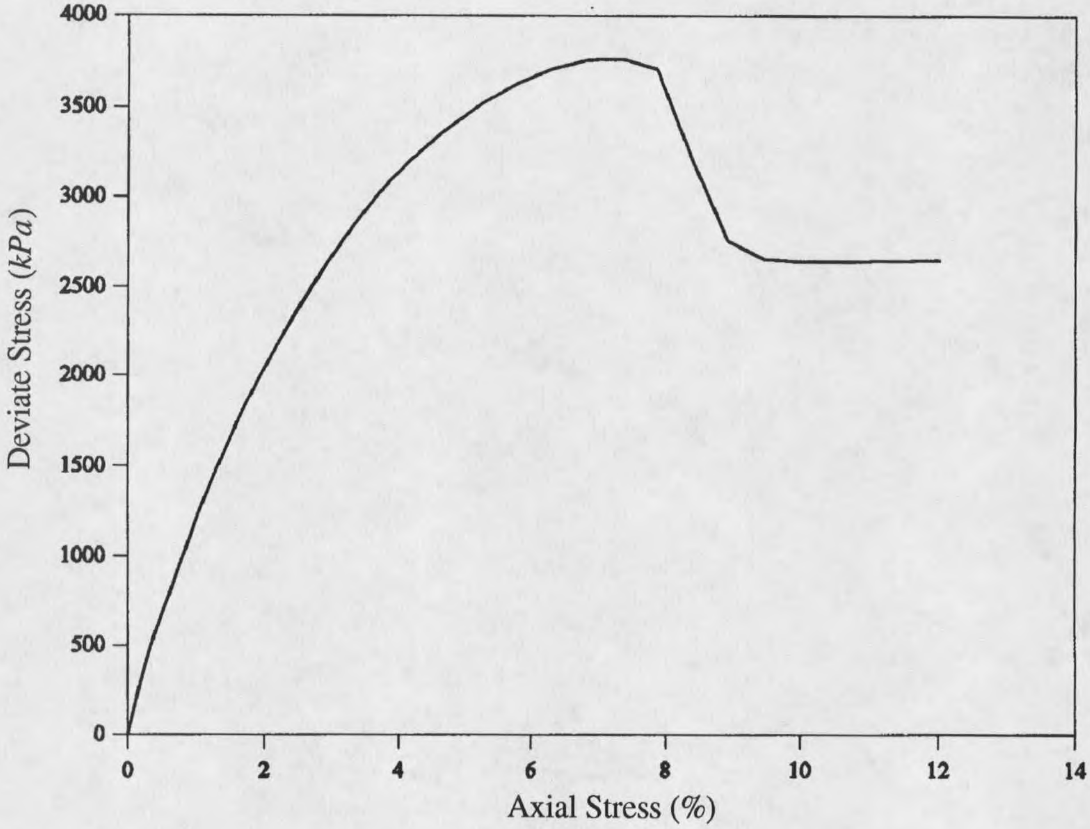

Figure 18 The stress - strain curve of a CTC test for confining pressure $\sigma_3 = 650\ kPa$

above which will be discussed in chapter 4. Fig.18 shows a particular CTC experiment result.

Experimental Set-up

A total of 30 bearing capacity experiments were performed in an increased gravity environment. The main variables included in the testing program were acceleration level and footing embedment. A rigid aluminum container was used in the experiments and a double acting hydraulic piston was used to apply loads to the footing.

Apparatus

The testing device consists of three basic components -- footing, specimen container and loading system. In order to ensure plane strain conditions, the footings were designed in a segmented fashion to allow independent measurement of load on each footing segment. The composite footing was constructed of five segments. The three interior segments each had a length equal to its width of 2 *cm*. The two end segments could be interchanged with various strip footings of a length varying from $1B$ to $3B$ (i.e. $2cm$ to $6cm$ in length) as shown in Fig.19. The end segments had the same width as the interior segments. The segments were designed to have 0.5 *mm* of clearance between each other. It is seen that a composite strip footing of a total length varying from $3B$ to $9B$ ($6cm$ to $18cm$) could be created. This feature was incorporated into the design to allow for the assessment of the plane strain condition for the center segment.

A rigid aluminum container was used in the test program. The container had an inside width and length of 1.09*m* and 1.14*m*, respectively and an inside height of 40*cm*. The walls of the container were 3.8*cm* in thickness. The container was reduced in size by inserting vertical walls supported by struts bearing against the aluminum container walls. These walls reduced the container width to 53*cm*, while the length and height remained unchanged. Fig.20 shows the configuration of the container.

The loading system was designed as shown in Fig.21. The three interior segments were instrumented with load cells having a range of 0 - 8.9*kN*. An uninstrumented steel rod was used to transmit load to the two end segments. The load to each segment was transmitted through an aluminum adapter which had a round tongue on its end. This tongue fits into a common size groove on top of the footing segment. The tongue and groove ran the length of the segment. This assembly allowed for rotation of the footing segments. Each loading adapter was connected to an aluminum cross-bar through the load cell or steel rods. A 3.2*cm* diameter, threaded, hardened steel rod was attached to the center of the loading cross-bar. This rod was threaded through a ring which was threaded to the bottom of a hollow hydraulic piston. The threaded rod could then extend upwards through the hollow cavity of the piston. The double acting hydraulic piston was used to support the weight of the footing assembly during the initial spin-up stage of the test and then used to apply loads to the footing. A control panel was designed to control the load system in the test and the four valves in the panel were used to apply the load on the footing or release the load.

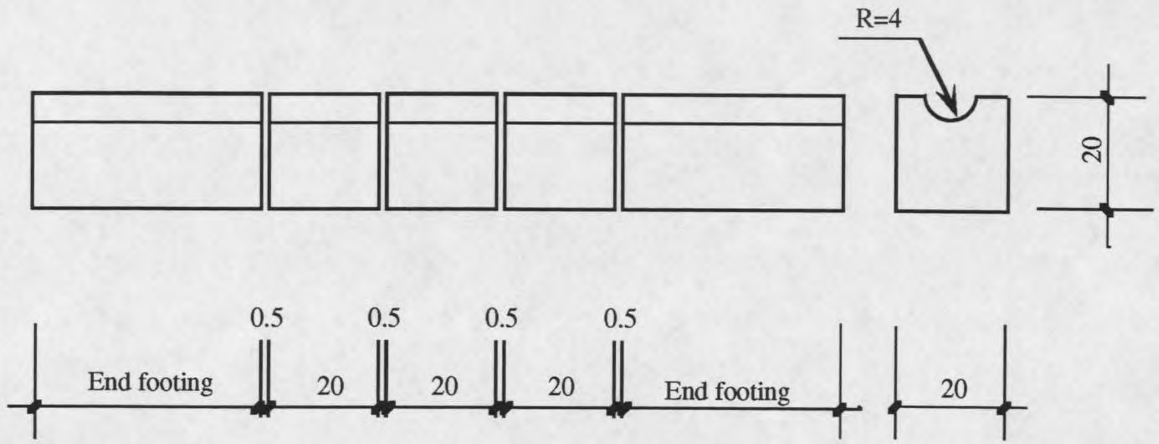

Figure 19 Configuration of footing segments (unit: *mm*)

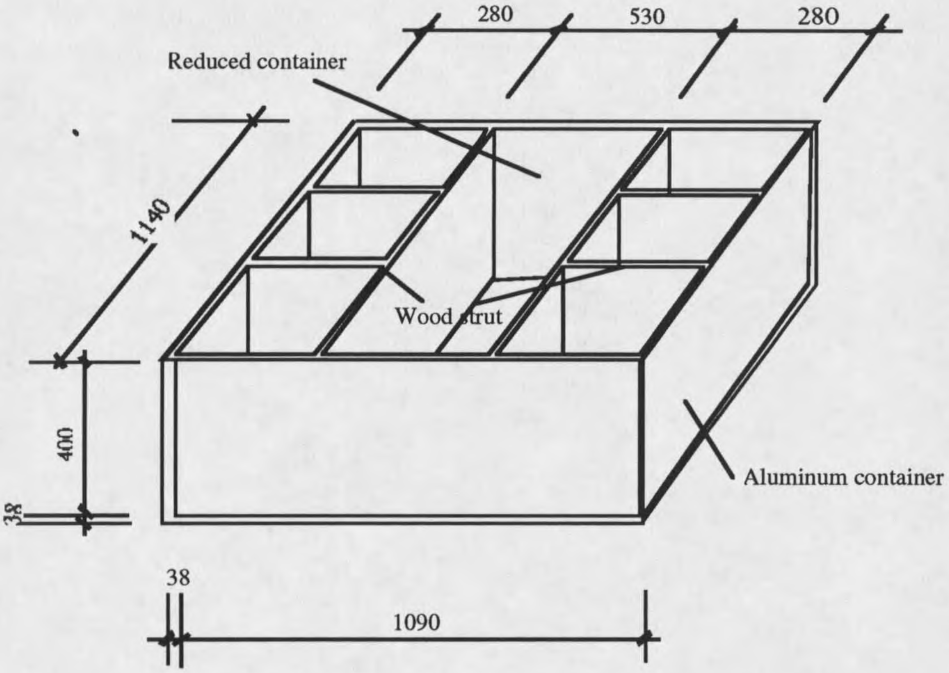

Figure 20 Configuration of the sample container (unit: *mm*)

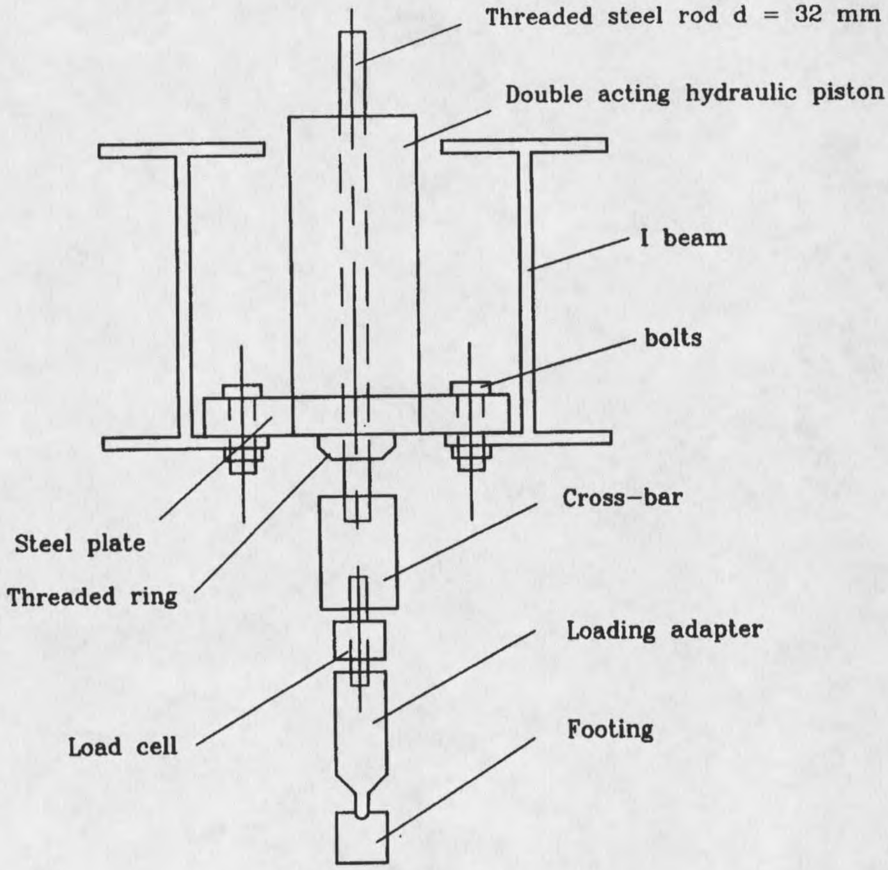

Figure 21 Configuration of the loading system

Sample Preparation

All test samples were prepared in equal lifts resulting in a final lift height of 4*cm*. To ensure that the soil was deposited uniformly, a wire screen was placed over the container and segmented into 105 equal areas approximately 7.5*cm* by 7.5*cm*. Atop each area, an equal mass of soil was gently deposited (Fig.22). After all areas had received the prescribed mass of soil, the screen was gently vibrated to allow the soil to fall uniformly. The screen was then removed and the lift received additional compaction. This compaction was provided by a pneumatic ball vibrator attached to a 23*cm* square steel plate. The plate was moved to different areas of the soil to compact the lift to a scribe lift height mark. The process was then repeated for the additional lifts. To model an embedded footing, several aluminum blocks were used to obtain the initial embedments of the footing. Each block was designed with the same width as the footing and yet was 1*cm* longer than the actual footing. The thickness of the blocks was designed to equal the required footing embedment in each test. When the last lift of soil had received initial compaction, two blocks were placed at the proper position where the soil was carefully excavated to the expected depths. Then the soil received additional compaction as shown in Fig.23. After the process of sample preparation was finished, the container was placed in the swinging platform of the centrifuge arm.

Testing Procedure

Generally, the following steps were performed in each test:

(1) set up the loading system and footing segments

(2) set up the data acquisition system and spin up the centrifuge

(3) loading and unloading process

(4) sample observation

In the first step, for the surface footing tests, the loading system was fixed on the container wall, which was already placed in the swinging platform, by eight bolts and the footing segments were attached to the corresponding loading adapters with rubber bonds as shown in the Fig.24. Rotating the threaded steel rod which was connected to the center of the cross-bar lowers the cross-bar along with the loading adapter and footing segments until the footing base was very close to the sample surface. When the position of the footing was carefully adjusted, the ring in the bottom of the hollow hydraulic piston was tightened to prevent rotations of the cross-bar and the footing. For the embedded tests, the footing segments no longer were attached to the loading adapters. They were placed in the

Figure 22 Sample preparation

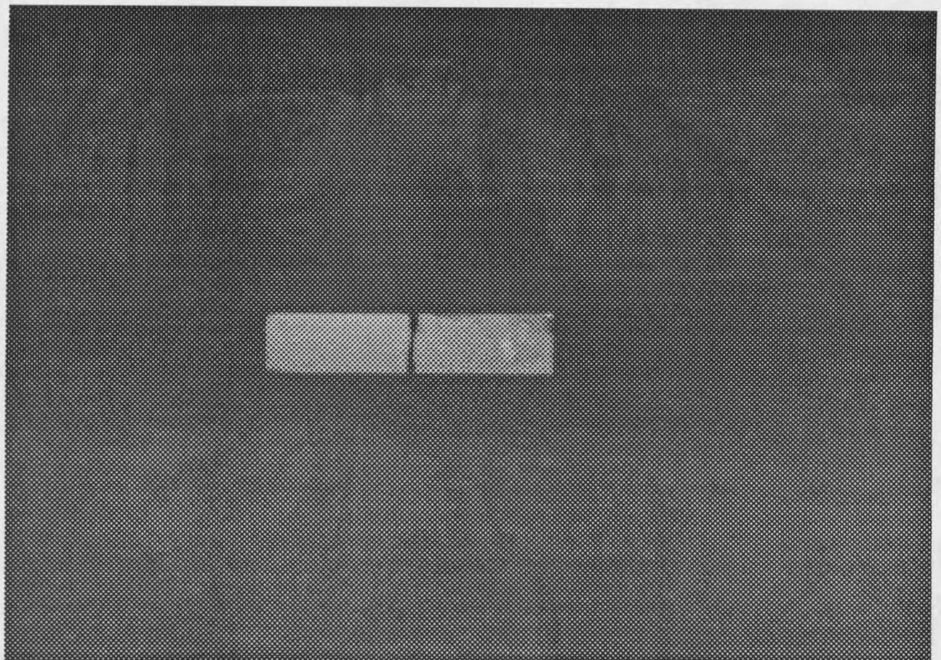

Figure 23 Photograph of the blocks

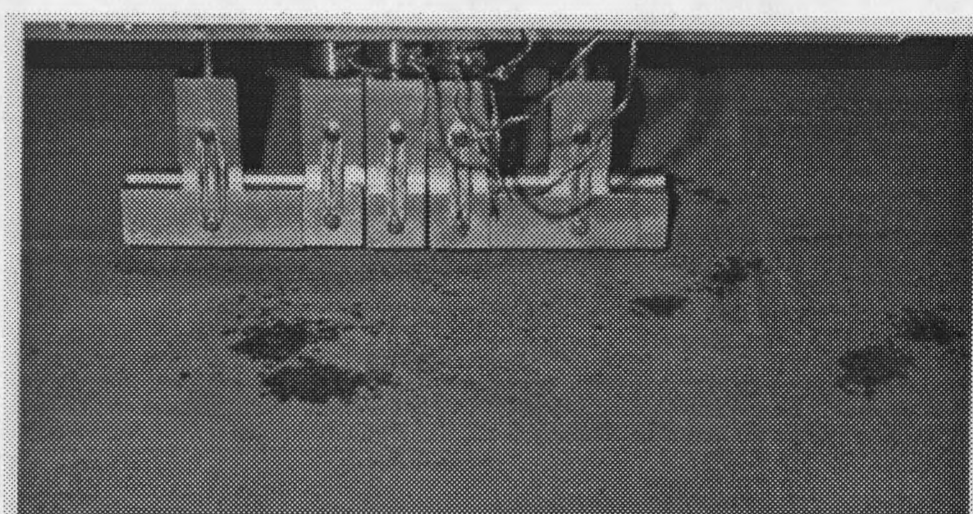

Figure 24 Photograph of the loading system

position to replace the blocks which were already embedded in the sample. The footing segments were then adjusted carefully to match the corresponding loading adapters. A small amount of the soil was used to fill the space in the two ends of the footing, and the soil was then compacted by a rigid steel block.

When the loading system and the footing were set up, a displacement transducer (LVDT) was mounted on the I beam, and all load cells as well as the LVDT were connected to the data acquisition system. The data acquisition system was set for all channels attached to the load cells and the LVDT. The value of the g-level for the test was also set in the centrifuge control computer. The data acquisition system was then started, and in the meantime the centrifuge spin up was started. The required g-level at the base of the footing was usually reached in 3 - 5 minutes.

When the required g-level was reached, a valve in the control panel was opened slightly to allow the hydraulic oil in the lower part of the cylinder to flow out and a valve was turned up continuously to apply the load on the footing through the cylinder. Meanwhile the readings of the load cells and LVDT were monitored on the screen. The load was continuously increased until the load readings of the three load cells dropped sharply accompanied by an increase in displacement. After about one minute of stable load shown on the screen, the valves were closed to prevent further deformation. Then, the centrifuge was gradually slowed down and finally stopped. The specimen was taken out of the centrifuge for observation.

Sample Observation

One of the objectives of this research is to study the failure mechanism of MLS-1 soil. A few ideas for trimming the sample were considered, but the experimental complicates prohibited these methods applying to the very big samples. Eventually, an acceptable method was applied in the sample observation. The basic principle is that, upon failure, the soil in the failure area is much looser than other regions. So it is possible to feel this difference by using a groove to cut the sample carefully. In addition, a vertical cut in MLS-1 soil is possible because of the slight cohesion of the soil. When the sample was trimmed, the one side wall of the container, normal to the footing length axis, was opened and the specimen is sliced into this sections by a groove. Slip lines were traced and maximum heights and widths of failure plane were measured for different sections. Plane strain conditions were also checked by comparing the failure planes at sections in the exterior footing sections and interior footing section. The plane strain condition is satisfied if these slip lines are basically identical.

Table 6 lists a comparison of maximum width and height between the observed failure surface in MLS-1 and theoretical failure mechanisms proposed by Prandtl (Fig.7), Terzaghi (Fig.8) and Hill (Fig.12). Theoretically, the maximum width X and height H of a failure surface in a soil can be calculated by the following equations, if the Prandtl failure mechanism is assumed to develop in the soil:

$$X = \frac{B}{2} + \frac{B\cos\left(45 - \frac{\phi}{2}\right)}{\cos\left(45 + \frac{\phi}{2}\right)} e^{\frac{\pi}{2}\tan\phi} + \frac{D_f}{\tan\left(45 - \frac{\phi}{2}\right)} \tag{38}$$

Table 6 Comparison of the experimental values of failure surface size in MLS -1 with theoretical values:

Test name	g-level g	Footing width cm	Observed failure surface		Prandtl failure mechanism		Terzaghi failure mechanism		Hill failure mechanism	
			Max. width cm	Max. height cm	Max. width cm	Max. height cm	Max. width cm	Max. height cm	Max. width cm	Max. height cm
BC3a01.O_1	25.69	51.4	326	98	863	194	695	156	444	97
BC3d01.O_2	25.1	50.2	311	80	843	190	679	153	434	95
BC3a01.O_4	24.68	49.4	439	94	829	187	667	150	427	93
BC3c01.O_5	24.64	49.3	407	94	828	186	666	150	426	93
BC1a01.O_6	25.8	51.6	360	115	867	195	697	157	446	97
BC1c01.O_7	24.69	49.4	376	75	830	187	667	150	427	93
BC3b01.O_8	24.88	49.8	664	63	836	188	673	152	430	94
BC3a01.O_9	25.5	51	453	130	857	193	689	155	445	96
BC2b01.O_{12}	24.79	49.6	315	76	833	187	670	151	429	93
BC1b01.O_{13}	24.86	49.7	303	76	835	188	672	151	430	94

$$H = \frac{B}{2\cos\left(45 + \frac{\phi}{2}\right)} e^{\omega \tan\phi} \sin\left(135 - \frac{\phi}{2} - \omega\right) + D_f \tag{39}$$

where B is the footing width, D_f is the footing embedment, ϕ is the friction angle in the soil, and ω is an angle corresponding to the deepest point of the failure surface (Fig.7). This value of ω can be obtained by setting $\partial H/\partial\omega = 0$.

From table 6 we can see that the experimental maximum width and height of the failure surface occurring in MLS-1 are much smaller than the values obtained from Prandtl's and Terzaghi's failure mechanisms. Comparing these experimental values with Hill's failure mechanism, however, close predictions for the size of the failure surface in MLS-1 are obtained as seen in table 6.

Results

Bearing capacity experiments were performed on samples subjected to three different acceleration levels and different footing embedments. An acceleration level of 25-g and footing resting on the sample surface were designed for the preliminary tests to evaluate the influence of container walls on the experimental results and to assess a plane strain condition. The experimental results will be presented in Appendix B.

Assessment of The Influence of The Container Walls

To prevent the influence of boundary effects from the bottom of the container on the experimental results, a single footing was designed to test in the container and repeated the testing with the soil depth of 10*B*, 8*B*, 6*B* and 4*B* (i.e. 20*cm*, 16*cm*, 12*cm*, 8*cm*). Therefore, a minimum depth of soil was found to sufficiently prevent the influence of the container bottom on the experimental results. Experiments performed for this purpose are listed in Table 7. The labeling of tests shown in Table 7 and in following tables conforms to the following guidelines. The first two letters of each name stand for "bearing capacity". The third slot, 0, 1, 2 or 3 stands for a total length of footing of 6*cm*, 10*cm*, 14*cm* or 18*cm*, respectively. The fourth slot for these tests stands for the depth of soil underneath the footing base, where *a* stands for 20*cm* depth of soil, and *b*, *c*, *d* represent the depth of soil 16*cm*, 12*cm*, 8*cm*, respectively. The fifth slot stands for the initial embedment of the footing which 0, 1, 2 represents the surface, 1 *cm* embedment and 2 *cm* embedment, respectively. The sixth slot 1, 2 or 3 stands for the g-level 25*g*, 16.7*g*, or 5*g* respectively.

In order to evaluate the influence stated above, the test results are expressed on a plot of initial stiffness *E* (i.e. the slope of initial portion of the load versus displacement curve) of the testing sample versus the relative depth of soil (*D/B*) in Fig.25. Theoretically, the sample should present the same value of stiffness under the same testing conditions, and it will cause a higher stiffness if there exists an influence from the container bottom. As we can see from Fig.25, the stiffness *E* presents a higher value as the depth of sample *D* is small, and it presents a lower value as *D* is high. A decreased value of the initial stiffness *E* can also be observed as the relative depth of sample increases, and it approaches a stable value of stiffness at $D/B = 7$. Therefore, relative depth of the sample $D/B = 7$, namely, the depth of soil $D = 16cm$, was used throughout the experiments to

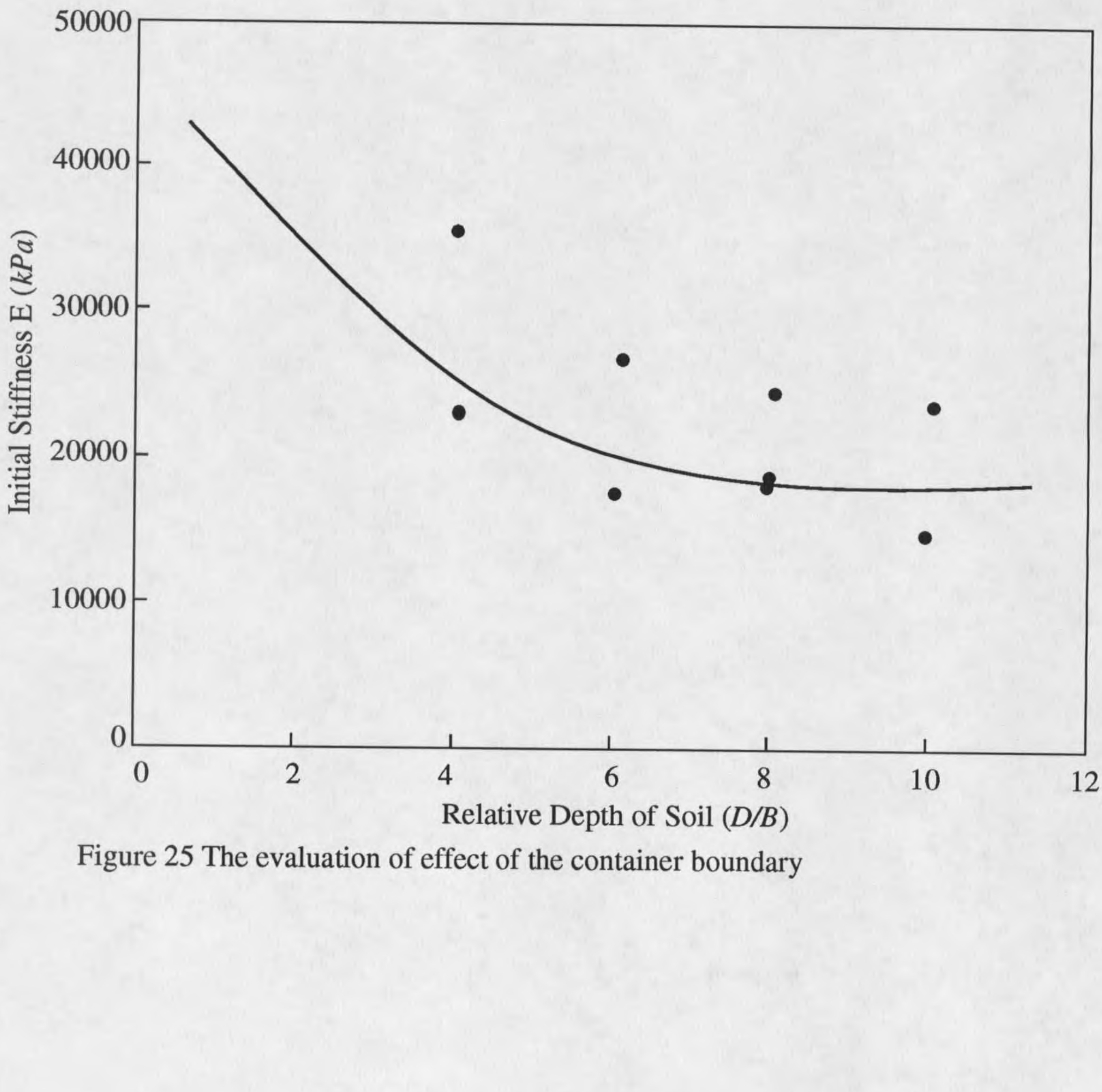

Figure 25 The evaluation of effect of the container boundary

sufficiently prevent the influence of the container bottom. To evaluate the influence of the container wall on the experimental results, two particular tests were conducted where the footings were placed on different positions, namely, the footing of BC3a01.O_1 test was placed at the center of the container where the container walls have no influence on the test results due to enough space between the footing and walls. The footing of BC3a01.O_4 test was placed in one side of the container which provided 18 *cm* of clearance between the edge of the end segments, as measured along the length of the footing, and 56 *cm* of clearance between the edges of the segments and the container wall, as measured along the width of the segments. These two tests showed very close experimental results so that it was calculated that two experiments could be conducted in a single container without the influence of the container walls.

The Assessment of Plane Strain Condition

In order to assess a plane strain condition, the experimental program was designed to allow the footing length to be varied from $3B$ to $9B$ ($6cm$ to $18cm$). Table 8 lists the experiments for the assessment of a plane strain condition, and Fig.26 shows a diagram of percentage difference of the initial stiffness versus m, where m is the ratio of footing length to width. The percentage difference of the initial stiffness describes the difference between the stiffness in the central segment of the footing and that in the two segments immediately adjacent to the central segment. Theoretically, a footing under a plane strain condition has the same vertical deformations under the footing at the central section and at the end section, which means the difference of the initial stiffness between the central

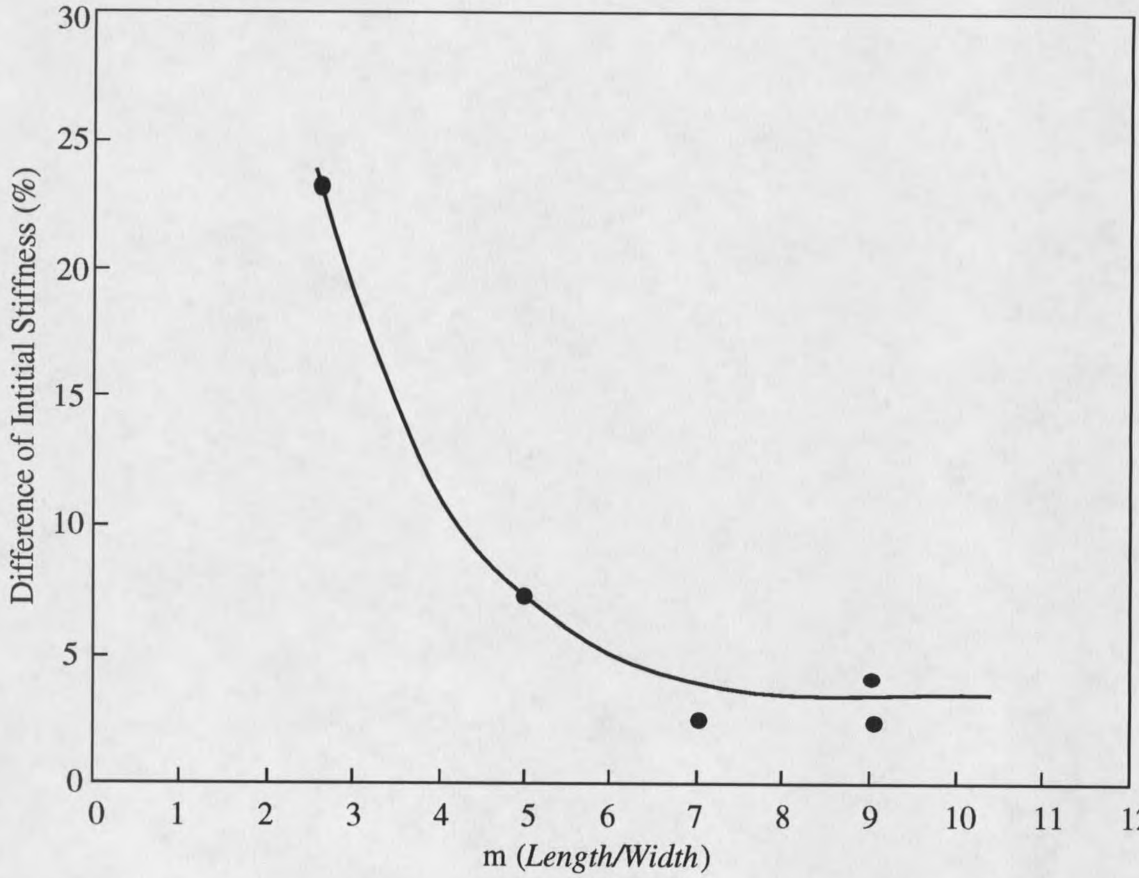

Figure 26 The evaluation of plane stain condition

segment and the adjacent segments should tend to a zero. Therefore, the values of this difference for a square footing should be a maximum. If we evaluate the difference of the initial stiffness with an increased footing length, the value of the difference should decrease and tends to zero. The footing length corresponding to this limiting value is the minimum footing length for which the plane strain condition can be simulated. It can be seen in Fig.26 that the percentage difference of stiffness decreases and then tends to a limiting value as m increases. Consequently, the footing length at $m = 7$ was determined to be used throughout the tests so that the plane condition can be simulated sufficiently.

Testing Program and Bearing Capacity Results

When all requirements were examined and validated as indicated above, an experimental program was designed to achieve the proposed goals. The main variables included in the testing program were the acceleration level and the depth of footing embedment. Three acceleration levels of approximately 25-g, 17-g, and 5-g were selected. A footing with a width B of 2cm was used for all experiments. Experiments were performed at the previously stated g-levels at initial footing embedments of 0B, 1B and 2B. Table 9 shows the testing program used to study the bearing capacity of the surface footings and the effect of the embedment on the bearing capacity. Results from three centrifuge experiments are shown in Fig.27. All three experiments were performed with the footings initially resting on the surface. The footing widths given for the experimental curves have been scaled to the prototype dimension in 1-g. The curve corresponding to "B =51cm" represents the test performed at approximately 25-g, while the experimental curves for "B = 35 *cm* "and "B = 11*cm* "correspond to acceleration levels of approximately 17-*g* and 5-*g*, respectively. The footing pressure is the actual pressure observed in the experiments and scales one to one. The relative displacement, given as the ratio of the footing displacement to the footing width, also scales one to one. Correction of the initial loading portion of the experimental curves has been achieved by extending the initial slope of the curves backwards to the zero load line. This necessitated shifting the displacements slightly to account for seating of the footing as load was applied. All the results of the centrifuge experiments will be given in Appendix B.

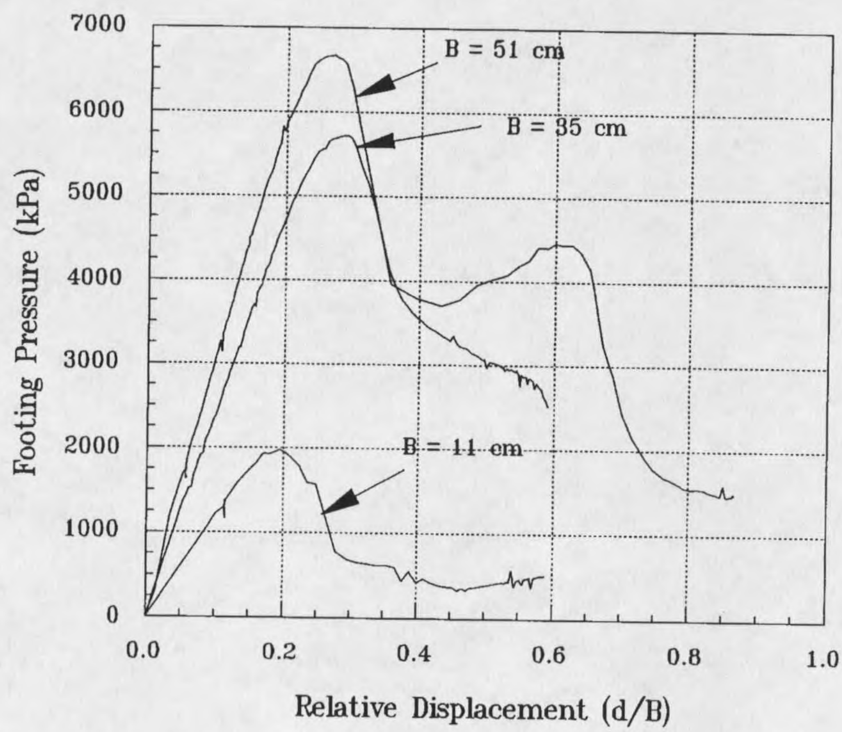

Figure 27 Centrifuge bearing capacity results

Table 7 Experiments performed for the evaluation of influence of container bottom

Test No.	Test Name	Model Footing Size			Depth of Soil	g-level
		Width	Length	Burial		
		cm	*cm*	*cm*	*cm*	*g*
1	BC3d01.O_2	2	18	0	8	25.10
2	BC3d01.O_3	2	18	0	8	24.96
3	BC3a01.O_4	2	18	0	20	24.68
4	BC3c01.O_5	2	18	0	12	24.64
5	BC3b01.O_8	2	18	0	16	24.88
6	BC3a01.O_{10}	2	18	0	20	25.14
7	BC3c01.O_{11}	2	18	0	8	24.77
8	BC2b01.O_{12}	1	14	0	16	24.79

Table 8 Experiments performed for the assessment of plane strain condition

Test No.	Test Name	Model Footing Size			Depth of Soil	g-level
		Width	Length	Burial		
		cm	*cm*	*cm*	*cm*	*g*
1	BC3a01.O_4	2	18	0	20	24.68
2	BC1a01.O_6	2	10	0	20	25.8
3	BC3b01.O_8	2	18	0	16	24.88
4	BC2b03.O_{18}	2	14	0	16	5.0
5	BC0c01.O_{24}	2	6	0	12	24.5

Table 9 Experiments performed for the study of bearing capacity on surface and embedded footings

Test No.	Test Name	Model Footing Size			Depth of Soil	g-level
		Width	Length	Burial		
		cm	*cm*	*cm*	*cm*	*g*
1	BC3a01.O_4	2	18	0	20	25.10
2	BC3b01.O_8	2	18	0	16	24.88
3	BC3a01.O_{10}	2	18	0	20	25.14
4	BC2b01.O_{12}	2	14	0	16	24.79
5	BC2b02.O_{14}	2	14	0	16	17.40
6	BC2b12.O_{15}	2	14	1	16	17.43
7	BC2b11.O_{16}	2	14	1	16	24.62
8	BC2b22.O_{17}	2	14	2	16	17.58
9	BC2b03.O_{18}	2	14	0	16	5.44
10	BC2b13.O_{20}	2	14	1	16	5.39
11	BC2b23.O_{21}	2	14	2	16	5.34

CHAPTER FOUR

BEARING CAPACITY OF MLS - 1

Introduction

This chapter discusses the comparison of the theoretical and experimental bearing capacity of shallow foundations on MLS-1. The chapter is composed of three sections. The first section is a presentation of analysis methods to obtain shear strength parameters for MLS-1. The shear strength of MLS-1 is computed by using both nonlinear tangent and secant analyses. In the second section a general expression is presented to describe the relationship of normal stress and bearing capacity in a soil, where the ratio of normal stress to bearing capacity is a function only of the internal friction angle of the soil by an approximation. The bearing capacity analysis of MLS-1 is presented in the third section. The bearing capacity values of MLS-1 predicted by Meyerhof's, Vesic's, and Chen's theories are compared with the experimental results using the two different shear strength analyses. The remaining section describes the procedure and results of the slip-line method. Three different boundary conditions of shear resistances at the interface of a foundation and soil are taken into account in the numerical solution. A computer program

(Perkins, 1994) of the slip-line method is used to predict ultimate bearing capacity values of shallow foundations on MLS-1 soil, and the predicted values are compared with the experimental results and with the aforementioned theories.

The Determination of Shear Strength Parameters for MLS-1

The Influence of Stress Level on Shearing Strength Parameters (c, ϕ)

Shear strength parameters of a soil, internal friction angle, ϕ, and the cohesion c, are two significant factors in the evaluation of stability problems such as bearing capacity. In most cases, the linear Mohr-Coulomb strength criterion is employed as the material law in most conventional bearing capacity theories. Using this strength criterion, the constant friction angle, ϕ_s' in Figure 28, can be obtained from conventional triaxial tests for a very low or a very high confining pressure by assuming a straight line between the low and the high stresses. However, many investigations have verified that realistic shear strength characteristics of soils cannot simply be defined by the linear criterion, and they vary with mean normal stress. Lee and Seed (1967) presented triaxial experimental results of drained shearing resistance of sand. They showed a significant difference of friction angles obtained at a very low confining pressure and at a very high confining pressure. For a dense sand tested by Lee and Seed, this difference was as high as 15°. Ponce and Bell (1971) performed triaxial experiments at extremely low confining pressures, and the shear strength behavior at the extremely low pressures is shown by the relationship between the effective principle stress ratio and the effective confining stress at failure.

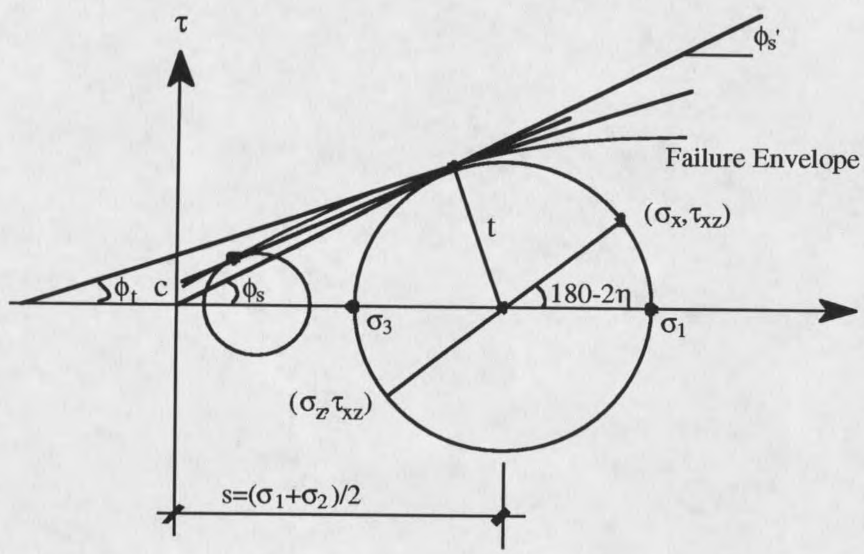

Figure 28 Mohr's circle and the failure envelope

However, the angle of shearing resistance as expressed by the slope of the Mohr envelope showed only a small change as the confining pressure changed from 0.2 *psi* to 5 *psi*. De Beer (1965) indicated that, for a given density, the shear strength parameters (ϕ, c) depend upon the value of the mean normal stress. The intrinsic law is not a straight line but a curve turning its concavity towards the normal stress axis in the $\tau\text{--}\sigma$ plane (Fig.28), or towards mean normal stress axis in the p -q plane (Fig.29). This curvature should be taken into account when studying bearing capacity problems if realistic shear strength parameters are expected to be used. De Beer (1965) also showed that the difference in the friction angle ϕ for different values of mean normal stresses is far from negligible if an ultimate bearing capacity has to be estimated accurately. He showed that a 5.5° variation

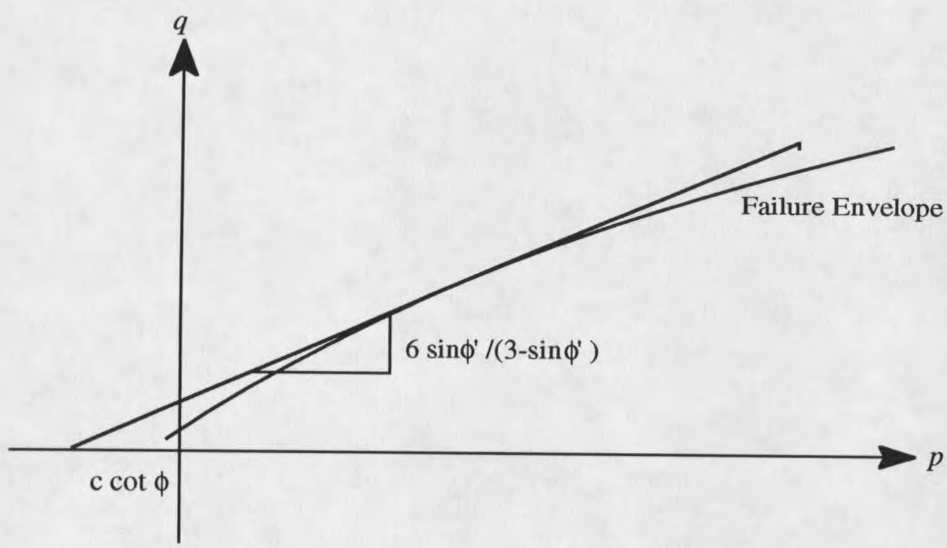

Figure 29 Shear strength in a p - q plane

in the friction angle was obtained, in a particular sand being tested, for a mean normal stress p which was varied from 0.2 kPa to 6 kPa.

As we know, using a bearing capacity solution to predict ultimate bearing capacity of a soil requires linear friction angle and cohesion. This linear friction angle and cohesion must be approximated from the non - linear failure envelope if a realistic failure is taken into account. There are two methods to obtain linear fiction angle and cohesion from a non-linear failure envelope. One method is the tangent method, where the friction angle can be obtained from the slope of a tangent line of the failure curve, and cohesion can be calculated from the intersection of the tangent line with the shear stress difference q axis as shown in Fig.29. For a p -q failure envelope, the yield function of the failure envelope is normally expressed as:

$$f(p, q) = 0 \tag{40}$$

The tangent friction angle ϕ, and cohesion c, at the point corresponding to normal stress p, are obtained from the following equations:

$$\frac{dq}{dp} = \frac{6\sin\phi}{3 - \sin\phi} \tag{41}$$

$$\frac{dq}{dp} = \frac{q}{p + c\cot\phi} \tag{42}$$

The second method is the secant method where the cohesion is assumed to be zero and the secant friction angle can be calculated from the following equation:

$$\frac{q}{p} = \frac{6\sin\phi}{3 - \sin\phi} \tag{43}$$

In order to use the nonlinear approach to obtain shear strength parameters using the above equations, the stress level, namely mean normal stress p, has to be determined first. This mean normal stress state is influenced by many parameters such as soil properties and footing physical characteristics. Therefore, if we can develop a function describing the relationship between ratio of mean normal stress to ultimate bearing capacity and the influenced parameters, the mean normal stress state can be determined for a given soil and given footing physical condition. In the next section, a new approach will be introduced to determine mean normal stress which considers the parameters of soil properties and footing conditions.

The Procedure to Obtain Linear Shear Strength Parameters

The procedure for computing linear friction angle and cohesion used in the bearing capacity equations for a given material and a given footing's physical characteristics is considered to consist of five steps:

Step 1: Assume a value of mean normal stress p. From this value of p, the corresponding value of principle stress difference can then be found from equation (41), where the point (p, q) lies on the failure envelop of the analyzed material.

Step 2: Calculate the tangent friction angle ϕ_t and cohesion c at the point corresponding to p, from equations (42) and (43) respectively. For the secant method, the secant friction angle ϕ_s can be obtained from equation (44). In this case, cohesion is always zero.

Step 3: Compute the ultimate bearing capacity, q_{ult}, from the predictions by using the shear strength parameters from step 2.

Step 4: Calculate the ratio m of the mean normal stress p assumed in step 1 to the ultimate bearing capacity obtained in step 3, compare it with the value of p/q_{ult} in Fig.33 or equation (48) using the same friction angle. Equation (48) will be presented in the next section.

Step 5: Redo steps 1 through step 4 if the ratio m is not close to the value obtained from equation (48).

Shear strength parameters (c, ϕ) of MLS-1

The main objective of this thesis is to compare the experimental results for bearing capacity of MLS-1 with three analytical approaches, limit equilibrium (e.g. the predictions of Meyerhof and Vesic), slip-line solutions, and the method of limit plasticity (e.g. the formulas of Chen). To calculate the bearing capacity by these approaches, the shear strength of MLS-1 has to be determined first. For analysis purposes, the "tangent" and "secant" shear strength parameters are computed by using the failure function corresponding to the peak strength of the CTC tests, and by using the failure function corresponding to the residual strength of the CTC tests. The peak strength is obtained by choosing values of maximum major principle stresses in CTC tests, and the residual strength is obtained by choosing values of residual stresses in the CTC tests. Using these peak and residual shear strength parameters, peak and low bearing capacity respectively will be obtained from the bearing capacity solutions, and the experimental bearing capacity results will be compared with the two extreme values of theoretical bearing capacity. Equations (36) and (37) describe the yield functions for the peak and residual strength, respectively. Table 10 lists the peak shear strength parameters corresponding to Meyerhof's, Vesic's and Chen's predictions and the slip-line method. In order to calculate the shear strength parameters in table 10, a Maple program was produced to perform the procedure for steps 1 to 5 for each of the bearing capacity solutions and the given experimental footing physical conditions.

It is noteworthy in table 10 that, for Meyerhof's, Vesic's, and Chen's approaches, most tangent friction angles fall in a range of 48° to 50°, and the secant friction angles are in range of 50° to 53°. The "tangent" analysis shows that the cohesion values are higher than $15kPa$, and some higher than $30kPa$ which are far from negligible. For the slip-line

Table 10 Shear strength parameters of MLS-1 from CTC peak strength results

Test Name	Meyerhof method			Vesić method			Chen method		
	Cohesion	Friction angle		Cohesion	Friction angle		Cohesion	Friction angle	
		Tangent	Secant		Tangent	Secant		Tangent	Secant
BC3a01.O4	17.6	48.9	51.2	16.7	49.0	51.4	25.2	48.3	50.5
BC2b11.O16	22.1	48.5	50.8	21.3	48.5	51.0	29.2	48.0	50.3
BC2b21.O23	27.3	48.1	50.4	27.0	48.2	50.5	34.3	47.8	50.0
BC2b02.O14	13.9	49.3	51.6	13.2	49.4	51.9	19.6	48.7	51.0
BC2b12.O15	17.3	48.9	51.2	16.9	48.9	51.5	22.9	48.5	50.7
BC2b22.O17	20.8	48.6	50.9	20.5	48.6	50.1	26.2	48.2	50.5
BC2b03.O18	6.7	50.6	53.2	6.2	50.7	53.7	9.2	50.0	52.6
BC2b13.O20	8.0	50.2	52.9	7.6	50.3	53.2	10.3	49.8	52.4
BC2b23.O21	9.3	50.0	52.6	9.0	50.0	52.8	11.5	49.6	52.2

Test Name	Slip-line method (smooth footing base)			Slip-line method (partially rough footing base)		
	Cohesion	Friction angle		Cohesion	Friction angle	
		Tangent	Secant		Tangent	Secant
BC3a01.O4	12.8	49.4	52.2	225.5	45.0	50.6
BC2b11.O16	18.5	48.8	51.5	293.5	44.5	49.9
BC2b21.O23	24.2	48.3	50.9	327.4	44.3	49.4
BC2b01.O14	10.2	49.8	52.6	174.3	24.2	48.3
BC2b12.O15	14.5	49.2	51.8	225.5	44.9	50.3
BC2b22.O17	18.3	48.8	51.5	259.5	44.7	49.8
BC2b03.O18	4.8	51.1	53.9	157.0	45.4	51.5
BC2b13.O20	6.4	50.6	53.5	208.4	45	51.5
BC2b23.O21	8.0	50.2	53.1	242.5	44.8	51.1

method, slightly lower cohesion and relatively higher tangent and secant friction angles were obtained for the smooth footing base boundary condition, but much higher cohesion and relatively lower friction angles can be obtained if a partially rough footing base is used in the computation.

Corresponding to the yield function of the residual strength, the shear strength parameters of MLS-1 are shown to have a constant friction angle and almost zero cohesion. All tangent and secant friction angles are calculated to be about 44^{o}.

Investigation of the Mean Normal Stress *p*

Introduction

It is somewhat complicated to evaluate mean normal stress in a soil because it changes with material properties, the physical characteristics of foundations, as well as the bearing capacity methods used. To the author's knowledge, no research work published has given a general expression to determine the mean normal stress in terms of the parameters stated above. Meyerhof (1948) suggested that values of one tenth the ultimate bearing capacity can be utilized as the mean normal stress along the failure surface for a friction angle in the range of 45^{o} to 46^{o}. He didn't present any theoretical or experimental proof for the assumption. Hansen (1975) suggested two ways to obtain a solution of shearing strength for practical purposes. One suggested method is that of defining a mean stress level which is somewhat higher than Meyerhof's assumption in the above range of friction angle, then the corresponding tangent in Mohr's envelop is used to find a value of ϕ_t and, by its intercept with the shear stress τ axis in the diagram, the apparent cohesion c_t. For the second method, he suggested that by using the method of characteristics, friction angle ϕ can be calculated by assuming the angle between the a and β lines to be $\pi/2 \pm \phi$.

As the ultimate bearing capacity and mean normal stress in a soil not only depend on the mechanical properties (cohesion c, friction angle ϕ and densityγ), but also on the physical characteristics of the footing (width B, depth D and roughness d) on the soil, we can express the ratio of the mean normal stress to the ultimate bearing capacity as the following function:

$$\frac{p}{q_{ult}} = f\,(\phi, B, \gamma, q_o, c) \tag{44}$$

where B represents the width of the footing, γ is the unit weight of the soil, q_o is the surcharge, and where c and ϕ represent the cohesion and friction angle of the soil respectively.

It is necessary to mention here that the mean normal stress p used in equation (44) is the average value of mean normal stresses in the entire failure area of the soil, and p is defined as:

$$p = \frac{\sum s_i A_i}{A} \tag{45}$$

where s_i represents a mean normal stress at ith point of intersection of the α and β characteristics, and $s_i = (s_{1i} + s_{3i})/2$ as shown in Fig.28. A_i is the area in influence of the pressure s_i at the ith point as shown in Fig.30, and A represents the total area of failure in the soil which is the sum of the areas in Zone I, Zone II and Zone III in Fig.30.

From equation (45) we can see that using Meyerhof's assumption of the constant

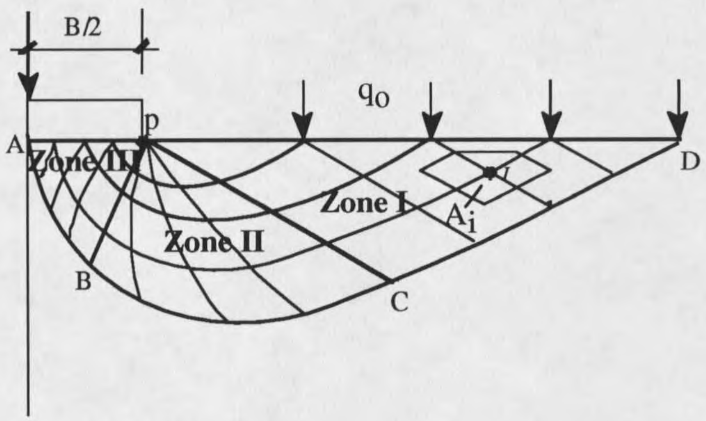

Figure 30 Net of Characteristics.

ratio, p/q_{ult}, to describe a normal stress state might be limited and arbitrary. To obtain a more universal expression to describe the variation of mean normal stress state with these parameters, a new approach is presented in this thesis where the numerical solution of the slip-line method is employed to analyze the changes of mean normal stress and ultimate bearing capacity with the above parameters. The basic principle of the slip-line method has been discussed in chapter two. This method is based on the theory of plastic equilibrium and obeys the associated flow rule. A detailed procedure of this method (Atkinson, 1981, Nordal, 1992) is presented in Appendix C.

Definition of A Dimensionless Factor B_o

In order to simplify the analysis, a dimensionless factor B_o is employed to reduce the number of variables in the approach, so that the fundamental dimensionless parameters associated with the stress characteristic equations are ϕ and B_o. The factor B_o is a function of B, γ, q_o, c as well as ϕ, and is defined as:

$$B_o = \frac{B\gamma\cot\phi}{q_o - c\cot\phi} \tag{46}$$

where the quantities here have the same meaning as in equation (45). For most practical materials we can expect that ϕ lies in the range 20^o to 60^o and B_o ranges from 0 to 60. Therefore, ranges of the parameters in equation (47) can be shown if it is rewritten as:

$$\frac{c}{B\gamma} = \frac{1}{B} - n\tan\phi \tag{47}$$

where n is introduced to represent a ratio of footing initial embedment D to the footing width B, namely $n = D/B = q_o/(\gamma B)$. For a shallow foundation, n can only be in the range of 0 to1, e.g. $0 \leq n \leq 1$, and the two limited values of the ratio n represent a surface footing condition or a buried footing with $1B$ embedment respectively. Fig.31 shows the range of $c/(\gamma B)$ corresponding to the non-dimensional factor B_o, friction angle ϕ, and the ratio n. From Fig.31, we can see that the value of $c/(\gamma B)$ should fall into the range between the line of $n = 0$ and the curve of $n = 1$, $\phi = 60^{o}$ by the limitation of equation (47). Several particular cases need to be discussed for using Fig.31:

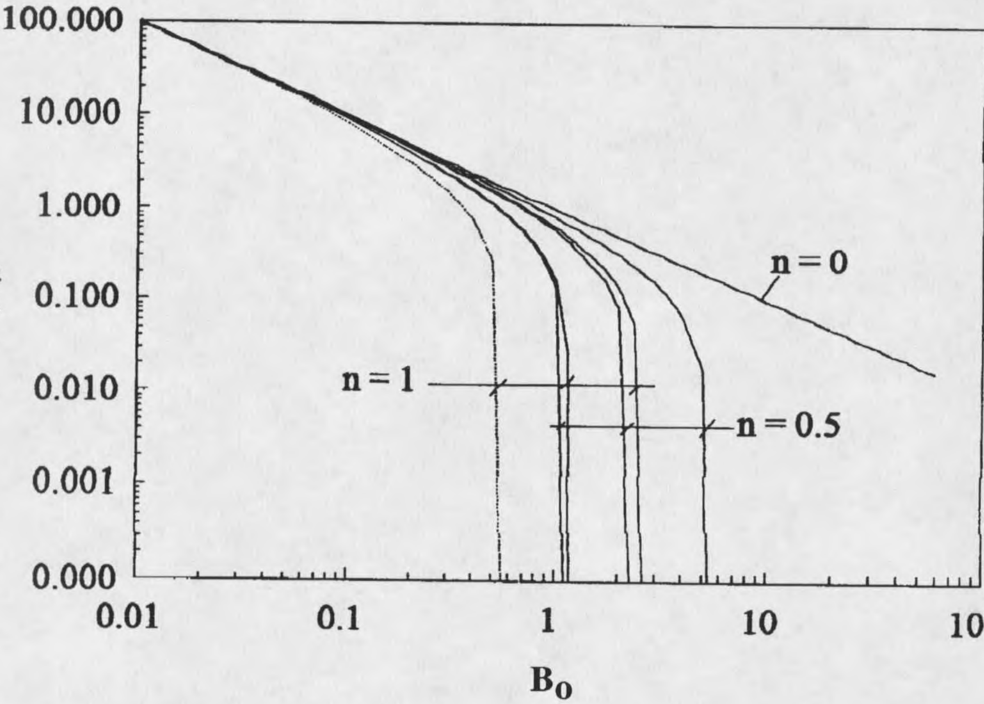

Figure 31 The ranges of the parameters $c/(\gamma B)$

(1) When $n = 0$, the line in the figure represents a surface footing and it establishes the maximum value of B_o. For $B_o = 60$, the ratio of $c/(\gamma B) = 0.02$, $c=0.02\ (\gamma B)$. Practically, the unit weight γ is usually about 20 kN/m^3, so the cohesion $c = 0.4B$. For $B_o = 0$, the point on the line represents a weightless soil ($\gamma = 0$), the cohesion can be any value from zero to infinite.

(2) When $0 < n \leq 1$, the value of $c/(\gamma B)$ changes with B_o and friction angle ϕ as

shown in Fig.31. Because the value of cohesion cannot be negative, the maximum value of B_o, for this case, depends upon the friction angle ϕ, and footing embedment, namely, $B_o = n \tan\phi$. For example, if $n = 1$ and $\phi = 60^{\circ}$, we can obtain the maximum $B_o = 1.73$, and it represents a cohesionless soil ($c = 0$).

Function of Determining the Mean Normal Stress p

Using the dimensional factor B_o, the ratio of the mean normal stress to ultimate bearing capacity can be simply expressed as a function of B_o and friction angle ϕ. Fig.32 shows the relationship between the ratio p/q_{ult} with B_o and ϕ. For each particular friction angle, the ratio of p/q_{ult} was obtained by increasing the different combinations of B, c, q_o which give the same values of B_o. From these curves it is seen that variations p/qult for different combinations of B, c, q_o and γ, leading to the same value of B_o, are significant only for low levels of friction angle. The impact of this variation will be explained later. From Fig.32 we can also see that for a relatively small friction angle, the ratio of p/q_{ult} has a slight increase with increasing B_o. For a higher friction angle, the ratio can be assumed to be approximately constant in the whole range of B_o. Therefore, the ratio of mean normal stress p to ultimate bearing capacity q_{ult} in a soil can be approximated as being independent of the dimensionless factor B_o, and dependent only on the internal friction angle ϕ, where Fig.33 describes the variation of the ratio p/q_{ult} only with the friction

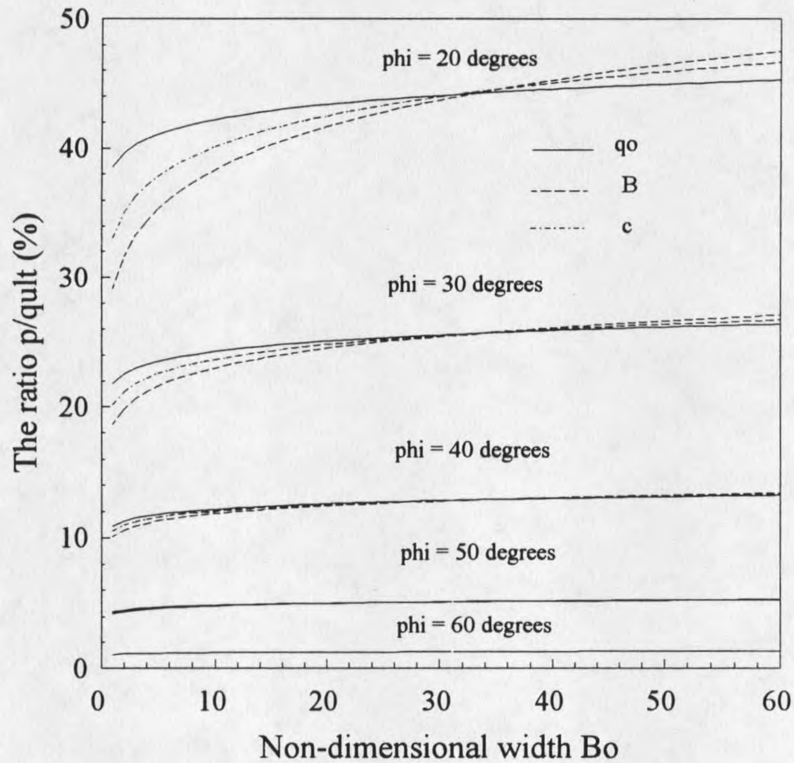

Figure 32 The relationship between the ratio (p/q_{ult}) and the friction angle and non-dimensional factor B_o

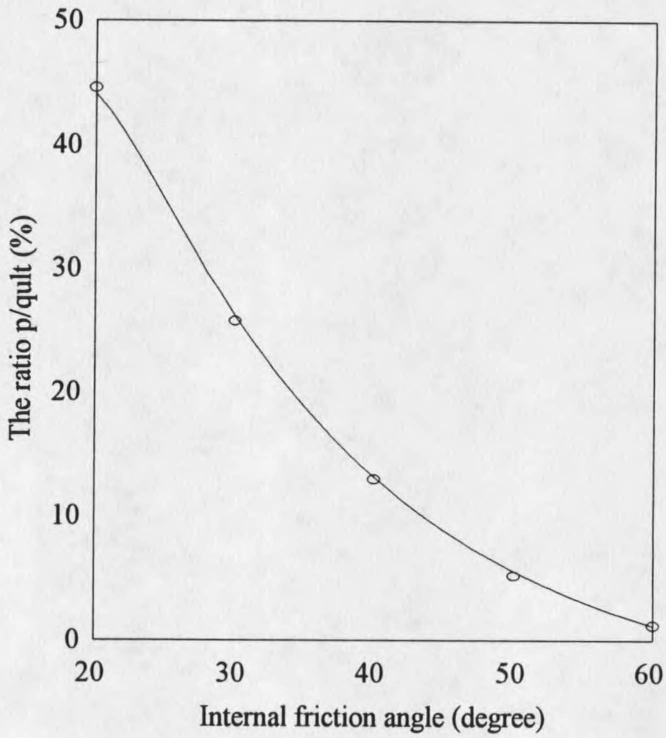

Figure 33 The relationship between the ratio (p/q_{ult}) and friction angleϕ

angle ϕ. It shows an inverse relationship between the ratio (p/q_{ult}) and the value ϕ. The ratio of the mean normal stress to the ultimate bearing capacity can be seen from Fig.32 to be about 7.5% in the friction angle range of 45^o-46^o, which is lower than Meyerhof's assumption of 10%. By regression, the curve in Fig.32 can be expressed by the following equation:

$$\frac{p}{q_{ult}} = -\frac{4.09}{\sin\phi^3} + \frac{19.06}{\sin\phi^2} + \frac{0.71}{\sin\phi} - 19.73 \tag{48}$$

Equation (48) is the proposed relationship between mean normal stress and ultimate bearing capacity in a soil. It can be used to obtain shearing strengths (c,ϕ) from related triaxial experimental results for plastic materials whose internal friction angles fall in the range of 20^o to 60^o.

Due to the slight change in curvature of the p/q_{ult} curve, for a given friction angle, approximating the curve by a constant induces error into the results of bearing capacity by using the shear strength obtained from equation (48). Because the approximation constant is chosen to be p/q_{ult} at B_o equal about 35, then for low friction angles and small value of B_o, the resulting error will be largest. The magnitude of the resulting error in the bearing capacity will depend upon soil properties, foundation physical characteristics, and predictions used. Calculations show that, for MLS-1 and the footings used in the centrifuge experiments, the error in the bearing capacity values is only about 5% using

Meyerhof's method, about 7% using Chen's and the slip-line methods, and for Vesic's method, the error is greater than 10%.

Bearing Capacity Analysis of MLS-1

Bearing Capacity for Surface Footings

Conventional bearing capacity solutions for a long footing resting on the surface of a horizontal soil are typically expressed as the sum of two components, namely a component reflecting the cohesive strength of the material and a component reflecting the frictional resistance due to self-weight normal stresses within the region experiencing shear. For this case, the bearing capacity equation is commonly written as:

$$q_{ult} = cN_c + \frac{1}{2}\rho g B N_\gamma \tag{49}$$

the expressions for the bearing capacity factors N_c and N_γ have been given in chapter 2 for different solutions. Here p is mass density of a soil, and g is the acceleration of gravity.

Centrifugal tests of surface footings with three different g-levels, approximately 5-g, 17-g and 25-g, were performed. In each test, the acceleration of gravity changed slightly from the designed value, and it has been accounted for in the analyses of the experimental results. The predicted values of ultimate bearing capacity of the footings obtained by the theoretical approaches, corresponding to the "tangent" shear strength and "secant" shear strength, are tabulated in table 11 along with the experimental results. The results of the three different g-level bearing capacity tests are compared with the conventional predictions given by Meyerhof (1963) and Vesic (1975), along with the solutions of limit plasticity theory derived by Chen (1975). The principles of the two different methods proposed by Chen (1975) have been described in chapter two, where one method is used in the analysis by assuming Prandtl failure mechanism, and the corresponding bearing capacity factor N_γ is given by equation (33). The results of the centrifuge tests are also compared for the slip-line solutions for both smooth footing bases and partially rough footing bases. In order to compare the predicted bearing capacity with the experimental values more adequately and to illustrate the effects of different shear strength analyses from CTC tests in the predictions, the "tangent" and "secant" shear strength parameters are used in aforementioned methods to predict the bearing capacities. The results are listed in the table 11. Fig.34 and Fig.35 show the predicted bearing capacity values and experimental results corresponding to the footing width, Fig.34 shows the predicted bearing capacity obtained by using the "tangent" shear strength parameters, and Fig.35 shows that obtained by using the "secant" shear strength parameters.

As we can see, by using the tangent shear strength parameters, almost all theories give higher values of ultimate bearing capacity compared to the experimental results except the slip-line method with a smooth footing base condition. Meyerhof's method overestimates the experimental values by about 75% for an 11*cm* footing, about 25% for $B = 35cm$, and 15% for $B = 50cm$. The bearing capacity values predicted by Vesic are about 60% higher than the test value for the 11*cm* footing width, approximately 20% higher at the 35*cm* footing width, and 10% higher at the 50 *cm* footing width. The bearing capacity values predicted by Chen's method are considerably higher than the experimental results, and about 60% to 130% higher values are given by this method. The slip-line method with the smooth footing base boundary condition provides the best prediction of the bearing capacity for all footing widths. However, rough footing bases were modeled in the centrifuge experiments, so the bearing capacity values obtained by the slip-line method with smooth footing base is not a realistic prediction. Note that in table 11, the bearing capacity values calculated by the slip-line method with the partially rough footing base boundary condition are above reasonable values.

The calculated values overestimate the experimental results by about ten times. A possible reason causing this bizarre result can be the boundary condition of partially rough footing base assumed in the slip-line method. This assumption of the boundary condition can lead to very high mean normal stresses obtained along the footing base. On the other hand, we can observe, from table 11 and Fig.34, that by using the "secant" shear strength ($c = 0$), Vesic's and Meyerhof's predictions give bearing capacity values close to the experimental results. Chen's prediction gives much higher values of bearing capacity, while the slip-line method with a smooth footing base provides a relatively lower bearing capacity.

From table 4.2 we can also see, all predicted values corresponding to the "tangent" shear strengths are higher than those corresponding to the "secant" shear strengths. For example, Meyerhof's method predicts about 15% -20% higher bearing capacity for the "tangent" analysis than for the "secant" analysis. Bearing capacities up to 45% higher are obtained from the slip-line method with smooth footing bases using the "tangent" shear strength parameters relative to the values obtained by using "tangent" shear strength parameters. In addition, for the theories of Meyerhof, Vesic and Chen, the rates of increased ultimate bearing capacity obtained by using "tangent" shear strengths increase as the footing width increases. The smaller the footing width, the higher the rate of increase for the predicted values.

A comparison was also conducted by using the shear strength obtained from the residual strength of the CTC tests. Table 12 lists the bearing capacity values obtained from the same methods as above when using the shear strengths corresponding to the residual strength. In table 11, the experimental results are lower than the predicted bearing capacity values obtained by using the peak shear strength of the CTC tests. This phenomenon can be explained by progressive failure in a soil during testing. During the gradual increase of the load on a footing, the shear strength is not immediately mobilized at all points of the potential slip surface, but only at the points where the shearing stresses are greatest, from there it extends to other places. This phenomenon of progressive failure has been clearly demonstrated and described by some researchers such as Muhs (1965a) and De Beer (1970). The large movements in the neighborhood of the footing, in the case of very dense soils, can produce distortions larger than the critical value which causes a drop of the shear strength, even though the limit equilibrium along the whole slip surface has not yet been reached. In other words, the shear strength can be less than the peak value of a soil due to the influence of progressive failure. However, it is believed that it is nearly impossible to take this influence into account in the equations for bearing capacity on a purely theoretical basis. The aim of the analysis is to compute the two extreme values

Table 11 Comparison of theoretical and experimental bearing capacity of surface strip footings from peak strength of CTC tests:

Test name	Footing Width B (cm)	Predicted q_{ult} for tangent shear strength (kPa)					Measured q_{ult} (Kpa)*	Predicted q_{ult} for secant shear strength (kPa)				
		M.hof	Vesić	Chen	Slip-line (s.f.)	Slip-line (p.r.f.)		M.hof	Vesić	Chen	Slip-line (s.f.)	Slip-line (p.r.f.)
BC3a01.O4	49.4	7360	7054	10228	5625	82330	6401	6369	5682	8729	3780	9469
BC2b02.O14	34.8	5970	5683	8142	4600	65418	4721	5113	4452	6868	3159	8199
BC2b03.O18	10.9	3167	2878	4092	2391	59329	1770	2546	2117	3307	2058	6190

Table 12 Comparison of theoretical and experimental bearing capacity of surface strip footings from residual strength of CTC tests:

Test name	Footing Width B (cm)	Predicted q_{ult} for friction angle $\phi = 44°$, cohesion $c = 0$ (kPa)					Measured q_{ult} (kPa)* peak	Measured q_{ult} (kPa) residual
		M.hof	Vesić	Chen	Slip-line (s.f.)	Slip-line (p.r.f.)		
BC3a01.O4	49.4	1131	1201	1912	598	1005	6401	3800
BC2b02.O14	34.8	801	850	1347	478	880	4721	3000
BC2b03.O18	10.9	248	264	421	273	655	1770	400

Note: * Measured q_{ult} is an average ultimate bearing capacity of the three interior footing segments.

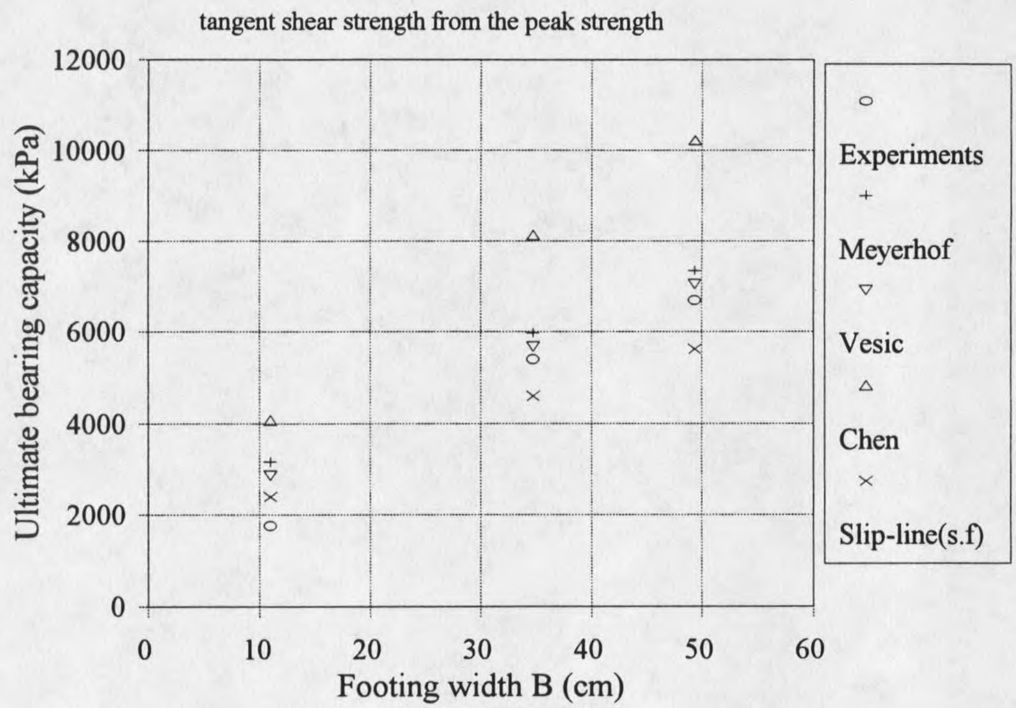

Figure 34 Comparison of theoretical and experimental bearing capacity values for surface footing using the peak tangent shear strength

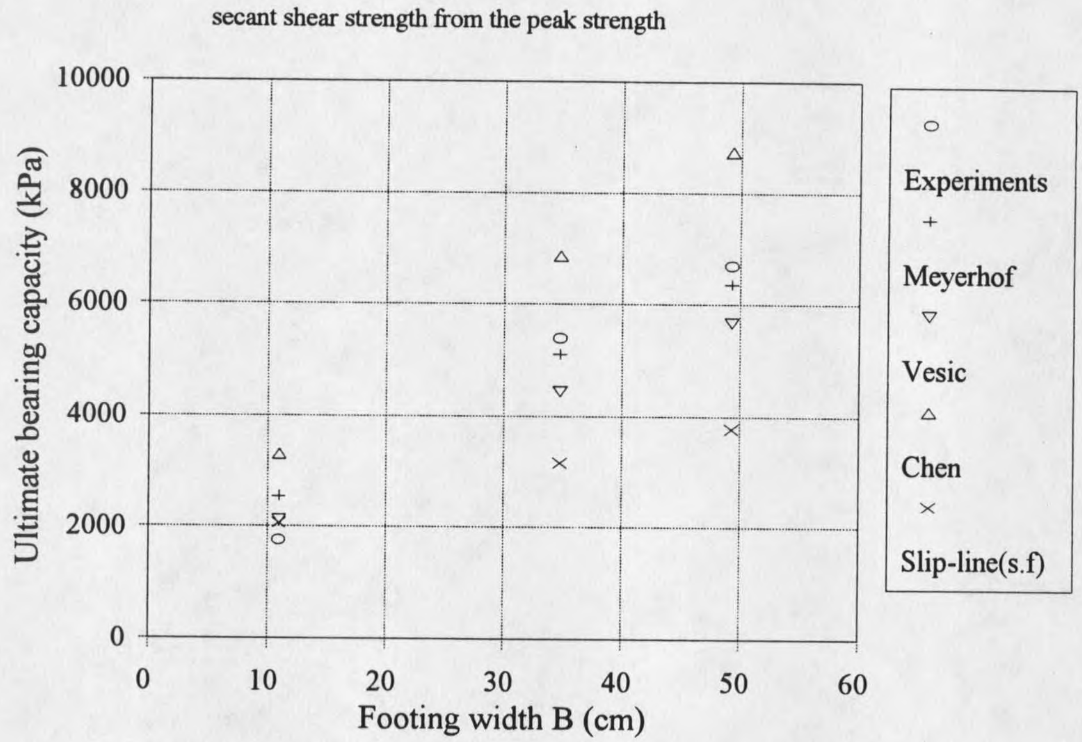

Figure 35 Comparison of theoretical and experimental bearing capacity values for surface footings using the peak secant shear strength

of bearing capacity by using the two extreme shear strengths--peak and residual. The peak bearing capacity can be predicted using the peak shear strength, and the lower bearing capacity prediction can be obtained from the residual shear strength. The experimental results for bearing capacity should fall in the range of the two extreme predicted values if progressive failure happens during the tests. Table 12 shows that all the predicted bearing capacity values are remarkably lower than the experimental values.

Bearing Capacity For Embedded Footings

For a strip footing with an initial embedment, the ultimate bearing capacity under a vertical load can be expressed by:

$$q_{ult} = cN_c + q_o N_q - \frac{1}{2}\gamma B N_\gamma \tag{50}$$

where the surcharge $q_o = \rho \cdot \gamma D$, D is the initial embedment of the footing.

The centrifuge experiments for embedded footing tests were conducted for three different initial embedments, $0B$, $0.5B$ and $1B$ for each of the three g-levels. The measured and predicted bearing capacity values obtained by using "tangent" and "secant" peak shear strength parameters are shown in table 13. These values are also plotted in the form of ultimate bearing capacity versus relative footing initial embedment (D/B) in Fig.36 through Fig.41. Table 14 presents all the bearing capacity values predicted by using the residual shear strength of the CTC tests. As it is shown in table 13 and the diagrams, the comparison of the experimental values for surface footings and embedded footings is interesting. All the measured bearing capacities for embedded footings are lower than the predicted values, especially for the footings with $1B$ embedment. The experimental results show considerably lower bearing capacity values for the three footing widths. The measurements also show that the bearing capacity for the footings with higher initial embedments are lower than those with lower initial embedments, which violate predictions of the basic theory of embedded foundations. No full explanation can be given here for the strange phenomenon, but it is felt that a local shear failure might occur for the footing tests with $1B$ embedments instead of general shear failure. For a local shear failure pattern, the stress-strain relation demonstrates a lower peak stress accompanied by a larger strain. The lateral compression in the soil required to spread the state of plastic equilibrium is greater than the lateral compression produced by settlement of the footing. In the case of a soil failing by local shear, the value of the shear strength is smaller than that for a general shear failure. Terzaghi (1943) suggested using shear strength c' and ϕ' to calculate bearing capacity of a soil with local shear strength, c' and ϕ' are given by

$$c' = \frac{2}{3}c, \qquad \phi' = \frac{2}{3}\phi \tag{51}$$

where c and ϕ are the shear strength corresponding to a general shear failure.

It is necessary to note that the conventional superposition methods such as Meyerhof and Vesic's, always give higher bearing capacity values than the slip-line method. Chen's method based on the limit plasticity theory and Prandtl failure mechanism gives much higher bearing capacity predictions compared with the conventional superposition methods as well as the slip-line method. Also, the slip-line method with a smooth footing base gives close values of the experimental bearing capacity, and the slip-line method with a partially rough footing base boundary condition gives very high bearing capacity values, which are not reasonable. The predicted bearing capacity values in table 14 are lower than the experimental results.

Fig.42 and Fig.45 show the percent difference of the theoretical bearing capacity to the experimental results with respect to the footing width. The results of tangent analysis and secant analysis for surface footings are plotted in Fig.42, the results for embedded footings are plotted in Fig.43 through Fig.45.

The Slip - line Method for Ultimate Bearing Capacity Analysis

As illustrated in the literature review, applications of the method of characteristics to geotechnical engineering have been studied by many researchers. The programs used in this thesis have been produced by Perkins (1994) which are presented in Appendix D. Three different boundary conditions of footing base are considered in the programs. They are smooth, rough, and partially rough footing base conditions. He introduced two non-dimensional factors p_o and B_o. The expression for B_o has been given in equation (46). The magnitude of the non-dimensional pressure p_o is:

$$p_o = q\left(\frac{\cot\phi}{q_o - c\cot\phi}\right) \tag{52}$$

where q represents the ultimate bearing capacity, and q_o represents the surcharge.

Table 13 Comparison of theoretical and experimental bearing capacity of embedded strip footings from peak strength of CTC tests:

Test name	Footing Width B (cm)	Footing Depth D (cm)	Predicted q_{ult} for tangent shear strength (kPa)					Measured q_{ult} (kPa)*	Predicted q_{ult} for secant shear strength (kPa)				
			M.hof	Vesić	Chen	Slip-line (s.f.)	Slip-line (p.r.f.)		M.hof	Vesić	Chen	Slip-line (s.f.)	Slip-line (p.r.f.)
BC3a01.O4	49.4	0	7360	7054	10223	5625	82330	6401	6369	5682	8729	3780	9469
BC2b11.O16	49.2	24.6	9056	8791	11665	7753	99814	6499	7682	7052	9846	6111	13069
BC2b21.O23	51.4	51.4	10972	10878	13534	9933	108669	5658	9218	8872	11352	7995	19104
BC2b02.O14	34.8	0	5970	5683	8142	4600	65418	4721	5113	4452	6868	3159	8199
BC2b12.O15	34.9	17.4	7299	7112	9360	6285	84824	4113	6112	5569	7803	4684	10563
BC2b22.O17	35.2	36.2	8590	8477	10525	7762	91348	4217	7130	6647	8764	6188	14569
BC2b03.O18	10.9	0	3167	2878	4092	2391	59329	1770	2546	2117	3307	2058	6190
BC2b13.O20	10.8	5.4	3638	3429	4676	3095	73200	2644	2931	2566	3658	2226	6547
BC2b23.O21	10.7	10.7	4144	4028	5039	3706	82395	1841	3305	2981	3998	2755	7995

Note: * Measured q_{ult} is an average ultimate bearing capacity of the three interior footing segments.

Table 14 Comparison of theoretical and experimental bearing capacity of embedded strip footings from residual strength of CTC tests:

Test name	Footing Width B (cm)	Footing Depth D (cm)	Predicted q_{ult} for tangent shear strength (kPa)					Measured q_{ult} (kPa)*
			M.hof	Vesić	Chen	Slip-line (s.f.)	Slip-line (p.r.f.)	
BC3a01.O4	49.4	0	1131	1201	1912	598	1005	6401
BC2b11.O16	49.2	24.6	1942	1987	1564	1325	2844	6499
BC2b21.O23	51.4	51.4	3025	3271	2266	2005	5105	5658
BC2b02.O14	34.8	0	801	850	1743	478	880	880
BC2b12.O15	34.9	17.4	1397	1411	1111	938	2014	4113
BC2b22.O17	35.2	36.2	2076	2244	1555	1428	3496	4217
BC2b03.O18	10.9	0	258	274	421	273	655	1770
BC2b13.O20	10.8	5.4	436	446	351	290	622	2644
BC2b23.O21	10.7	10.7	642	692	480	433	1058	1841

Note: * Measured q_{ult} is an average ultimate bearing capacity of the three interior footing segments.

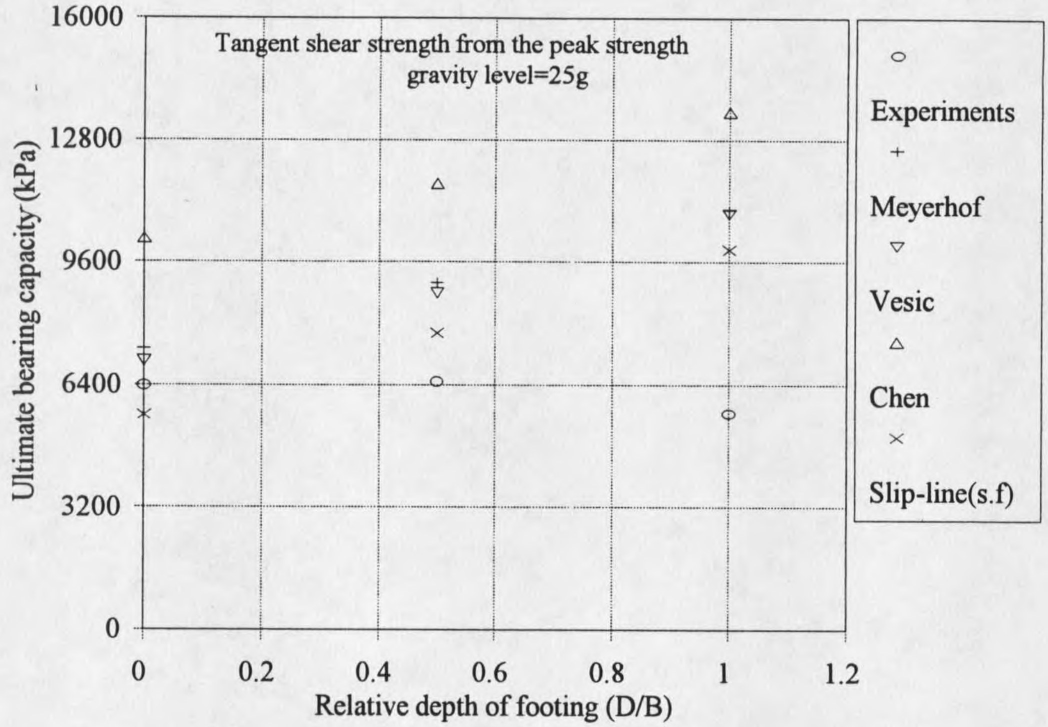

Figure 36 Comparison of theoretical and experimental bearing capacity values for embedded footings using the peak tangent shear strength

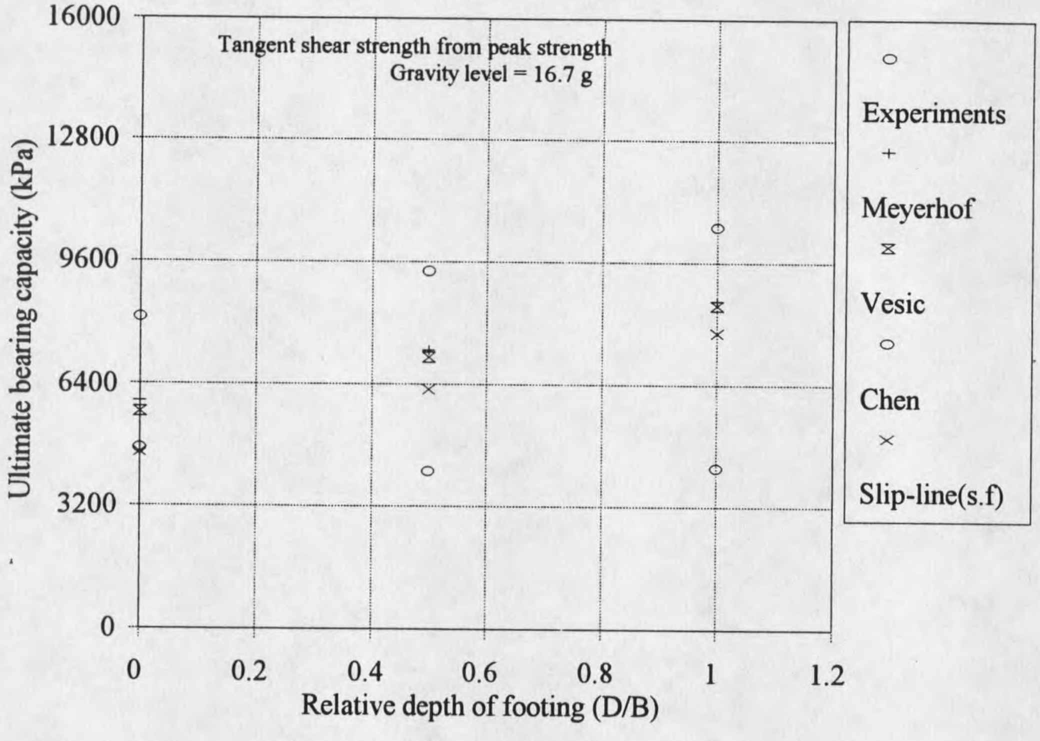

Figure 37 Comparison of theoretical and experimental bearing capacity values for embedded footings using the peak tangent shear strength

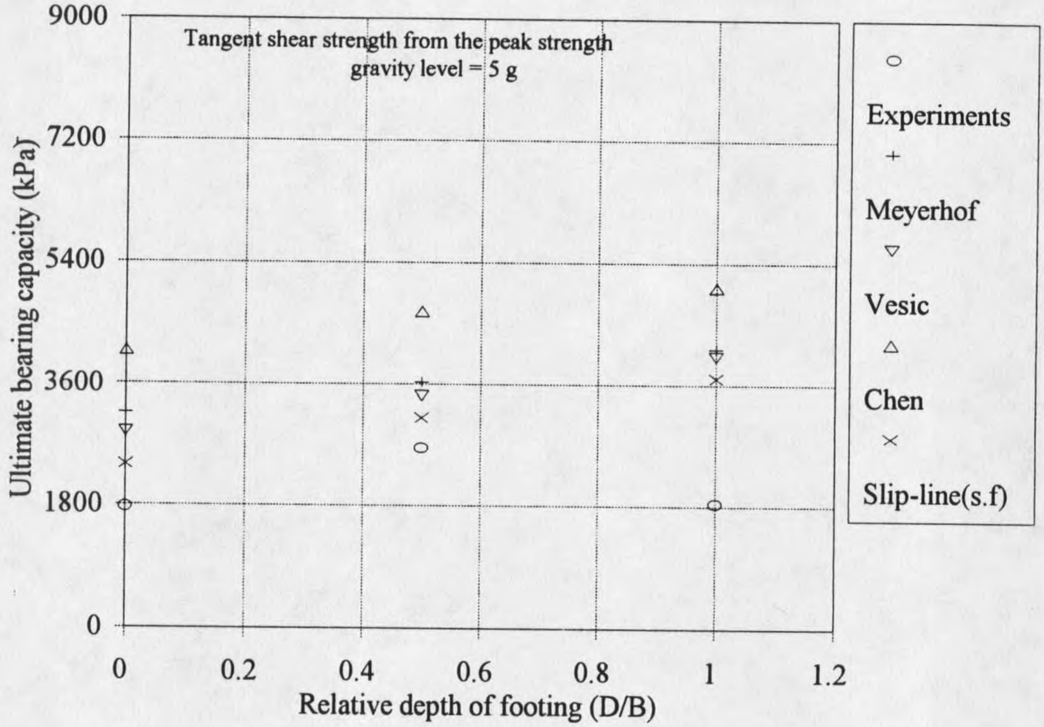

Figure 38 Comparison of theoretical and experimental bearing capacity values for embedded footings using the peak tangent shear strength

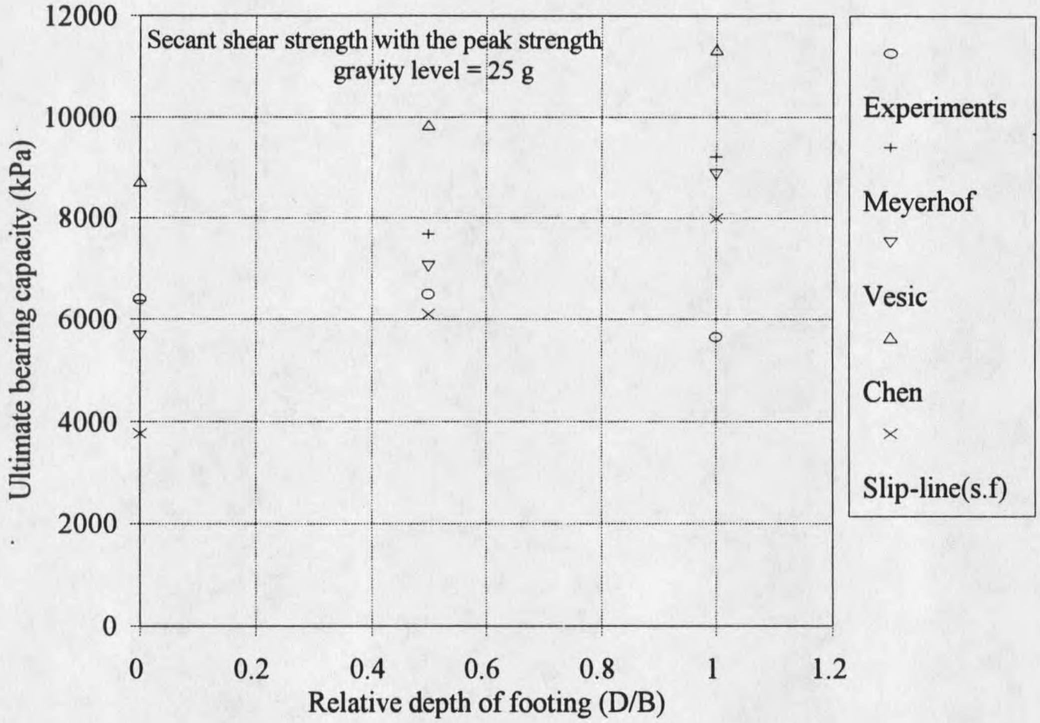

Figure 39 Comparison of theoretical and experimental bearing capacity values for embedded footings using the peak secant shear strength

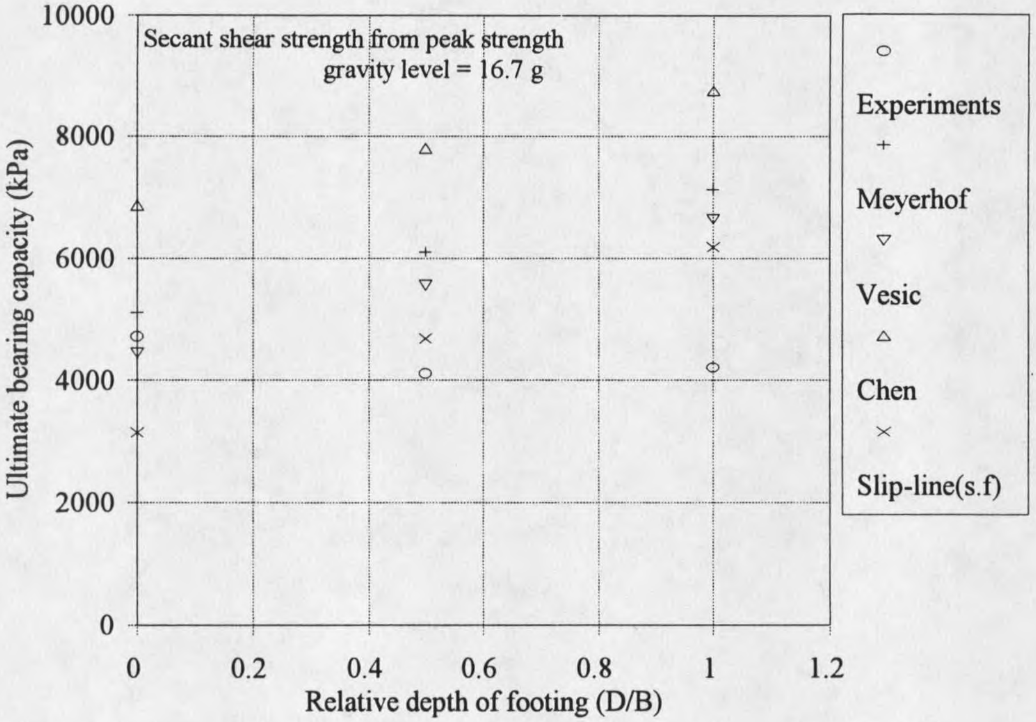

Figure 40 Comparison of theoretical and experimental bearing capacity values for embedded footings using the peak secant shear strength

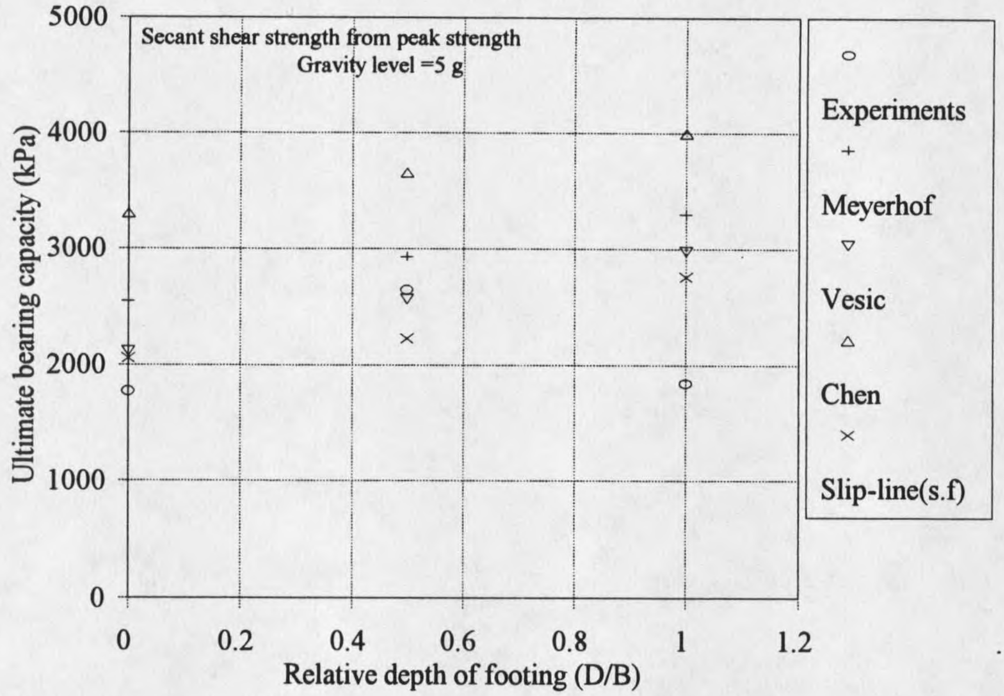

Figure 41 Comparison of theoretical and experimental bearing capacity values for embedded footings using the peak secant shear strength

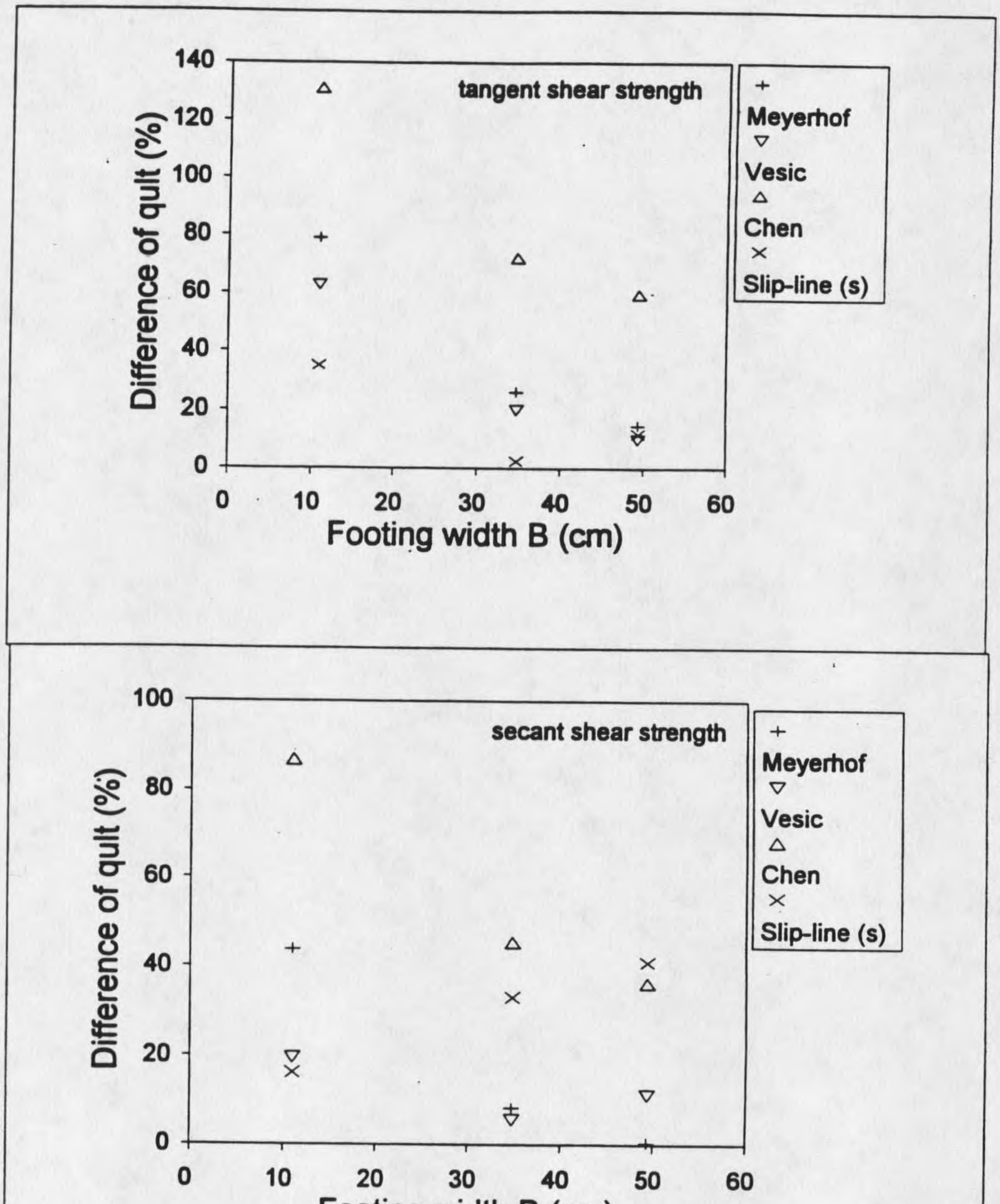

Figure 42 The percentage difference of the theoretical and experimental bearing capacity for surface footings.

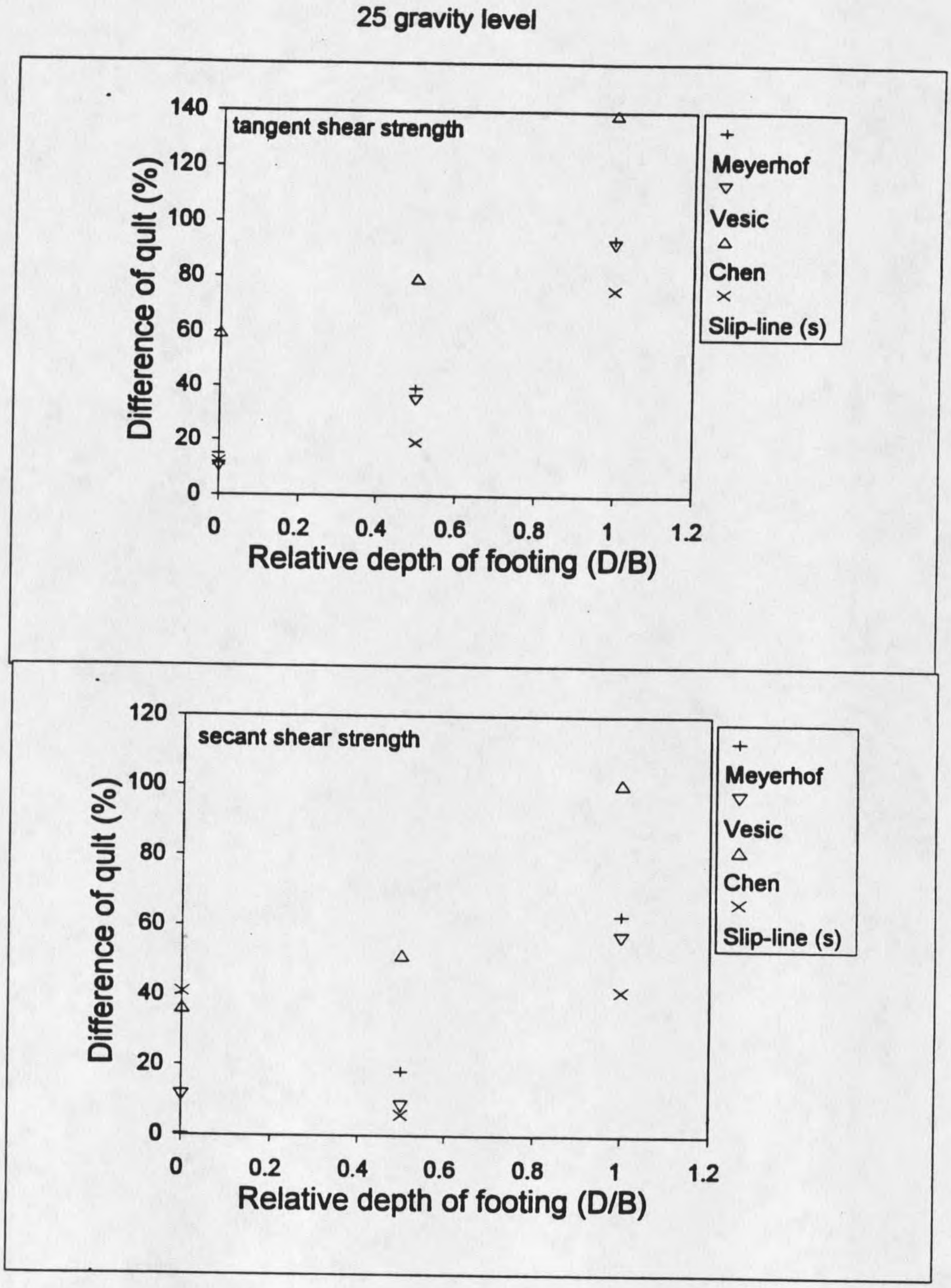

Figure 43 The percentage difference of the theoretical and experimental bearing capacity for embedded footings at 25g -level

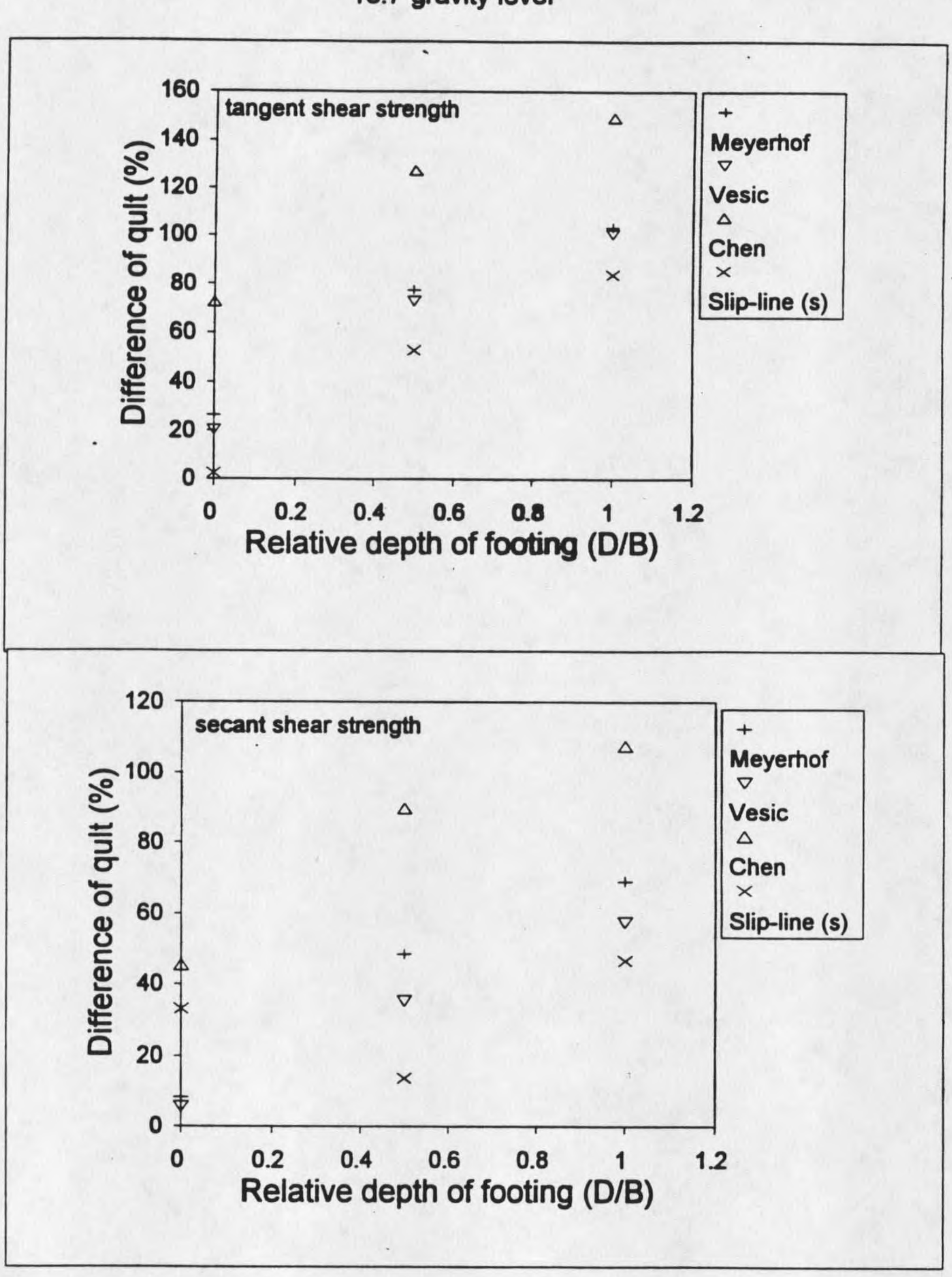

Figure 44 The percentage difference of the theoretical and experimental bearing capacity for embedded footings at 16.7g -level

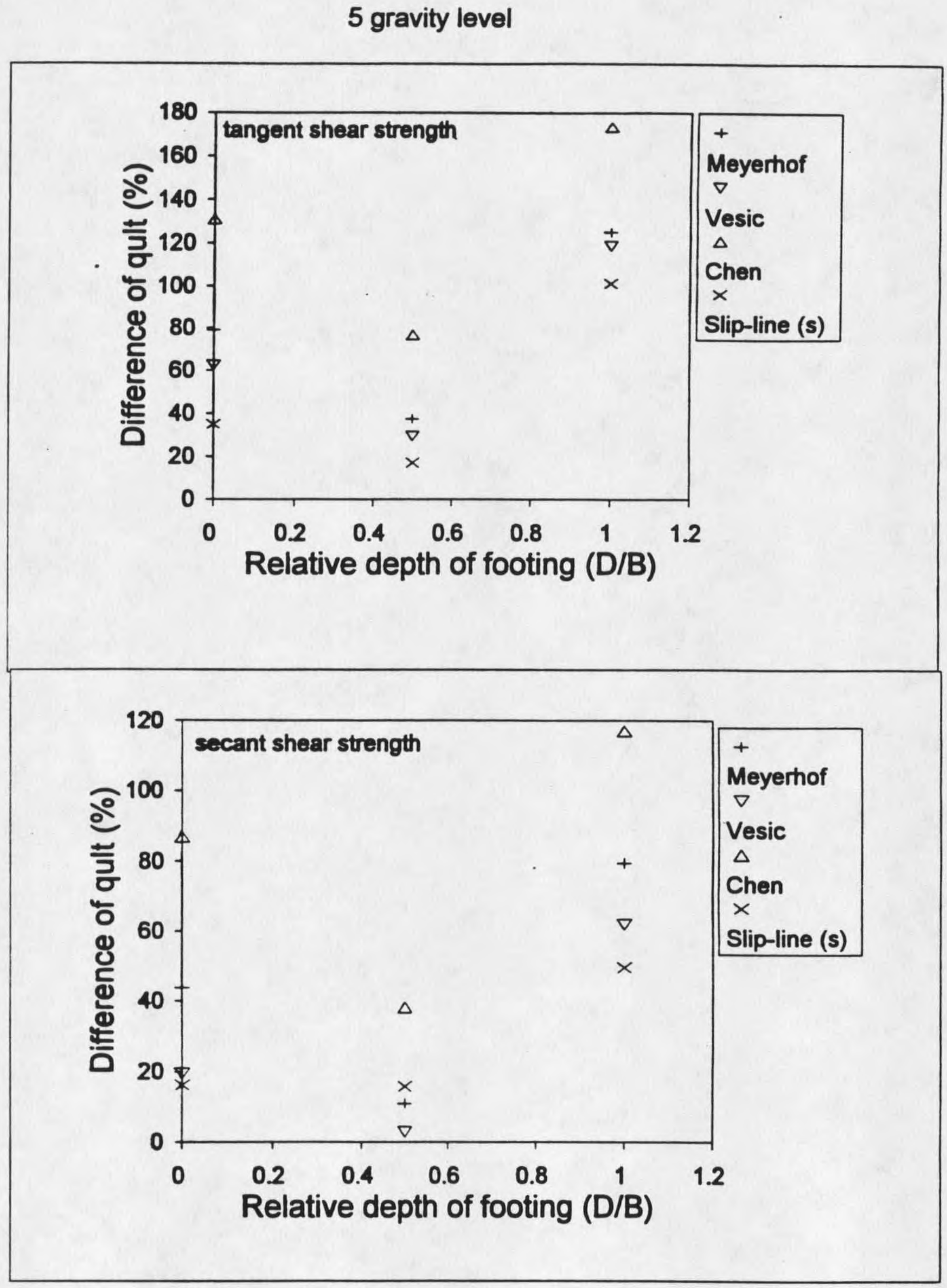

Figure 45 The percentage difference of the theoretical and experimental bearing capacity for embedded footings at 5g -level

Non-dimensional charts in terms of p_0 and B_0 are plotted in Fig.46 and Fig.47 for both the smooth and partially rough footing base conditions. Values of ultimate bearing capacity, calculated by the computer programs corresponding to the aforementioned footing physical characteristics, and the shear strengths, have been listed on table 11 though table 13. It should be noticed that the program with the condition of smooth footing base gives quite reasonable values of ultimate bearing capacity. When compared to the theories of Meyerhof (1963), Vesic (1975) and Chen(1975), the slip-line method with a smooth footing base gives values of bearing capacity close to Vesic's prediction. As can be seen from table 11 to table 13, the program with the boundary condition of a partially rough footing base gives extremely high bearing capacities for both surface footings and buried footings which is not a realistic prediction.

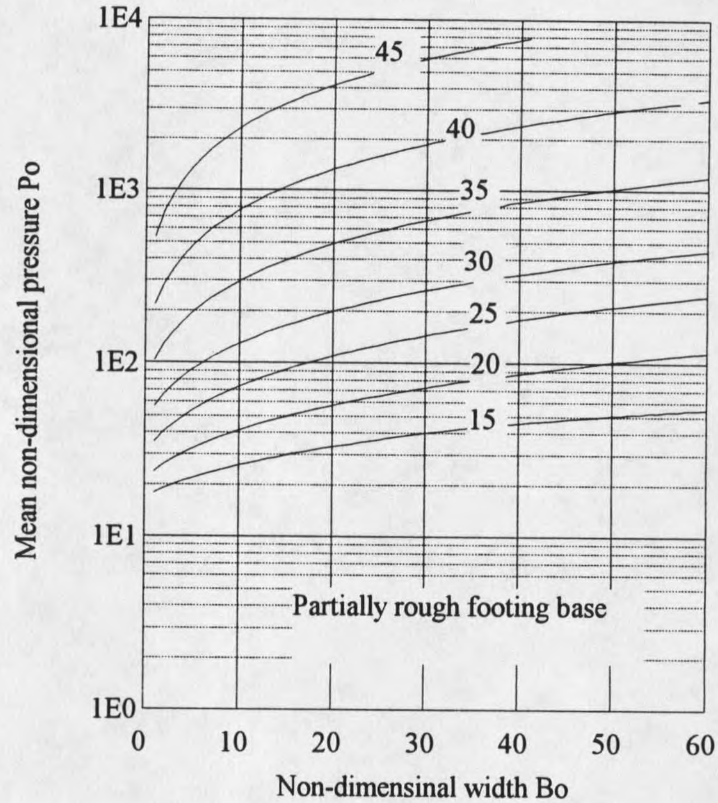

Figure 46 Chart for mean non-dimensional pressure with non-dimensional width for smooth footing base

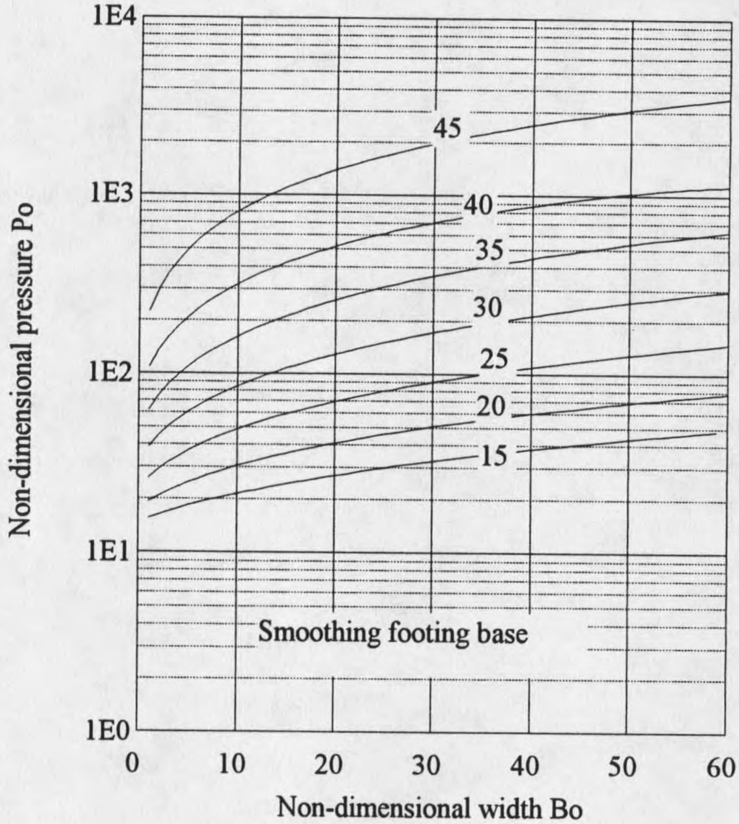

Figure 47 Chart for mean non - dimensional pressure with non - dimensional width for partial rough footing base

CHAPTER FIVE

SUMMARY, CONCLUSIONS AND RECOMMENDATIONS FOR FURTHER WORK

Summary

The design of foundations for constructed facilities relies on the use of classical bearing capacity theories for the evaluation of the ultimate load carrying capacity of soils. These classical bearing capacity theories have been validated only for terrestrial soils which possess moderate friction angles. However, the internal friction angle of lunar soils has been shown to be higher than terrestrial soils (Perkins, 1991). To evaluate the bearing capacity of the lunar regolith by using the classical bearing capacity theories, these theories, used to predict the bearing capacity of high frictional soils, has to be validated. This thesis is a presentation of research work on this topic.

A basic knowledge of the similarity laws of modeling were introduced in Chapter Two. The principle of conventional small-scale model tests and centrifuge model tests were then described. Several issues impacting centrifuge model tests were discussed. The issues of experimental and theoretical approaches related to bearing capacity evaluations have also been presented. These experimental approaches include full-scale model tests, 1-g small-scale model tests and centrifuge small scale model tests. The issue of theoretical approaches include the limit equilibrium method, the slip-line method, and the method of limit plasticity. The experimental work related to the evaluation of the bearing capacity of shallow foundations on the lunar simulant, MLS-1, was presented in Chapter Three, in which centrifuge small scale model tests were conducted by using the 400g-ton centrifuge at Boulder, Colorado. The preliminary testing programs were designed and conducted to assess the plane strain conditions and the effects of the container walls and bottoms on test results. A reasonable minimum depth of soil was determined which prevented effects from the container bottom and a rational configuration of the test footings designed to ensure a plane strain condition was obtained by assessment of the test results. In addition, the bearing capacity values of surface footings and embedded footings on MLS-1 were tested.

A proposed expression for the relation between the normal stress and ultimate bearing capacity in a soil was studied in Chapter Four, and steps using the proposed expression to determine the shear strength parameters of a soil by "tangent" analysis and "secant" analysis have also been developed. The bearing capacity values of MLS-1 were predicted by the theories of Meyerhof, Vesic and Chen by using the two shear strength analyses. A comparison of the bearing capacity values given by the aforementioned theories and experimental results were performed in this chapter. Computer programs based on the slip-line method were used to predict bearing capacity values of MLS-1 soil, and three different boundary conditions of shear resistance at a foundation - soil interface were taken into account in the programs. The bearing capacity values from the slip-line method were also compared with the aforementioned theoretical values as well as the experimental results.

Conclusions

Plane strain conditions were modeled properly for the centrifuge experiments by evaluating the test results of varied footing lengths. The assessment shows that a footing with a minimum footing length of seven times the footing width can perform the plane strain condition very well. The effects of the container walls and bottom on the experimental results were also evaluated, and a minimum sample height of 16*cm* was determined to prevent these effects on the experimental bearing capacity results.

A general expression related the ratio of normal stress to ultimate applied pressure in a soil was developed, which is a function of the friction angle of the soil. The ratio obtained from the function is about 7.5% for $\phi = 45^{o}$, and it is lower than Meyerhof's assumption of 10%. The shear strength parameters of MLS-1, cohesion c and friction angle ϕ, were different for different analytical methods. It was shown that about 2^{o} to 3^{o} differences of the internal friction angle result between the "tangent" analysis and the "secant" analysis. The cohesion obtained was in the range of 15*kPa* to 35*kPa* for the "tangent" analysis.

Compared to the experimental results, it can be seen that the conventional bearing capacity prediction of Meyerhof's theory overestimates the bearing capacity of MLS-1 by about 15% to 75% for the surface footings using the tangent shear strength parameters, and about 0.5% to 40% by using the secant shear strength parameters. Vesic's theory overestimates about 10% to 60% of experimental bearing capacity values by using the tangent shear strength and about 5% to 20% discrepancy (lower or higher than the experimental results) by using the secant shear strength. Chen's method based on the theory of limit plasticity provides much higher bearing capacity predictions. Approximately 60% to 130% higher values than the experimental bearing capacity were found from Chen's method corresponding to the tangent shear strength, and 40% to 90% higher corresponding to the secant shear strength. The slip-line method with the smooth footing base condition gives the best predicted values if the tangent shear strength is used, and the predicted values are lower than the experimental results when using the secant shear strength. The slip-line method with the partial rough footing base condition gives a much higher bearing capacity for both cases compared to the experimental results and other predictions. Remarkably higher bearing capacities were obtained from all the theoretical approaches for the maximum footing initial embedments compared to the experimental results. No full explanation can be given here for the strange phenomenon.

It can be seen that, for the particular soil property of MLS-1, directly using the conventional approaches to evaluate ultimate bearing capacity cannot give a satisfactory explanation of the experimental work, especially for the problems with embedded footings. Further research work regarding exploration of the lack of conventional solutions' ability and investigation of reasonable modification is necessary

Recommendations For Further Study

The research work presented in this thesis is just a starting point for further investigation of the bearing capacity of shallow foundations on lunar soil. Further study is necessary in order to understand thoroughly the suitability of the existing theories for lunar regolith application. More bearing capacity experiments regarding embedded footings need to be conducted to study initial embedment effects for the lunar simulant soils such as MLS-1. This thesis indicated the possibility of progressive failure happening in the testing process. Further study can also be involved investigation of this topic, where a related testing program and equipment setup need to be designed to conduct an effective research activity. One suggestion for examining progressive failure phenomenon is embedding several stress sensors in test soil in the range of expected failure zone, progressive failure may be examined from the time of stress response for each sensor. For centrifuge model tests, however, initial stress response would be observed from the embedded sensors due to centrifugal force, so the sensor should be placed appropriately to distinguish stresses from the soil deformation and from centrifugal force.

Further research work can focus on the determination of mean normal stress state. As we can see, using an average expression for mean normal stress from the slip-line solution to obtain the general expression of p/q_{ult} is somewhat arbitrary. For instance, if predictions given by Meyerhof's method is assumed to equal the experimental bearing capacity of MLS-1, normal stresses can be calculated by using the failure function of the soil corresponding to the different foundation conditions. The ratios of mean normal stress over ultimate bearing capacity obtained from above are plotted in Fig.48, and are compared with those obtained from Fig.33. We can see that the theoretical curve does not predict the experimental values and considerably underestimates them as friction angle decreases from 53°. To improve the fit, one might try the following weighting scheme instead of the equation (45) in order to obtain a higher mean normal stress:

$$p = s_i \frac{s_i A_i}{p_{avg}} \tag{53}$$

where s_i and A_i represent the same meanings as those in equation (45), and $p_{avg.}$ is the average mean normal stress obtained from equation (45).

Then using the slip-line method, higher values of p/q_{ult} can be obtained, and results can be seen as the upper curve in Fig.48. This weighting scheme overestimates p/q_{ult}. A better approximation can be obtained by combining both weighting schemes as in the next equation:

$$p = p_1 + \frac{(60 - \phi)}{40} (p_2 - p_1) \tag{54}$$

where p_1 is from equation (45), and p_2 is from equation (54). This produces the middle curve in Fig.48. Even though this approach is not consistently under or over estimating p/q_{ult}, the results are still not acceptable. One problem is lack of knowledge as to whether one or multiple curves are required to fit p/q_{ult} outside of the friction angles between roughly 48° and 50°. Developing a single p/q_{ult} curve valid for friction angles from 20° to 60°, based upon the limited data available, is unreasonable without having data from which to chose among the many curves which fit the experimental data. In short, an appropriate method to obtain mean normal stress still needs to be explored.

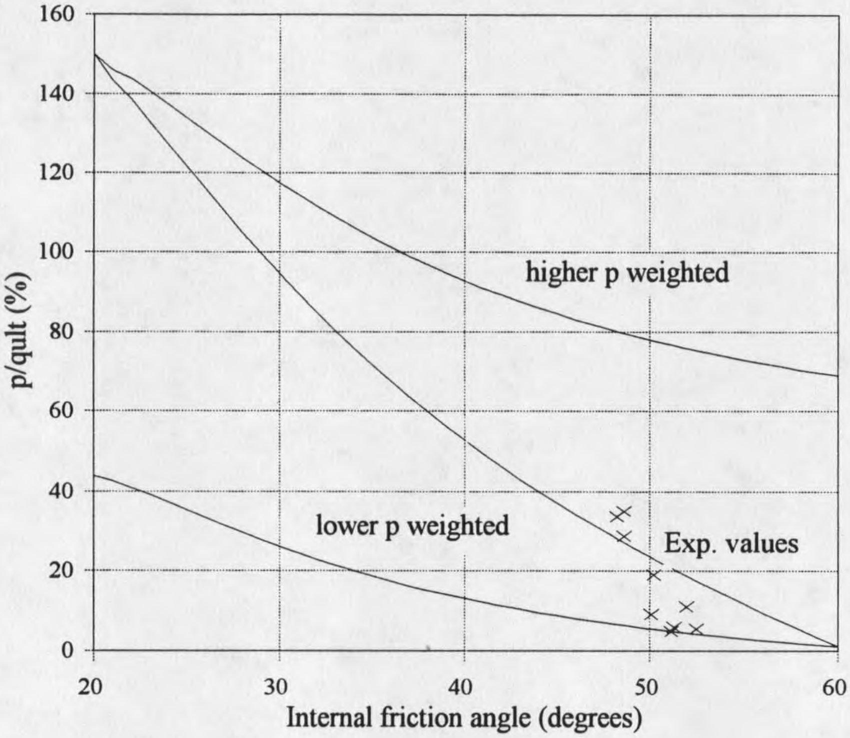

Figure 48 The relationship between the ratio (p/q_{ult}) and friction angle obtained from experimental results and predictions.

REFERENCES

REFERENCES

Aiban, S. A., Znidarcic, D., "Shallow Footings on Sand Under Vertical Central, Eccentric and Inclined Loads", *Centrifuge 91.*

Atkinson, J. H. The Mechanics of Soils, Chapter 7: Associated Fields and Slip Line Method, *McGraw Hill Ltd., Maidenhead, England*, 1981.

Balla, A., "Bearing Capacity of Foundations", Journal of the Soil Mechanics and Foundations Division, ASCE, Vol. 88, No. SM5, Oct. 1962, pp.13-14.

Bishop, A. W., "Discussion of Soil Properties and Their Measurement", *Proc. 4th Int. Conf. on Soil Mech. and Found. Engineering*, Vol. III, 1957, pp.100.

Caquot, A., Kerisel, J., "Table for the Calculation of Passive Pressure, Active Pressure and Bearing Capacity of Foundations", *Gauthier-Villars, Paris, France*, 1948.

Caquot, A., Kerisel, J., "Sur le Terme de Surface dans le Calul des Foundations en Milien Pulverulent", *Proc. 3rd Int. Conf. on Soil Mech. and Found. Engineering*, Vol. I, 1953, pp.336-337.

Carrier, W. D., Olhoeft, G., Mendell, W. W, "Physical Properties of the Lunar Surface", Lunar Source book Heiken, G., Vaniman, D., and French, B. M., *Cambridge University Press, New York*, 1991, pp. 475-567.

Chen, W. F. and Davidson, H. L., "Bearing Capacity Determination By Limit Analysis", *Journal of the Soil Mech. and Found. Divisions, ASCE*, Vol. 99, No. SM6, June, 1973.

Chen, W. F., Limit Analysis and Soil Plasticity, *Elsevier*, 1975.

Cherkasov, I. I., Mikheev, V. V., et. al., "Influence of Gravity on the Mechanical Properties of Soil", Translated from *Osnovanlya, Fundamenty Mekhanika Grunton*, Jan.-Feb. No. 1, 1970, pp.14-18.

Chummer, A. V., "Bearing Capacity Theory from Experimental Results" *Journal of the Soil Mechanics and Foundations Divisions, ASCE*, Vol. 98, No. SM12, Dec., 1972.

Cox, A. D., Eason, G. and Hopkins, H. G., "Axially Symmetric Plastic Deformations in Soil", *Phil. Trans. R. Soc.* A 254, 1961.

Cox, A. D. "Axially Symmetric Plastic Deformation in Soil - II. Indentation of Ponderable Soils", *International Journal Mech.* Science 4 September-October, 1962.

De Beer, E. E., "Bearing Capacity and Settlement of Shallow Foundations on Sand" *Proc. of a Symposium held at Duke University*, 1965, pp.15-34.

De Beer, E. E., "Influence of the Mean Normal Stress on the Shearing Strength of Sand" *Proc. 6th Int. Conf. on Soil Mech. and Found. Engineering*, Vol.I, 1965, pp.165-169.

De Beer, E. E., "Experimental Determination of the Shape Factors and the Bearing Capacity Factors of Sand", *Géotechnique*, Vol. 20, No. 4, 1970, pp.387-411.

Drucker, D. C. and Prager, W., "Extend Limit Design Theorems For Continuous Media", *Quarterly of Applied Mathematics*, Vol. 9, 1952. pp.381-389.

Fuglsang, L. D. and Ovesen, N. K., "The Application of the Theory of Modeling to Centrifuge Studies", *Proc. of the Int. Conf. on Geotech. Centrifuge Modeling, Paris*, April, 1988, pp.19-138.

Graham, J., "Plane Plastic Failure in Cohesionless Soil", *Géotechnique*, Vol. 18, 1968, pp.301-316.

Graham, J., Stuart, J. G., "Scale and Boundary Effects in Foundation Analysis", *Journal of the Soil Mech. and Found. Divisions, ASCE*, Vol.97, 1971, pp.1533-1548.

Graham, J., Hovan, J. M., "Stress Characteristics for Bearing Capacity in Sand Using a Critical State Model", *Canadian Ceotech. Journal*, Vol. 23, 1986, pp.195-202.

Hansen, J. B. "A General Plasticity Theory for Clay", *Géotechnique*, Vol.3, 1952.

Hansen, J. B. "A General Formula for Bearing Capacity", *Bull. Geotek. Inst.*, No.II, 1961.

Hansen, J. B. "A Revised and Extended Formula for Bearing Capacity", Bulletin No. 28, *Danish Geotechnical Institute, Copenhagen, Denmark*, 1970, pp.5-11.

Hansen, B. "Bearing Capacity of Footings in Theory and Experiment", *Proc. of 1st Baltic Conf. on Soil Mech. and Found. Engineering*, Vol. I, 1975, pp.83-104.

Jumikis, A. R., "Rupture Surface in Sand Under Oblique Loads", *Journal of the Geotechnical Divisions, ASCE*, Vol. 82, No. SM1, Jan., 1956, pp.1-26.

Jumikis, A. R., Soil Mechanics, *Robert E. Krieger Publishing Company, Inc.*, 1984

Kimura, T., Kusakabe, O., and Saitoh, K., "Geotechnical Model Tests of Bearing Capacity Problems in a Centrifuge", *Géotechnique* 35, No.1, 1985, pp.33-45.

Ko, H. Y. and Davidson, L. W., "Bearing Capacity of Footings in Plane Strain", *Journal of the Soil Mech. and Found. Divisions, ASCE*, Vol. 99, No. SM1, Jan., 1973, pp.1-23.

Ko, H. Y. and Scott, R. F., "Bearing Capacity of Footings in Plane Strain", *Journal of the Soil Mech. and Found. Divisions, ASCE*, Vol.99, No. SM1, Jan., 1973, pp.1-23.

Ko, H. Y. "400g-ton Centrifuge Facility in University of Colorado", *Centrifuge* 90.

Lee, Kenneth L. and Seed, H.B., "Drained Strength Characteristics of Sands" *Journal of the Soil Mech. and Found. Divisions, ASCE*, Vol.93, No. SM6, May. 1967, pp.117-141.

Lundgren, H. and Mortensen, K., "Determination by the Theory of Plasticity of the Bearing Capacity of Continuous Footings on Sand", *Proc. of the 3rd Int. Conf. on Soil*

Mech. and Found. Engineering, Vol. I, 1953, pp.409-412.

Lysmer, J., "Limit Analysis of Plane Problems in Soil Mechanics", *Journal of the Soil Mech. and Found. Divisions, ASCE*, Vol.96, No. SM4, July, 1970. pp.1311-1333.

Meyerhof, G. G. "An Investigation of the Bearing Capacity of Shallow Footings on Dry Sand" *Proc. 2nd Int. Conf. on Soil Mech. and Found. Engineering*, Vol. I, 1948, pp.237-243.

Meyerhof, G. G. "The Ultimate Bearing Capacity of Foundations", *Géotechnique* Vol.2, 1951, pp.301-332.

Meyerhof, G. G. "Influence of Roughness of Base and Ground-water Conditions on the Ultimate Bearing Capacity of Foundations" *Géotechnique* 5, No. 3, 1955 pp.227-242.

Meyerhof, G. G., "Some Recent Research on the Bearing Capacity of Foundations", *Canadian Geotechnical Journal*, Vol. 21, 1963, pp.1-7.

Mikasa, M., Takada, N., "Significance of Centrifugal Model Test in Soil Mechanics" *Proc. of the 8th Int. Conf. on Soil Mech. and Found. Eng.*, Vol. 12, 1973, pp.273-278.

Milovic, D. M., "Comparison Between the Calculated and Experimental Value of the Ultimate bearing Capacity", *Proc. of the 6th Int. Conf. on Soil Mech. and Found. Engineering*, Vol. II, 1965, pp.142-144.

Muhs, H., "Comparison between the calculated and Experimental Value of the Ultimate Bearing Capacity", Discussion, *Proc. of the 6th Int. Conf. on Soil Mech. and Found. Engineering*, Vol. III, 1965a, pp.439-440.

Muhs, H., "Calculations for the stability of a Sand Bed by a Solution Combining the Theories of Elasticity and Plasticity" Discussion, *Proc. of the 6th Int. Conf. on Soil Mech. and Found. Engineering*, Vol. III, 1965b, pp.436-439.

Muhs, H., "On the Phenomenon of Progression Rupture in Connection with the Failure Behavior of Footings in Sand" Discussion, *Proc. of the 6th Int. Conf. on Soil Mech. and Found. Engineering*, Vol. III, 1965c, pp.419-421.

Nordal, S., "The Method of Characteristics for Failure Load Analysis", *Lecture Notes*, April, 1992.

Ovesen, N. K., "Centrifugal Testing Applied to Bearing Capacity Problems of Footings on Sand", Géotechnique, Vol. 25, No. 2, 1975, pp.394-401.

Ovesen, N. K., "The Scale Law Relationship", Panel Discussion, *Proc. of the 7th European Conf. on Soil Mech. and Found. Engineering*, Vol.V, 1979,pp.319-323.

Perkins, S. W., "Modeling of Regolith Structure Interaction in Extraterrestrial Constructed Facilities" *Ph. D Thesis*, 1991, pp.249-258.

Perkins, S. W., "Programs of Bearing Capacity Solution Using the slip-Line Method"

Private Communication, 1994.

Ponce, V. M. and Bell, J. M., "Shear Strength of Sand at Extremely Low Pressures", *Journal of the Soil Mech. and Found. Divisions, ASCE*, Vol. 97, No. SM4, April, 1971, pp.625-636.

Pope, R. G., "Non-dimensional Chart for the Ultimate Bearing Capacity of Surface and Shallow Foundations", *Géotechnique* 25, No. 3, 1975, pp.593-597.

Pu, J. L. and Ko, H. Y., "Experimental Determination of Bearing Capacity in Sand by Centrifuge Footing Tests", *Proc. of the Int. Conf. on Geotech. Centrifuge Modeling*, Paris, April, 1988, pp.293-299.

Rocha, M., "The Possibility of Solving Soil Mechanics Problems by The Use of Models", *Proc. 4th Int. Conf. on Soil Mech. and Found. Engineering*, London, 1957, pp.1-183.

Roscoe, K. H., Journal of Strain analysis, Vol. 3 No. I, 1968.

Shield, R. T. et. al., "The Application of Limit Analysis to Punch-Indentation Problems", *Presented at the National Conf. of the Applied Mech. Division*, Minneapolis, Minn. June, 1953.

Sokolovskiî, V. V., Static of Soil Media, 2nd edition, *Butterworth Scientific Publishers*, London, England, 1960. Statics of Granular Media, *Pergamon Press*, 1965.

Sture, S., Runesson, K. and Macari-Pasqualina, E.J. "Analysis and Calibration of a Three-Invariant Plasticity Model for Granular Materials", *Ingenieur-Archiv.*, V.59, 1989, pp.253-266.

Terzaghi, K., Theoretical Soil Mechanics, *John Wily*, 1943.

Vesic, A. S., "Analysis of Ultimate Loads of Shallow Foundations", *Journal of the Soil Mech. and Found. Divisions, ASCE*, Vol. 99, No. SM1, Jan., 1973, pp.45-73.

Vesic, A. S., Chapter 3: Bearing Capacity of Shallow *Foundations in Foundation Engineering Handbook, Van Nostrand Reinhold Book CO.*, NY, 1975, pp.751.

Weiblen, P. W., Gorden, K. L., "Characteristics of a Simulant for Lunar Surface Materials", *Symp. on Lunar Bases and Space Activities in the 21st Century*, Paper No. LBS - 88 - 213, Huston, 1988.

Yamaguchi, H., Kimura, T., and Fuji - i, N., "On the Influence of Progressive Failure on the Bearing Capacity of Shallow Foundations in Dense Sand", *Soils and Foundations*, Vol.16, No. 4, 1976, pp.11-22.

Yamaguchi, H., Kimura, T., "On the Scale Effect of Footings on Dense Sand", *Proc. of the 9th Int. Conf. on Soil Mech. and Found. Engineering*, Vol. I, 1977, pp.795-798.

APPENDICES

APPENDIX A

CONVENTIONAL TRIAXIAL COMPRESSION RESULTS

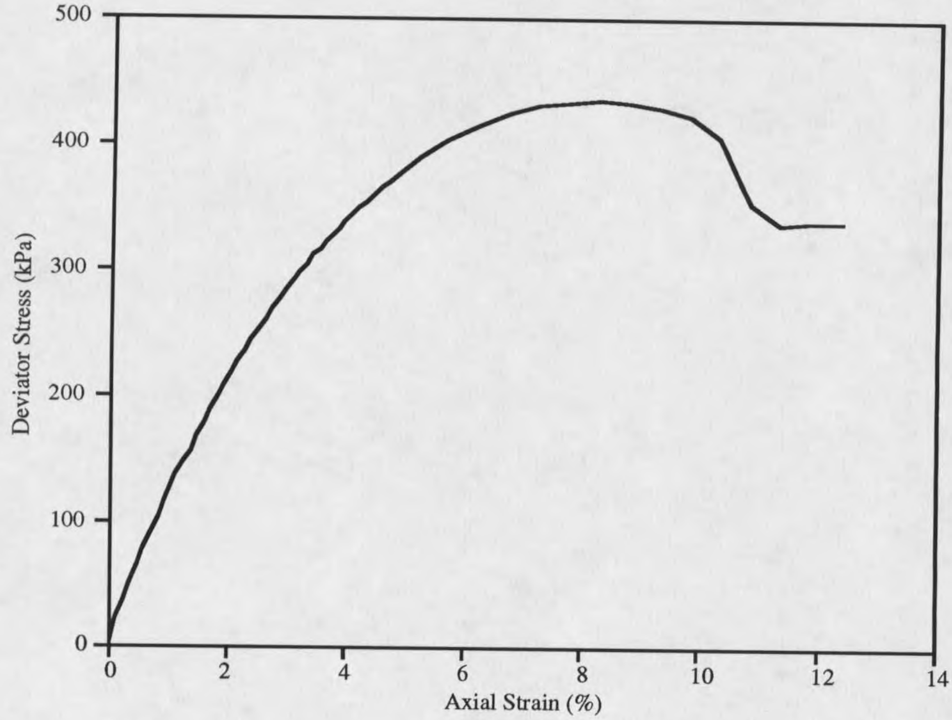

Figure 49 CTC experiment on MLS-1 at $\sigma_3 = 750\ kPa$

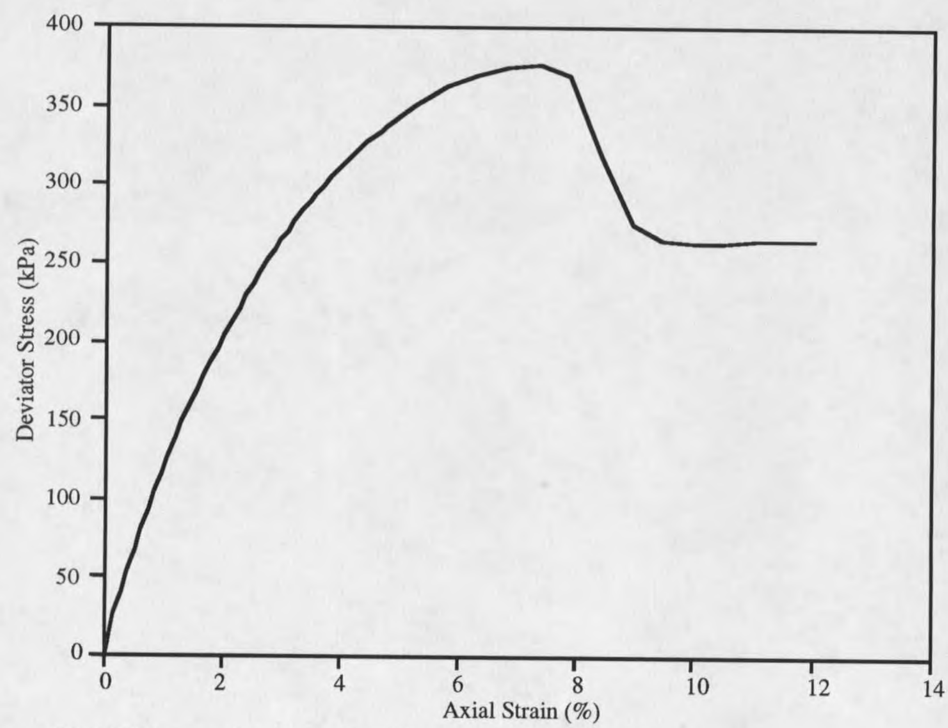

Figure 50 CTC experiment on MLS-1 at $\sigma_3 = 650\ kPa$

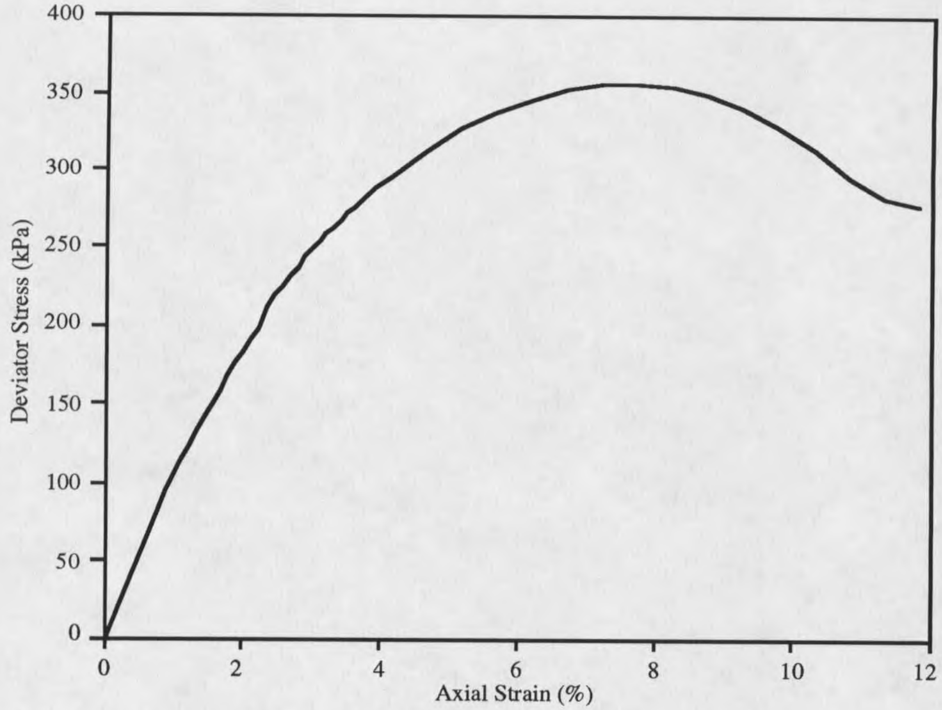

Figure 51 CTC experiment on MLS-1 at $\sigma_3 = 650\ kPa$

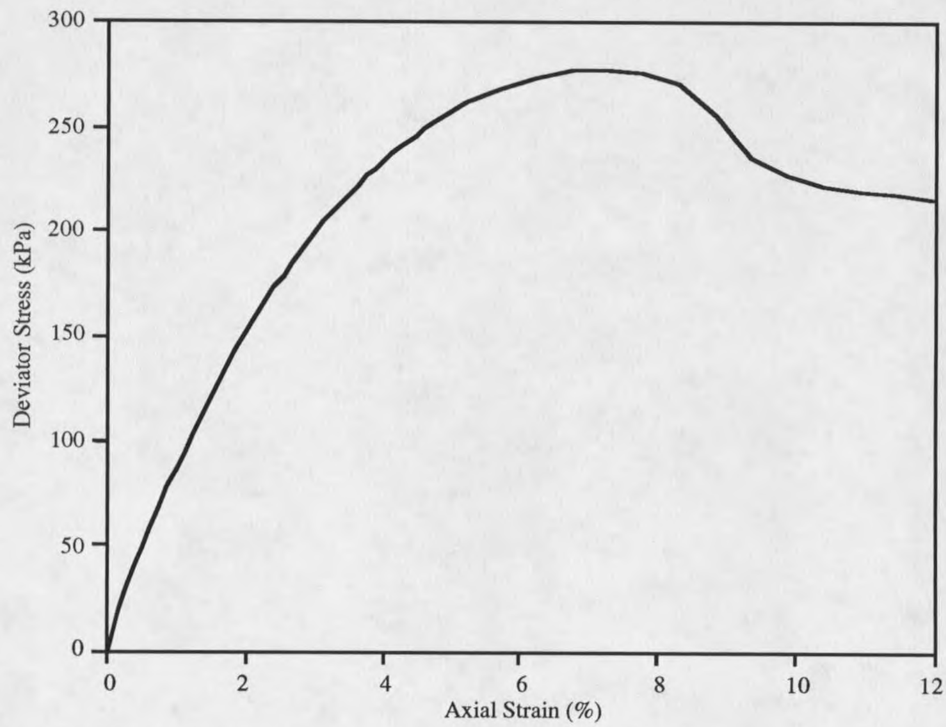

Figure 52 CTC experiment on MLS-1 at $\sigma_3 = 500\ kPa$

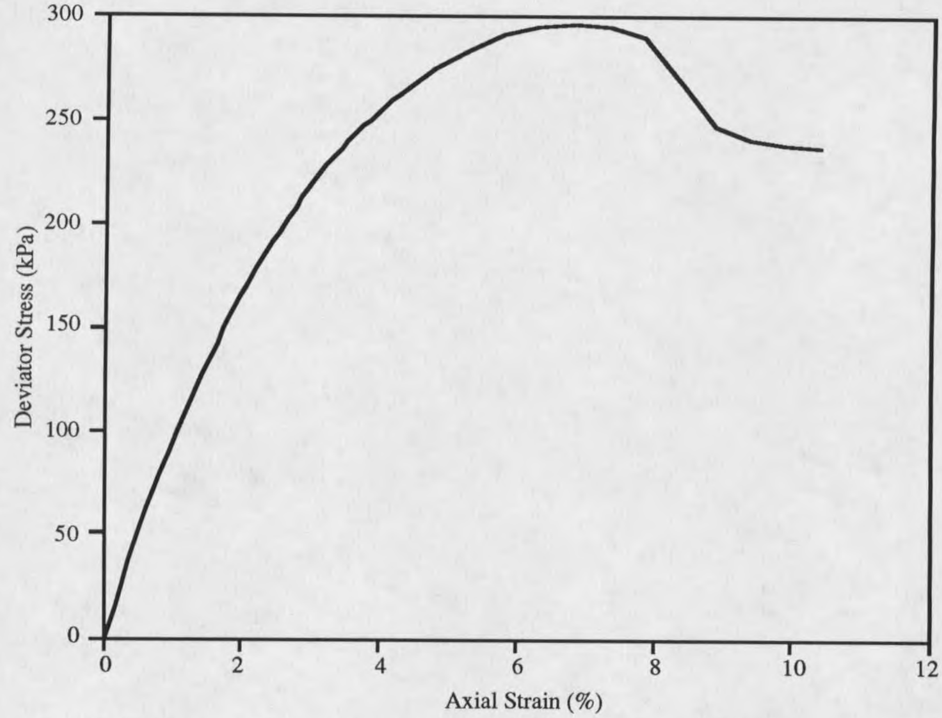

Figure 53 CTC experiment on MLS-1 at $\sigma_3 = 500$ *kPa*

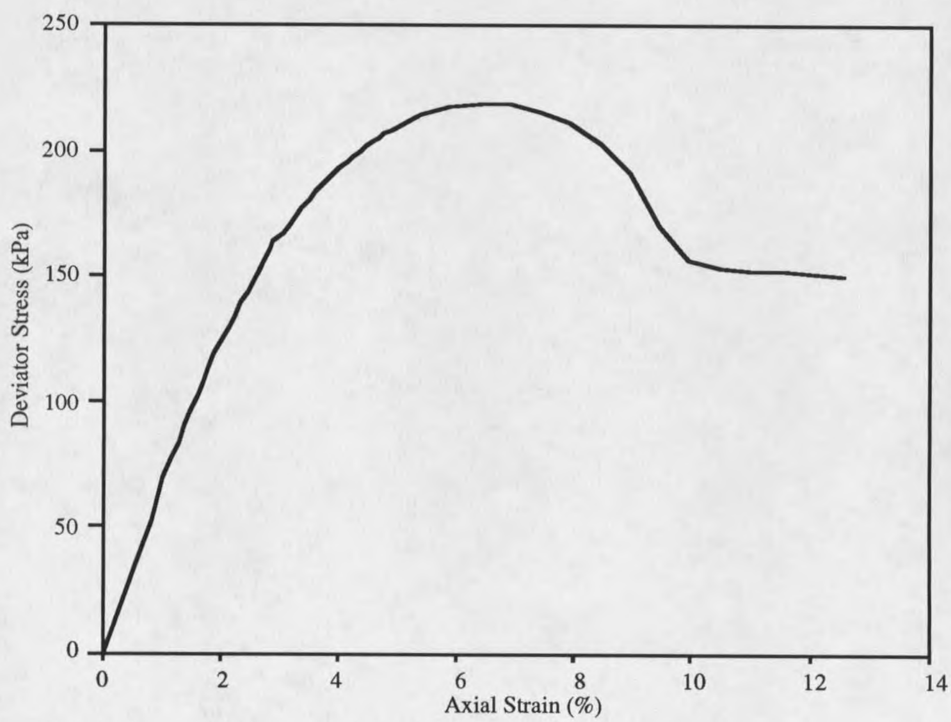

Figure 54 CTC experiment on MLS-1 at $\sigma_3 = 350$ *kPa*

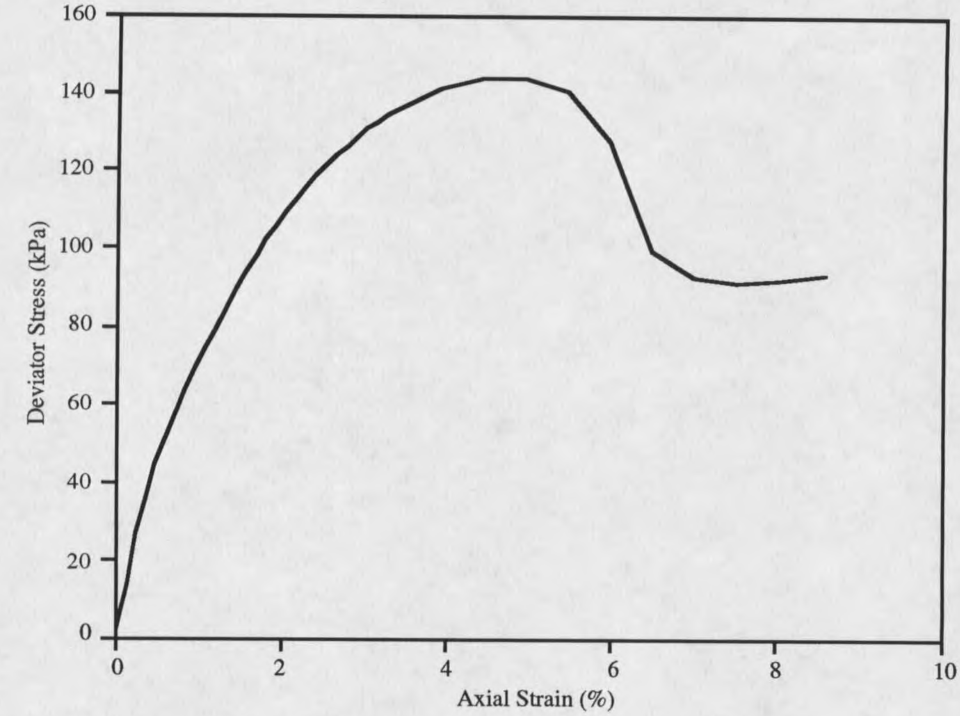

Figure 55 CTC experiment on MLS-1 at $\sigma_3 = 200\ kPa$

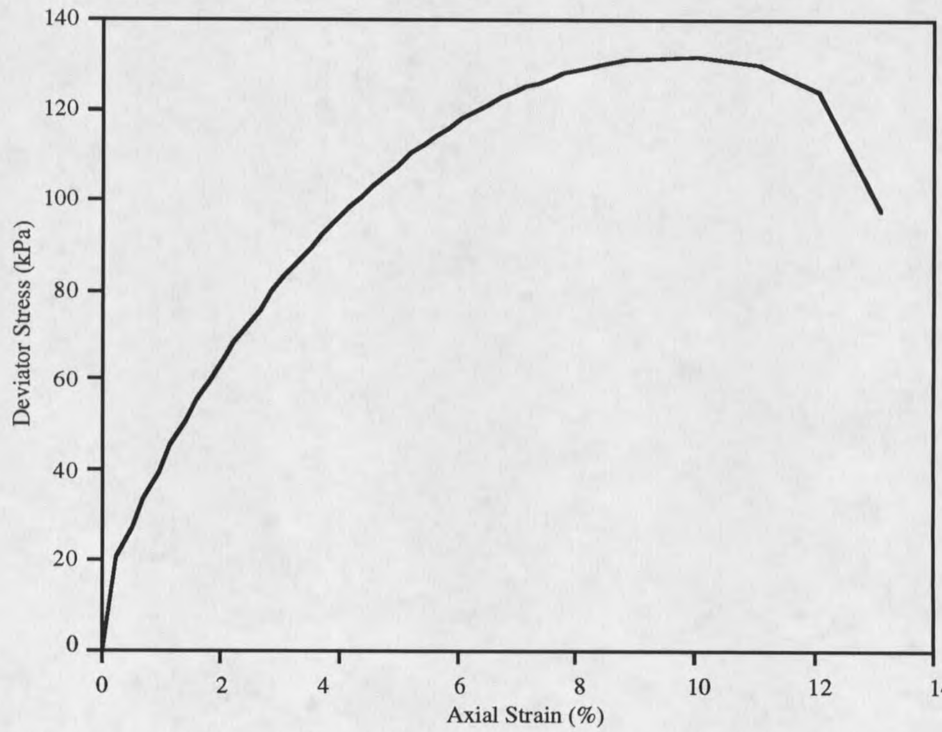

Figure 56 CTC experiment on MLS-1 at $\sigma_3 = 200\ kPa$

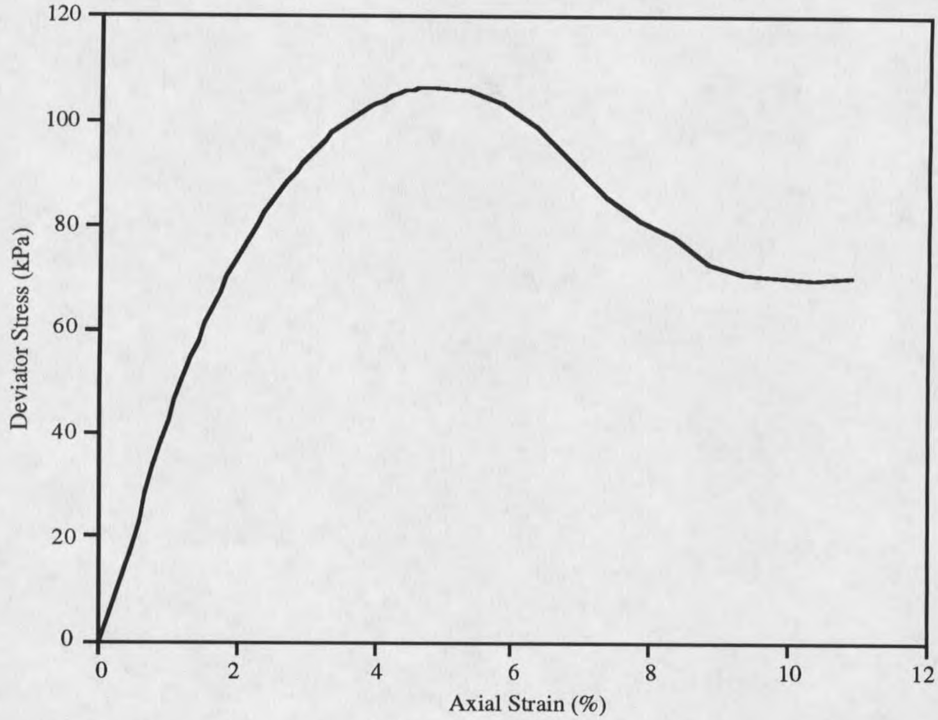

Figure 57 CTC experiment on MLS-1 at $\sigma_3 = 150\ kPa$

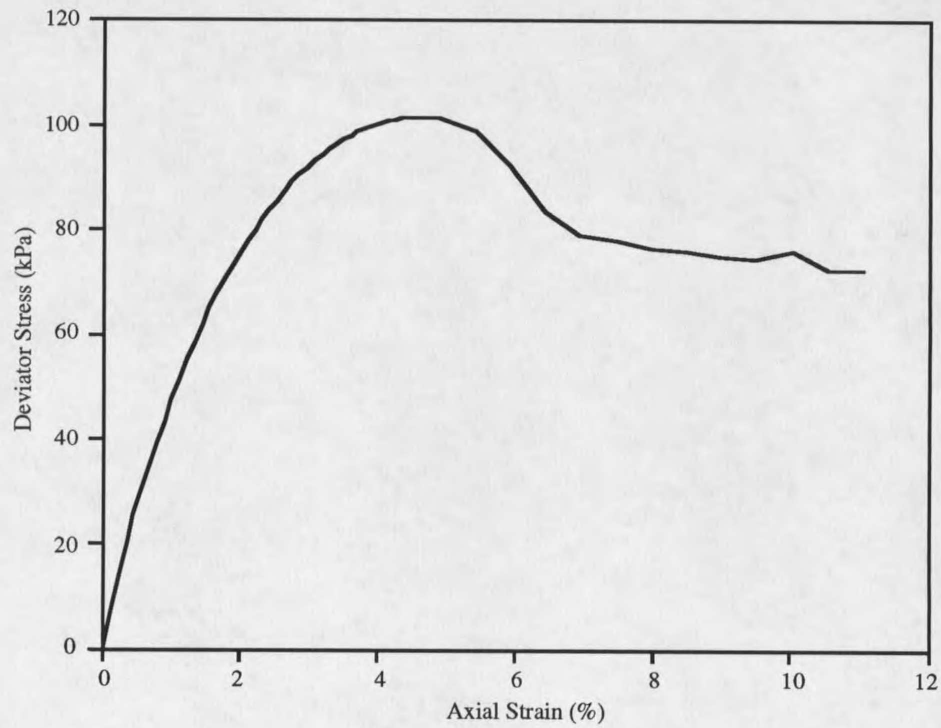

Figure 58 CTC experiment on MLS-1 at $\sigma_3 = 150\ kPa$

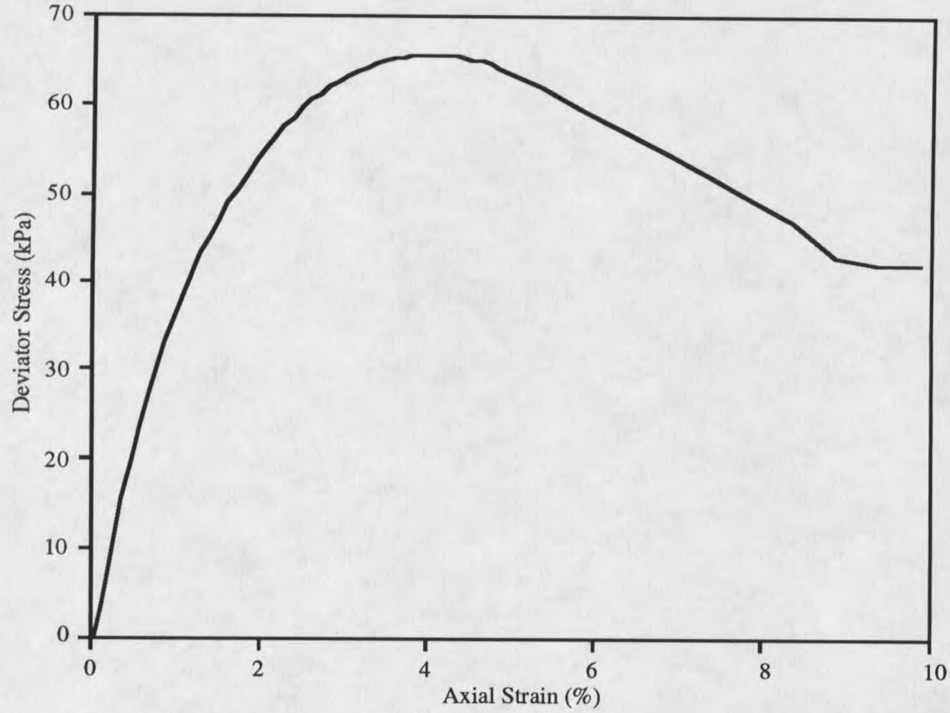

Figure 59 CTC experiment on MLS-1 at $\sigma_3 = 100\ kPa$

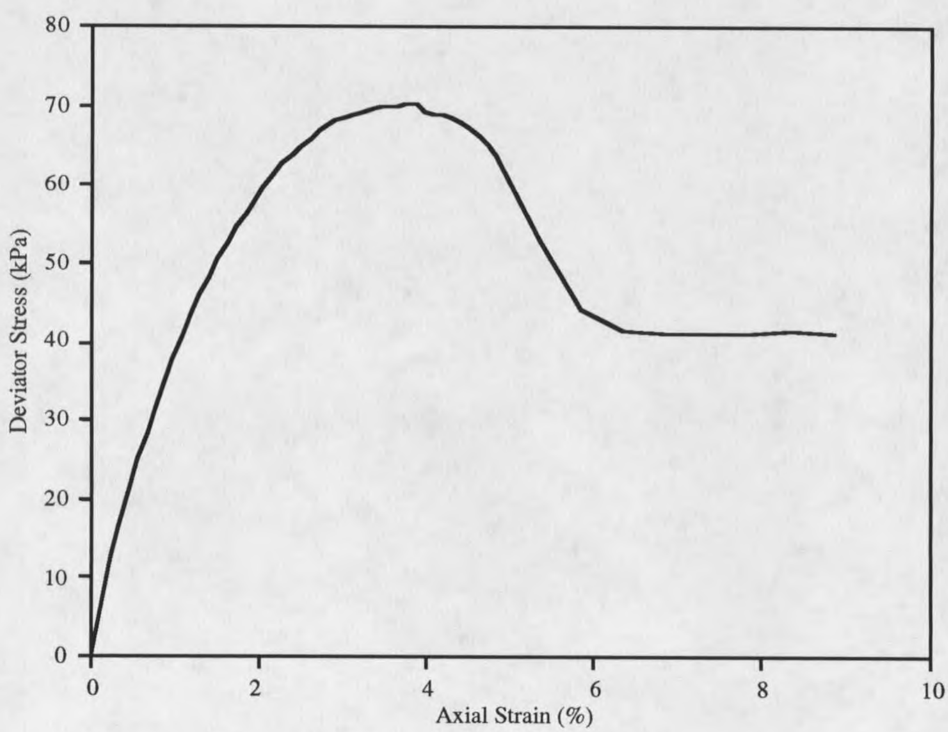

Figure 60 CTC experiment on MLS-1 at $\sigma_3 = 100\ kPa$

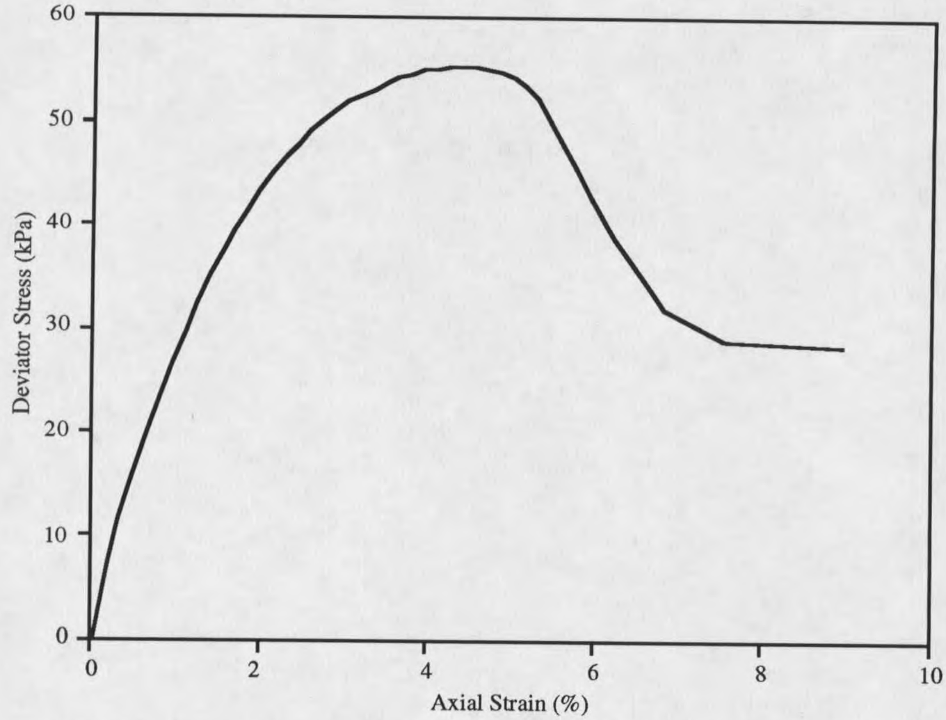

Figure 61 CTC experiment on MLS-1 at $\sigma_3 = 50\ kPa$

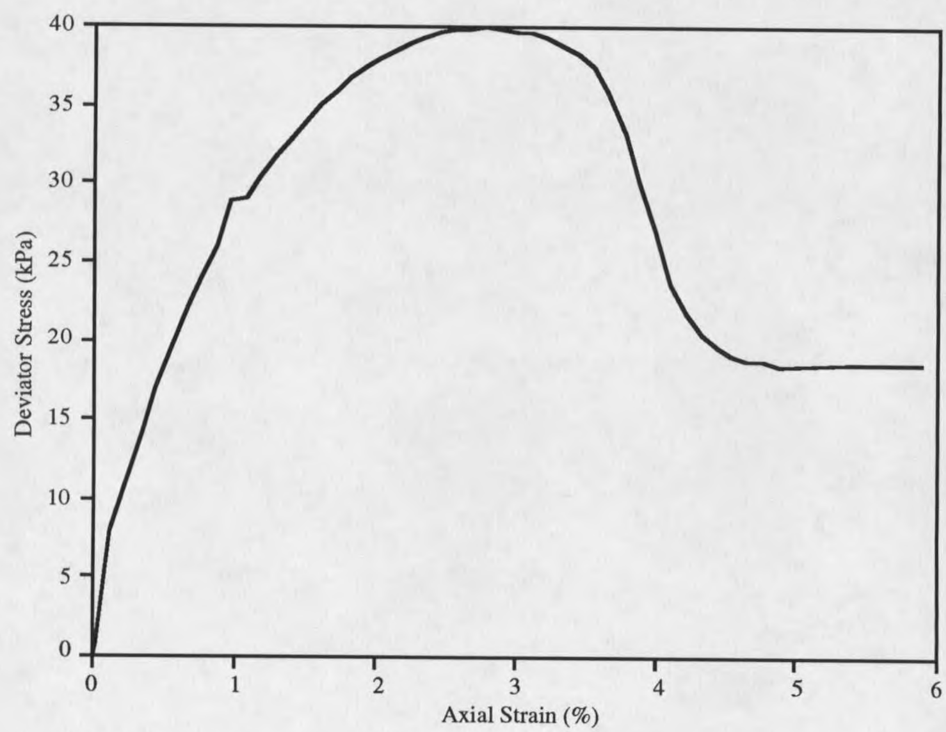

Figure 62 CTC experiment on MLS-1 at $\sigma_3 = 50\ kPa$

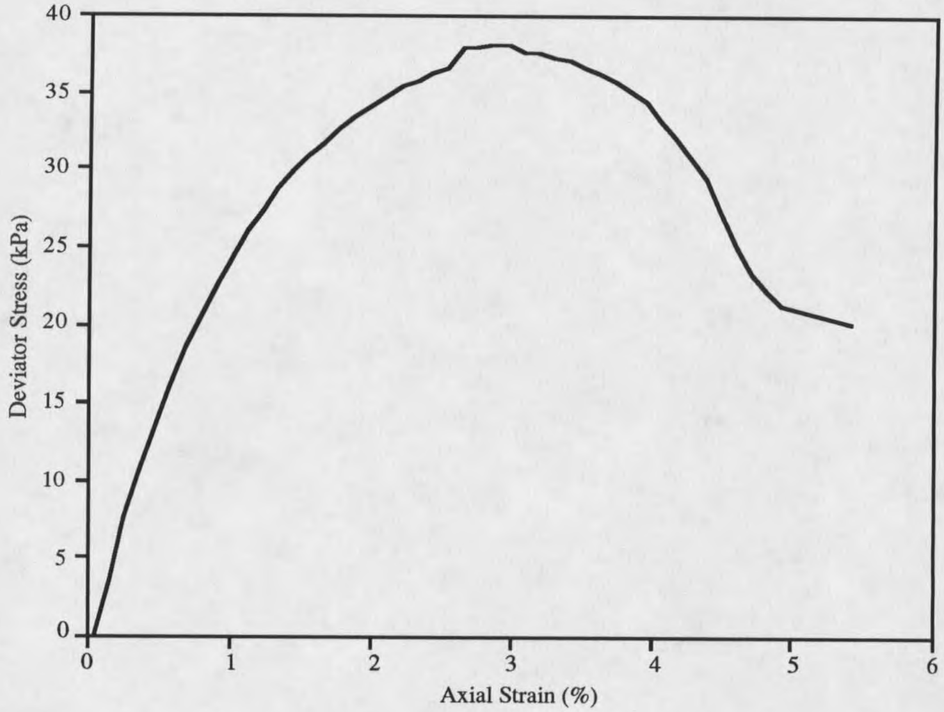

Figure 63 CTC experiment on MLS-1 at $\sigma_3 = 50\ kPa$

APPENDIX B

BEARING CAPACITY RESULTS

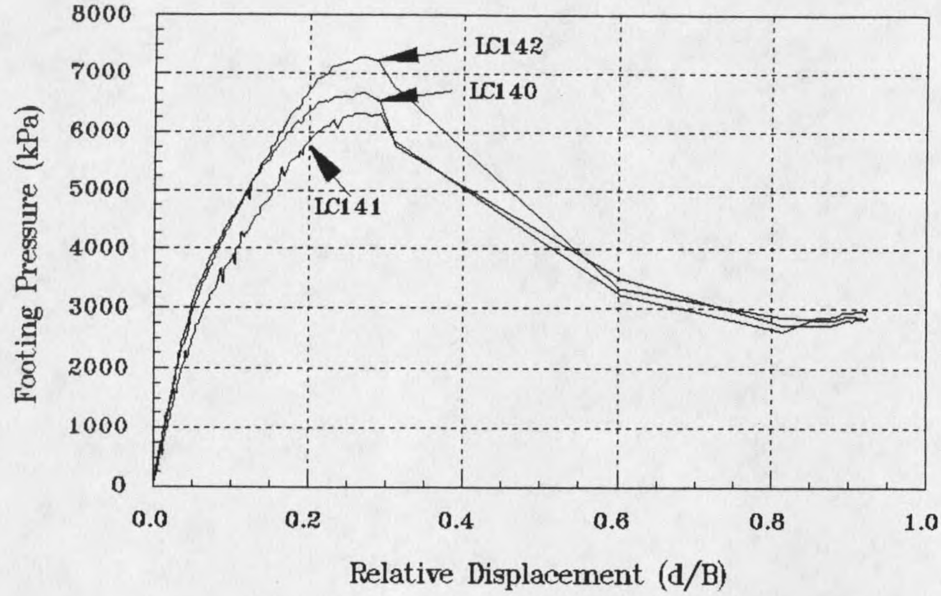

Figure 64 Bearing Capacity Result of BC3a01.O_1

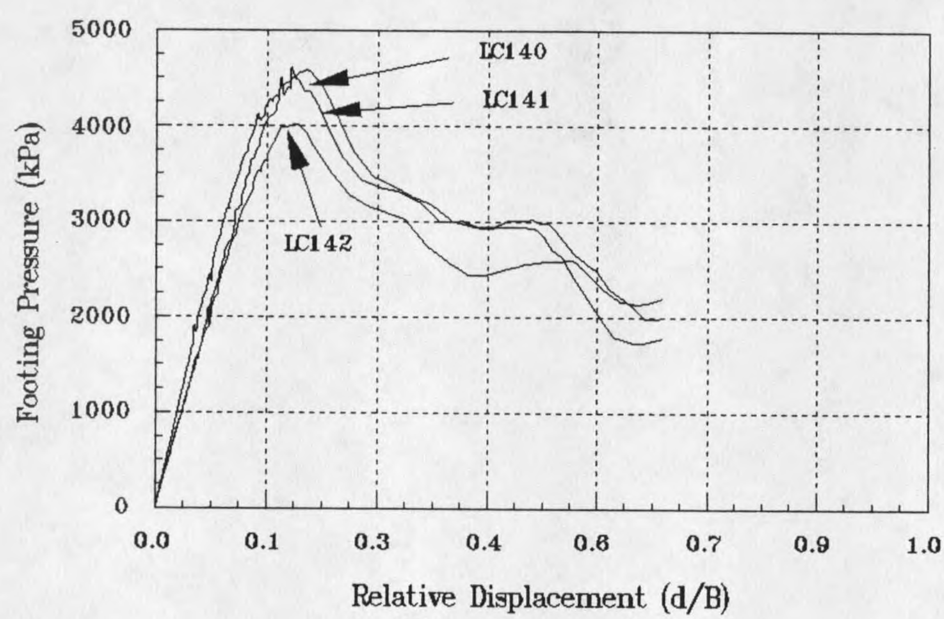

Figure 65 Bearing Capacity Result of BC3d01.O_2

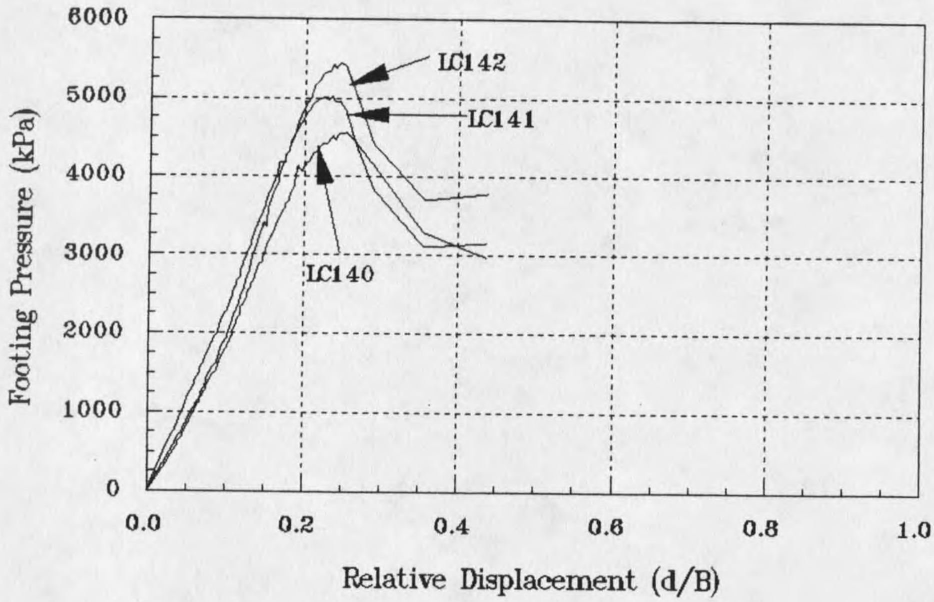

Figure 66 Bearing Capacity Result of BC3d01.O_3

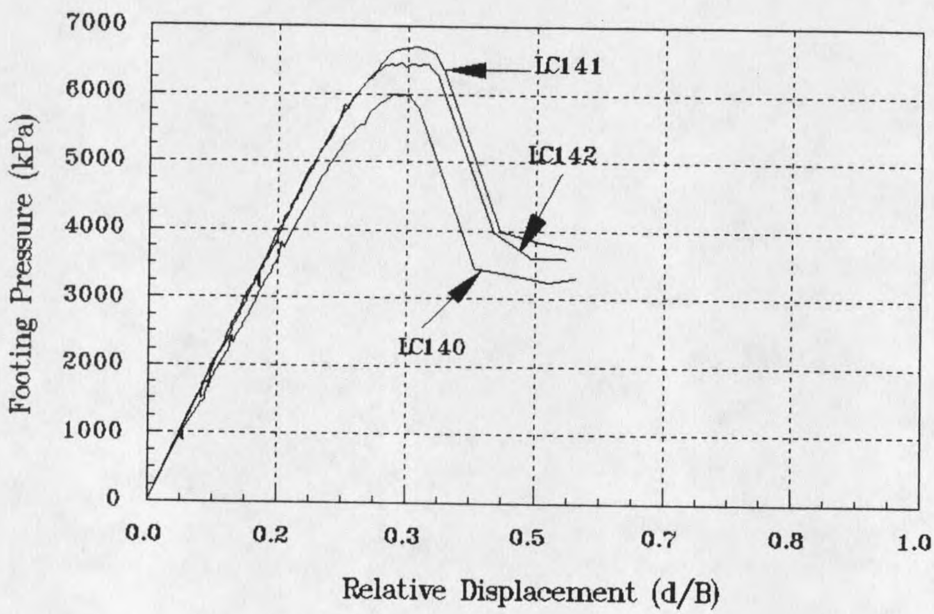

Figure 67 Bearing Capacity Result of BC3a01.O_4

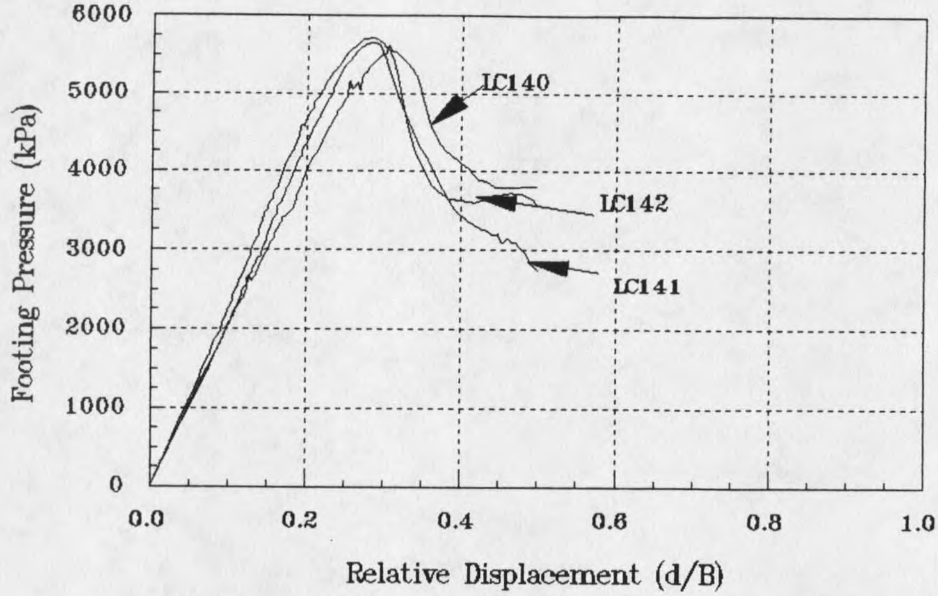

Figure 68 Bearing Capacity Result of $BC3c01.O_5$

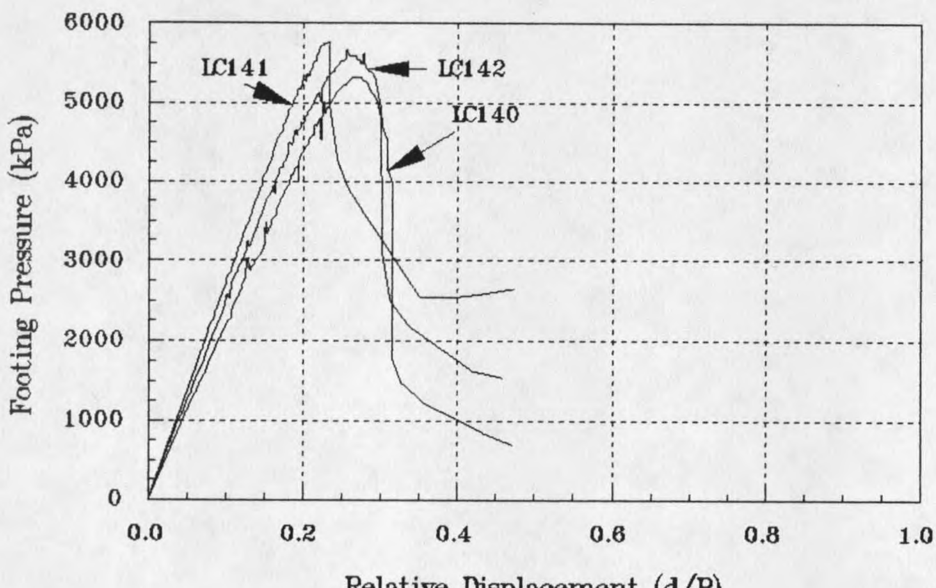

Figure 69 Bearing Capacity Result of $BC1a01.O_6$

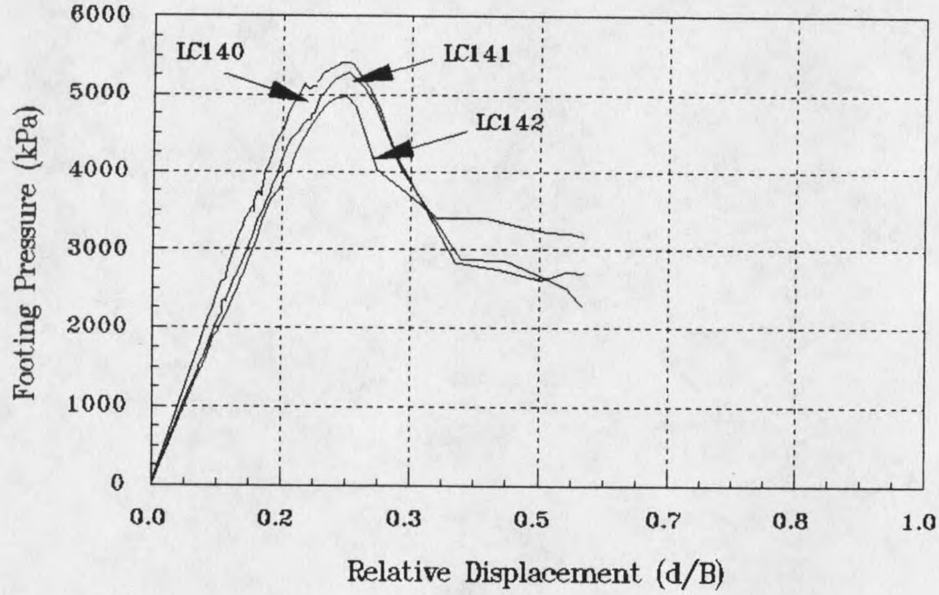

Figure 70 Bearing Capacity Result of BC1c01.O_7

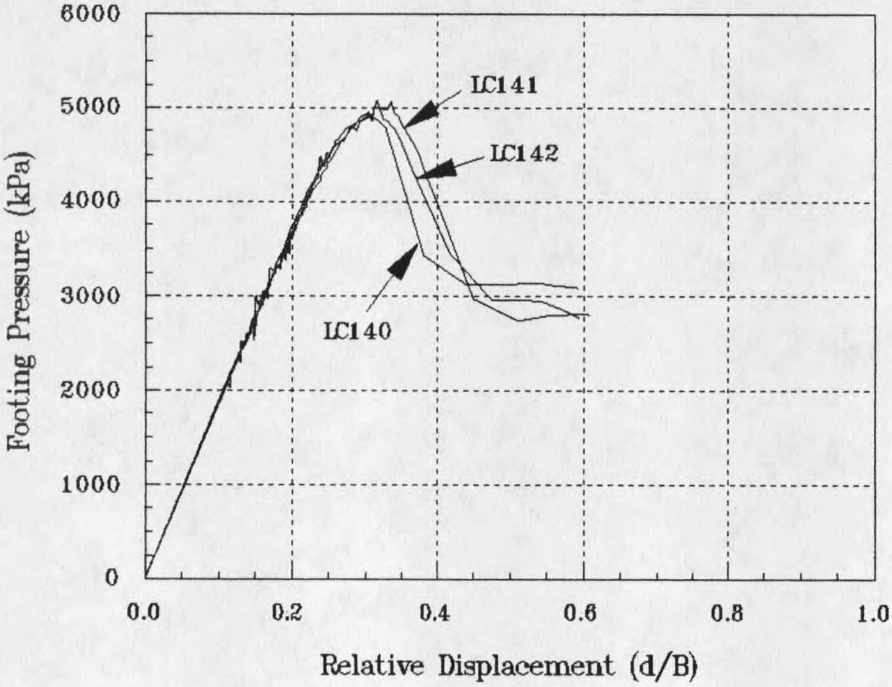

Figure 71 Bearing Capacity Result of BC3b01.O_8

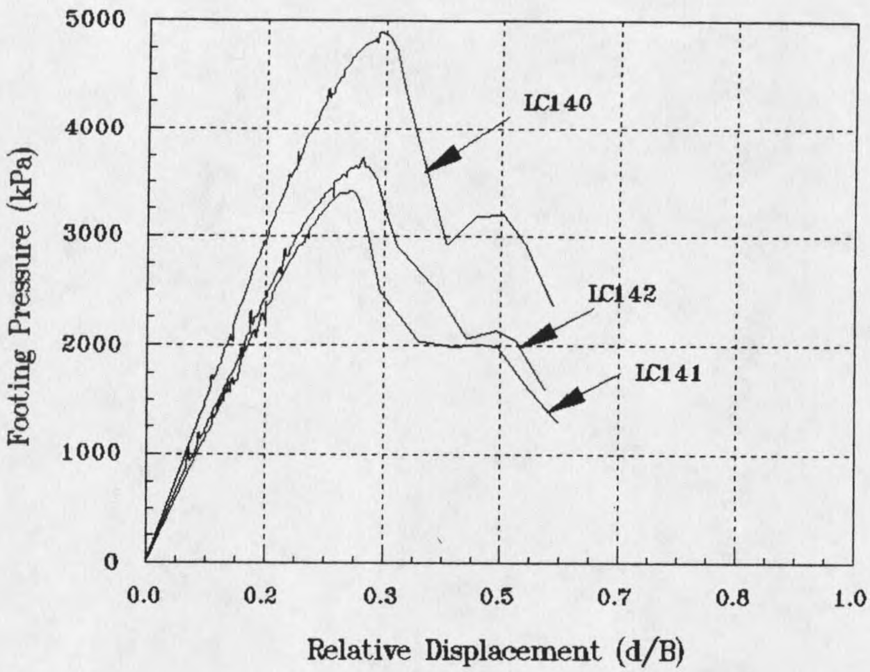

Figure 72 Bearing Capacity Result of BC3a01.O_9

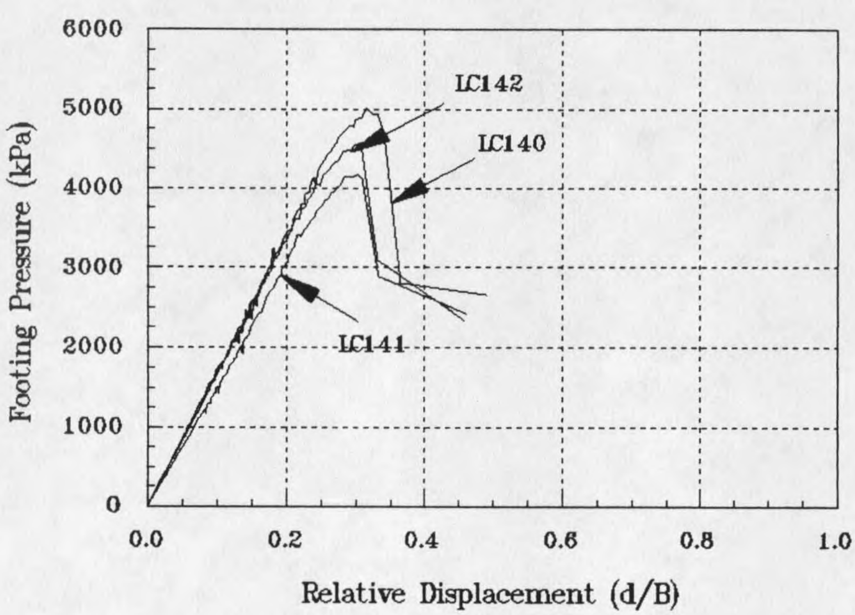

Figure 73 Bearing Capacity Result of BC3a01.O_{10}

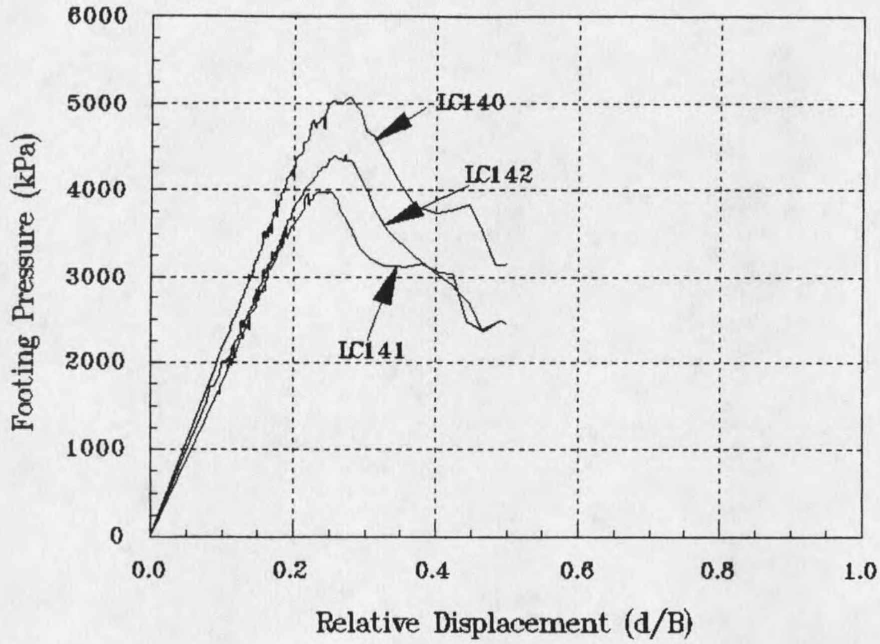

Figure 74 Bearing Capacity Result of BC3c01.O_{11}

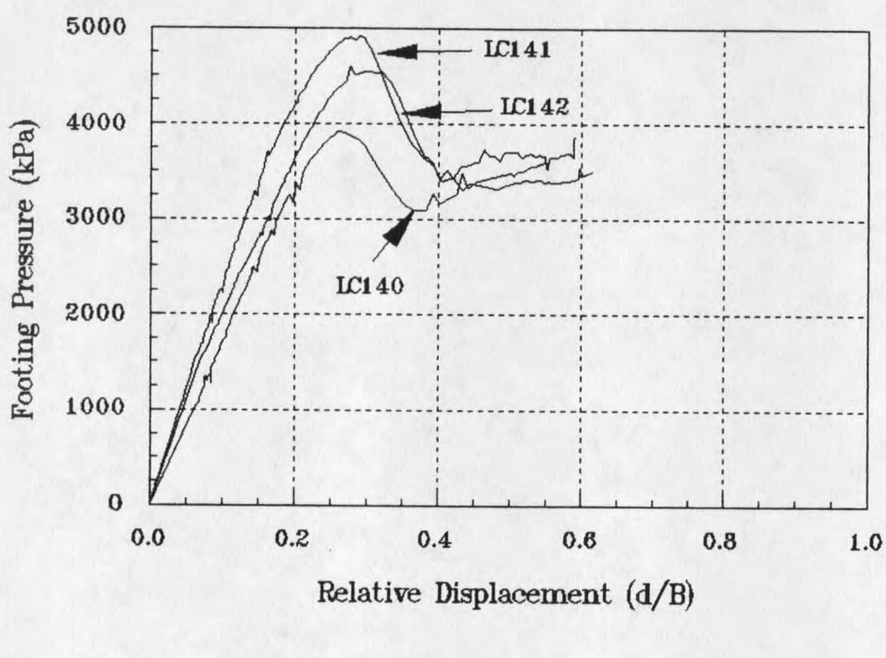

Figure 75 Bearing Capacity Result of BC2b01.O_{12}

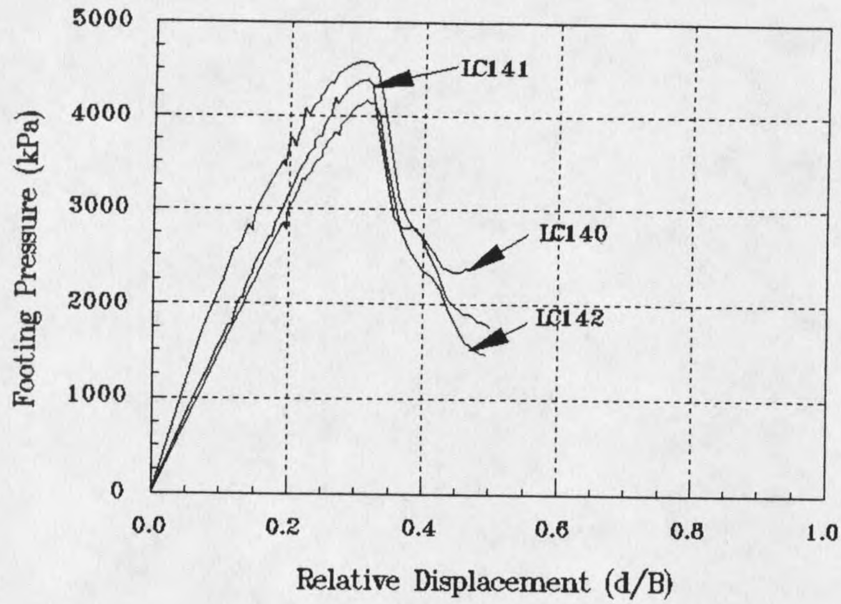

Figure 76 Bearing Capacity Result of BC1b01.O_{13}

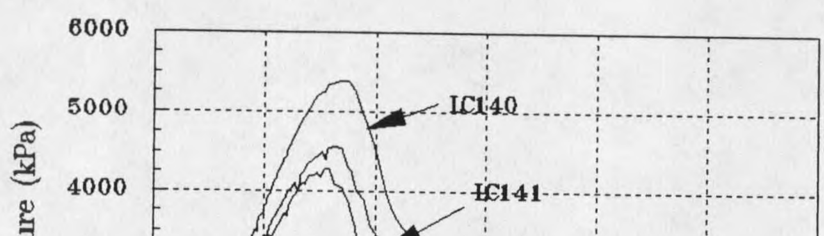

Figure 77 Bearing Capacity Result of BC2b02.O_{14}

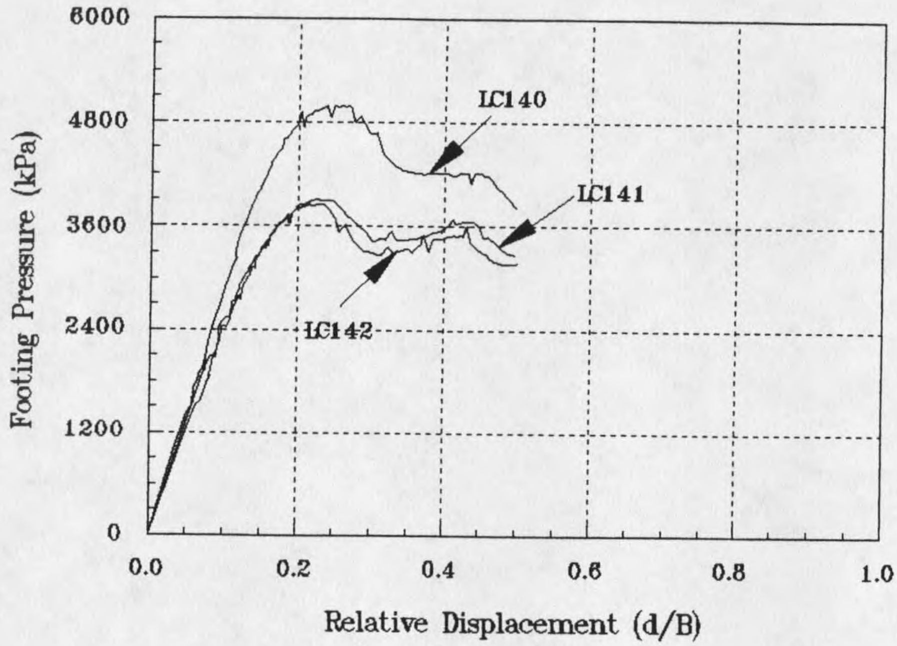

Figure 78 Bearing Capacity Result of $BC2b12.O_{15}$

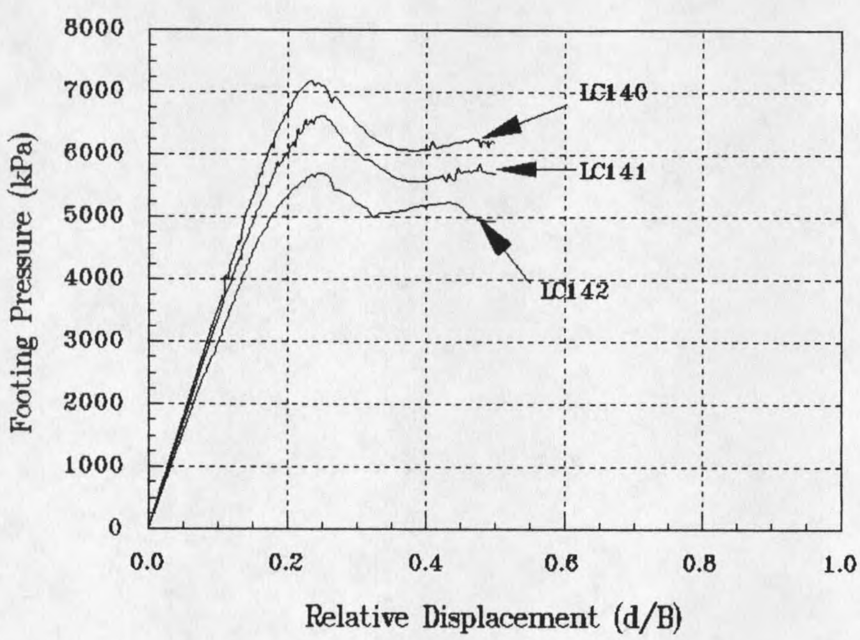

Figure 79Bearing Capacity Result of $BC2b11.O_{16}$

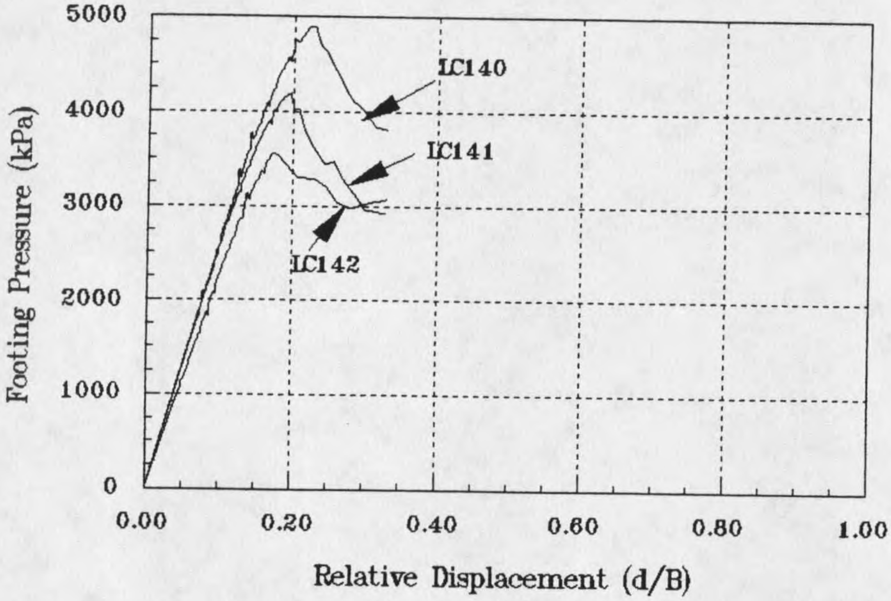

Figure 80 Bearing Capacity Result of $BC2b22.O_{17}$

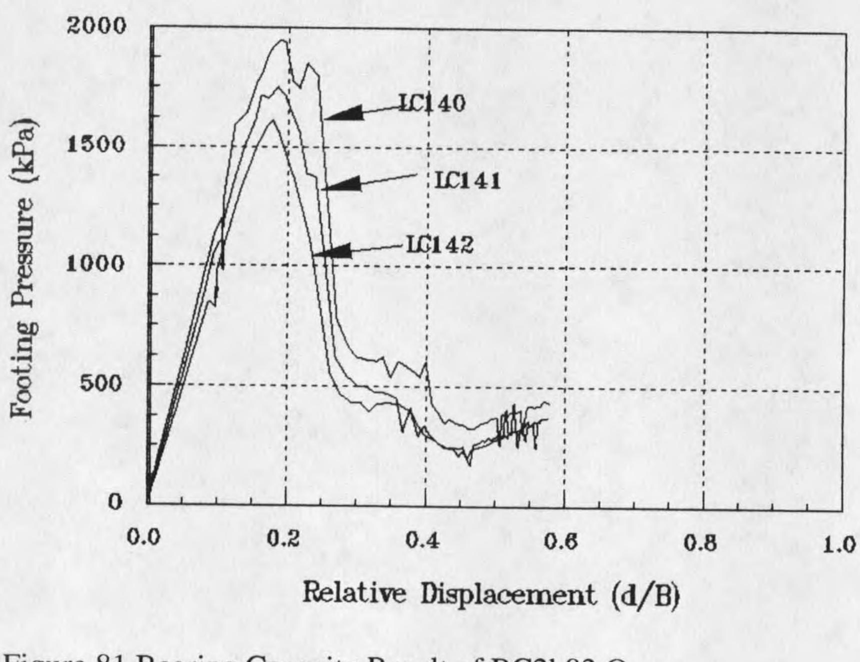

Figure 81 Bearing Capacity Result of $BC2b03.O_{18}$

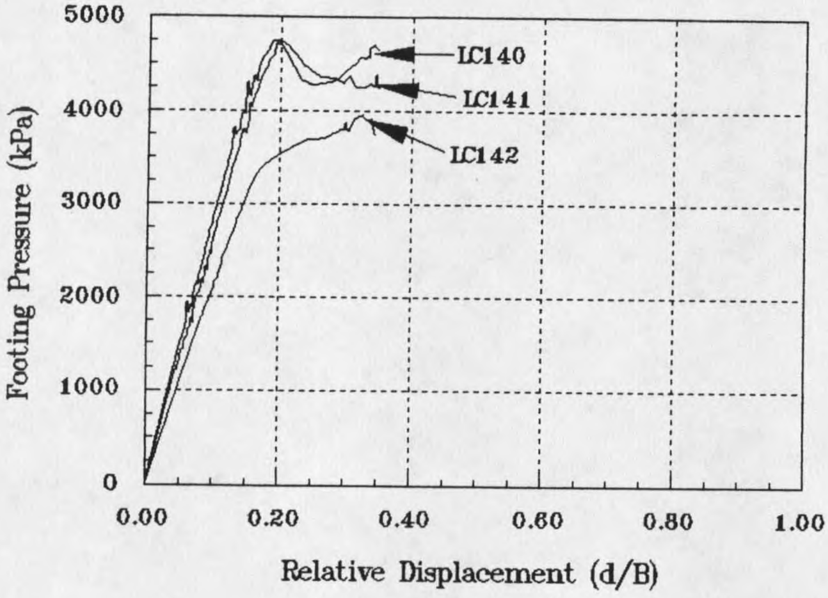

Figure 82 Bearing Capacity Result of BC2b21.O_{19}

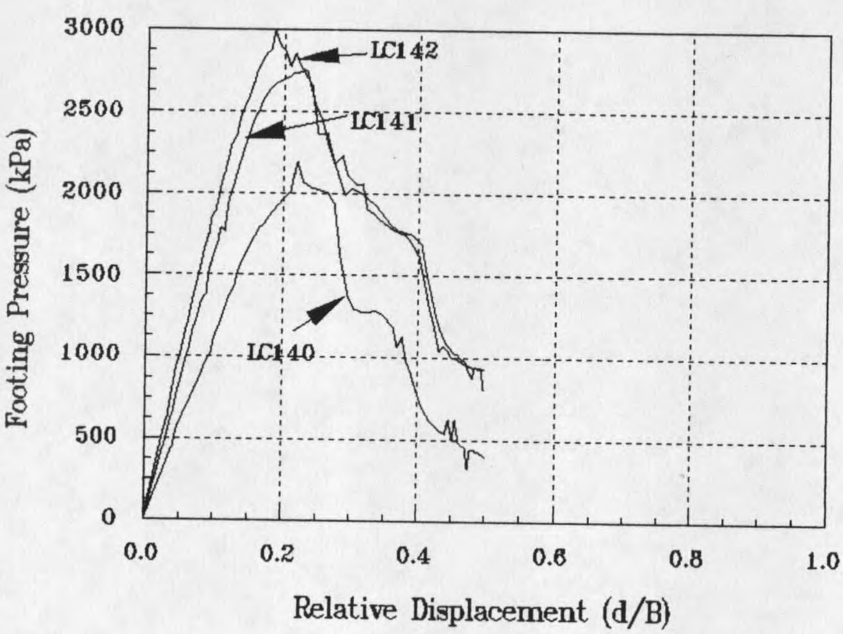

Figure 83 Bearing Capacity Result of BC2b13.O_{20}

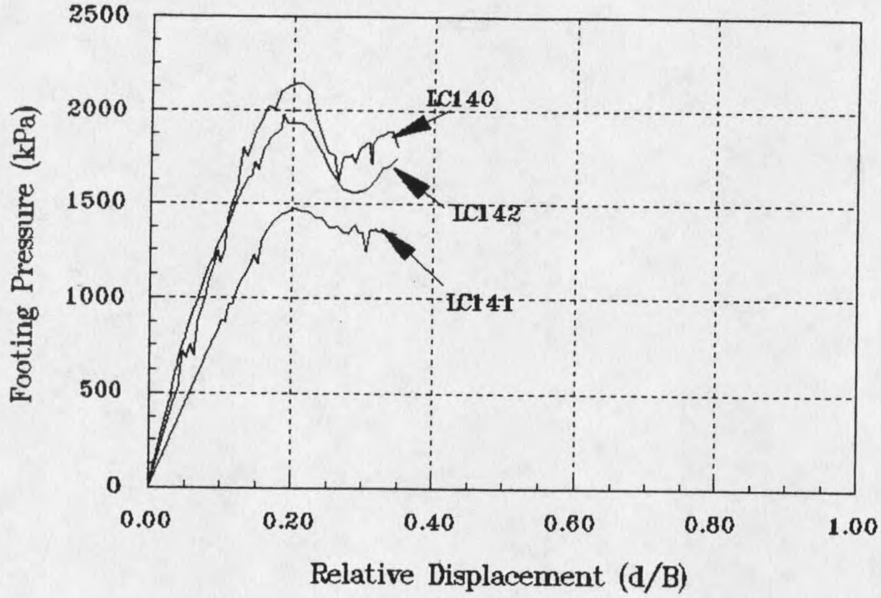

Figure 84 Bearing Capacity Result of BC2b23.O_{21}

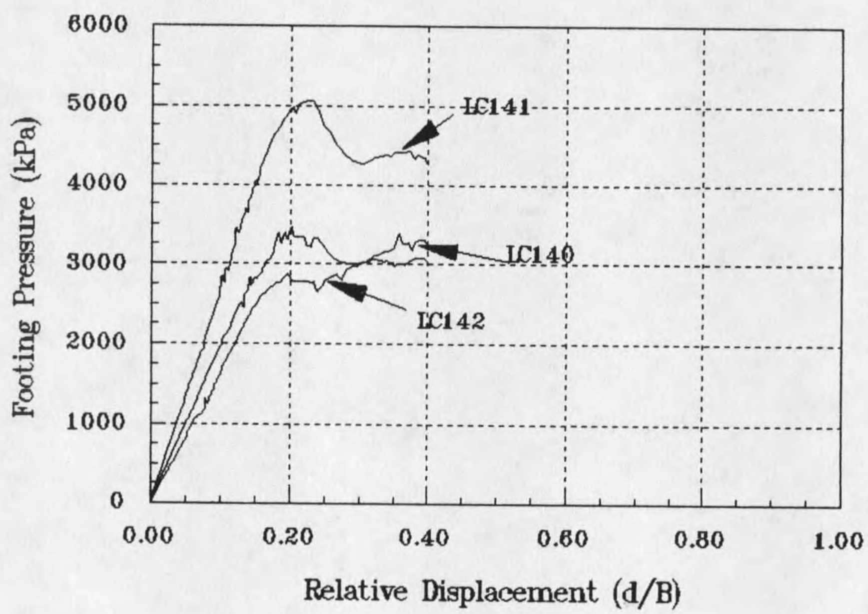

Figure 85 Bearing Capacity Result of BC2b21.O_{22}

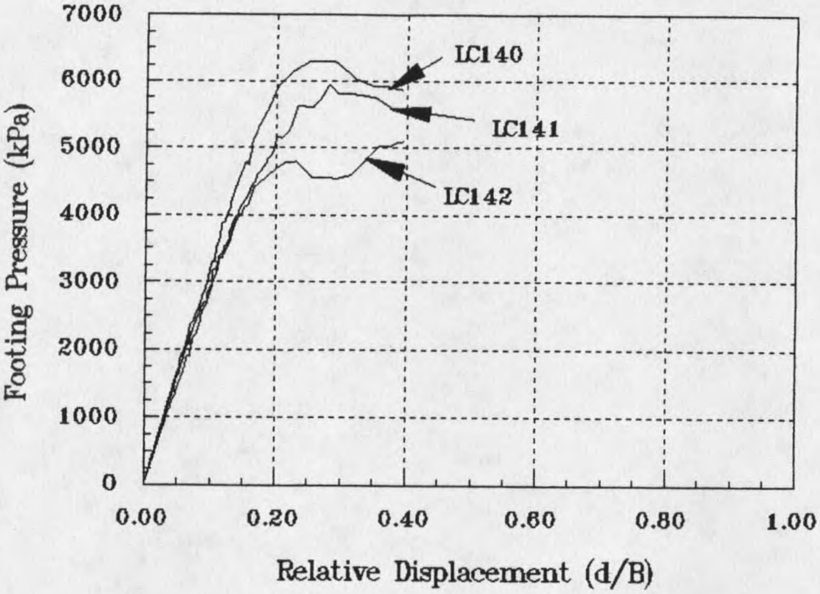

Figure 86 Bearing Capacity Result of BC2b21.O_{23}

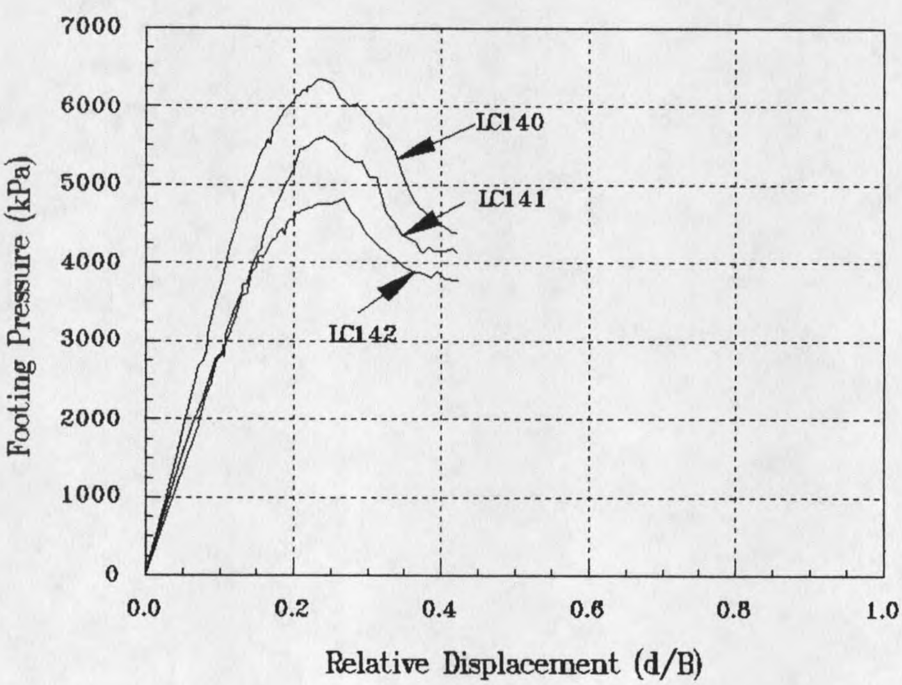

Figure 87 Bearing Capacity Result of BC9c01.O_{24}

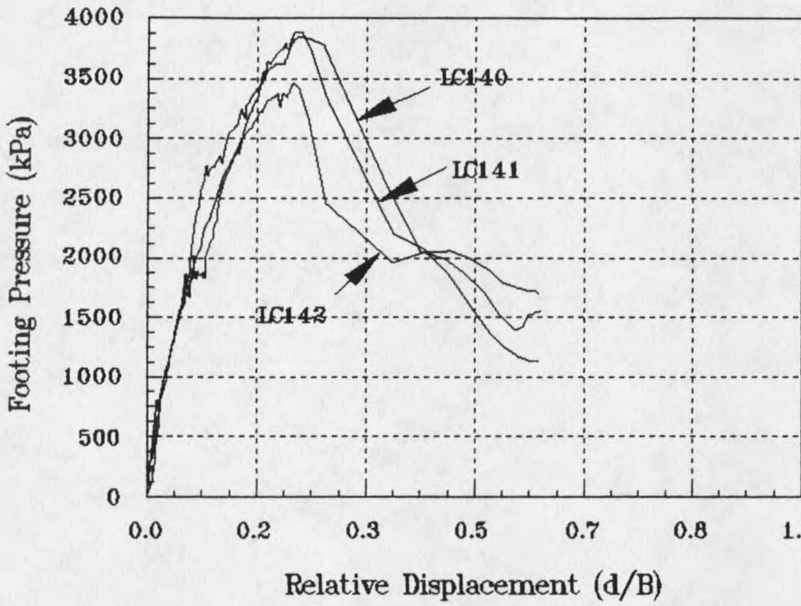

Figure 88 Bearing Capacity Result of BC3b01.O_{25}

APPENDIX C

DERIVATION OF THE SLIP - LINE METHOD

Introduction

The derivation of the slip-line method is demonstrated in this appendix. The following sections describe the process of the derivation.

Orientation of Slip Lines and Their Relations Conditions of Strain

For a general x - z coordinate system, subject to some general state of stress, σ_x, σ_z, τ_{xz}, we would like to describe the orientation of plane, or lines, where incipient failure occurs as shown in Fig.89, and this orientation can also be described as in a Mohr-Coulomb circle in Fig.90.

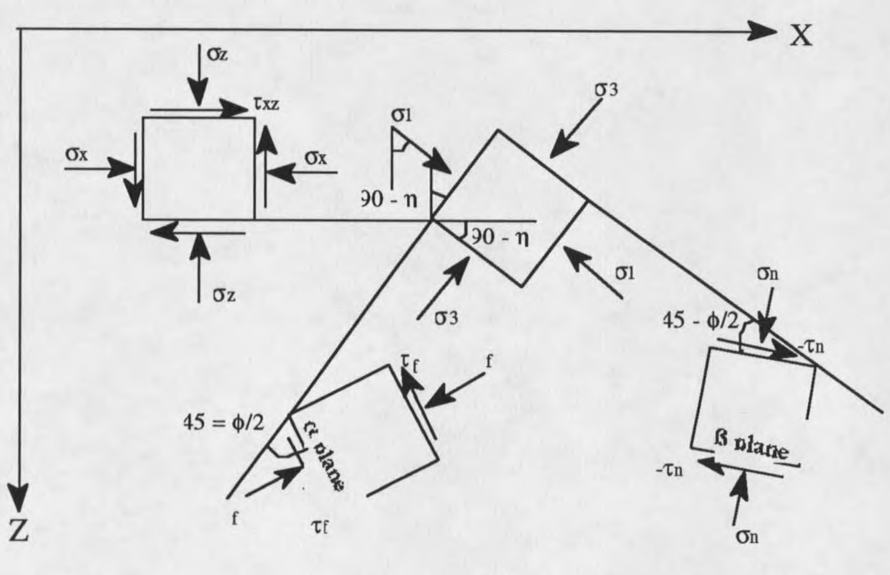

Figure 89 Orientation of the stress plane

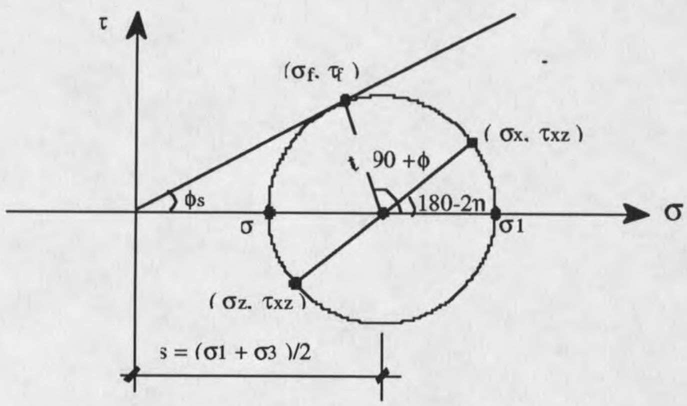

Figure 90 Mohr-Coulomb circle

The α plane and β plane in Fig.89 present two stress characteristics upon which slip occurs. From the geometry of Mohr's circle in Fig.90, we obtain expressions of σ_x, σ_z, τ_{xz} in terms of mean normal stress *s* and principle stress difference *t* for cohesionless soil:

$$\sigma_x = s + t\cos(180 - 2\eta) = s(1 - \sin\phi\cos 2\eta) \tag{55}$$

$$\tau_{xz} = t\sin(180 - 2\eta) = s\sin\phi\sin 2\eta \tag{56}$$

$$\sigma_z = s - t\cos(180 - 2\eta) = s(1 + \sin\phi\cos 2\eta) \tag{57}$$

Stress Equilibrium Equations:

For a undrained loading, we have stress equilibrium equations as following:

$$\frac{\partial \sigma_x}{\partial x} + \frac{\partial \tau_{zx}}{\partial z} = 0 \tag{58}$$

$$\frac{\partial \sigma_x}{\partial z} + \frac{\partial \tau_{xz}}{\partial x} = \gamma \tag{59}$$

we inset expressions for σ_x, σ_z, τ_{xz} from equations (55), (56) and (57) into the equilibrium equations. we then have a set of equations which satisfy equilibrium and the failure criterion for all soil within the set of stress characteristics.

$$\frac{\partial \sigma_x}{\partial x} = (1 - \sin\phi\cos 2\eta)\frac{\partial s}{\partial x} + 2s\sin\phi\sin 2\eta\frac{\partial \eta}{\partial x} \tag{60}$$

$$\partial \tau_{zx} = \sin\phi\sin 2\eta\frac{\partial s}{\partial z} + 2s\sin\phi\sin 2\eta\frac{\partial \eta}{\partial z} \tag{61}$$

$$\frac{\partial \sigma_z}{\partial z} = (1 + \sin\phi\cos 2\eta)\frac{\partial s}{\partial z} - 2s\sin\phi\sin 2\eta\frac{\partial \eta}{\partial z} \tag{62}$$

$$\partial \tau_{xz} = \sin\phi\sin 2\eta\frac{\partial s}{\partial x} + 2s\sin\phi\cos 2\eta\frac{\partial \eta}{\partial x} \tag{63}$$

substituting equations (60) to (63) into (58) and (59) we obtain:

$$(1 + \sin\phi\cos 2\eta)\frac{\partial s}{\partial z} + \sin\phi\sin 2\eta\frac{\partial s}{\partial x} - 2s\sin\phi\sin 2\eta\frac{\partial \eta}{\partial z} + 2s\sin\cos 2\eta\frac{\partial \eta}{\partial x} = \gamma \tag{64}$$

$$(1-\sin\phi\cos 2\eta)\frac{\partial s}{\partial x}+\sin\phi\sin 2\eta\frac{\partial s}{\partial z}-2s\sin\phi\sin 2\eta\frac{\partial \eta}{\partial x}+2s\sin\cos 2\eta\frac{\partial \eta}{\partial z}=0 \tag{65}$$

<u>**Solution Via Method of Characteristics**</u>

In order to use the method of characteristics, re-express equations (64) and (65) as:

$$A\frac{\partial s}{\partial x}+B\frac{\partial s}{\partial z}+C\frac{\partial \eta}{\partial x}+D\frac{\partial \eta}{\partial x}+E \tag{66}$$

$$a\frac{\partial s}{\partial z}+b\frac{\partial s}{\partial x}+c\frac{\partial \eta}{\partial z}+d\frac{\partial \eta}{\partial x} = e \tag{67}$$

Multiply equation (67) by a factor m and add to equation (66):

$$(a+mA)\frac{\partial s}{\partial x}+(b+mB)\frac{\partial s}{\partial z}+(c+mC)\frac{\partial \eta}{\partial x}+(d+mD)\frac{\partial \eta}{\partial z} = e+mE \tag{68}$$

Combine to get:

$$(b+mB)\left[\left(\frac{a+mA}{b+mB}\right)\frac{\partial s}{\partial x}+\frac{\partial s}{\partial z}\right]+(d+mD)\left[\left(\frac{c+mC}{d+mD}\right)\frac{\partial \eta}{\partial x}+\frac{\partial \eta}{\partial z}\right] = e+mE \tag{69}$$

Now, consider the total differential of s and of η:

$$ds = \frac{\partial s}{\partial x}dx+\frac{\partial s}{\partial z}dz \rightarrow \frac{ds}{dz} = \frac{\partial s}{\partial x}\frac{dx}{dz}+\frac{\partial s}{\partial z} \tag{70}$$

$$d\eta = \frac{\partial\eta}{\partial x}dx + \frac{\partial\eta}{\partial z}dz \rightarrow \frac{d\eta}{dz} = \frac{\partial\eta}{\partial x}\frac{dx}{dz} + \frac{\partial\eta}{\partial z} \tag{71}$$

If we let $\frac{dx}{dz} = \frac{a+mA}{b+mB} = \frac{c+mC}{d+mD}$, equations (70) (71) become:

$$\frac{ds}{dz} = \frac{a+mA}{b+mB}\frac{\partial s}{\partial x} + \frac{\partial s}{\partial z} \tag{72}$$

$$\frac{d\eta}{dz} = \frac{c+mC}{d+mD}\frac{\partial\eta}{\partial x} + \frac{\partial\eta}{\partial z} \tag{73}$$

Substitute equations (72) and (73) into equation (69) we obtain:

$$(b+mB)\frac{ds}{dz} + (d+mD)\frac{d\eta}{dz} = e+mE \tag{74}$$

which holds true along

$$\frac{dx}{dz} = \frac{a+mA}{b+mB} = \frac{c+mC}{d+mD}$$

This requires *m* to be given by:

$$m^2(DA-BC) + m(aD+dA-cB-Cb) + (ad-cb) = 0 \tag{75}$$

The above equation provides two real roots of *m*, from which we can solve for *s* and η along the two directions defined $\frac{dx}{dz} = f(m_1, m_2)$.

Compared equations (66) and(67) with equations (64) and (65), we have:

$A = 1 - \sin\phi\cos2\eta \quad B = \sin\phi\sin2\eta \quad C = 2s\ \sin\phi\sin2\eta \quad D = 2s\ \sin\phi\cos2\eta \quad E = 0$

$a = \sin\phi\sin2\eta \quad b = 1 + \sin\phi\cos2\eta \quad c = 2s\ \sin\phi\cos2\eta \quad d = -2s\ \sin\phi\sin2\eta \quad e = \gamma$

We now insert values for *a, b, c, d, e, A, B, C, D, E* to equation (56) to obtain the two roots of *m* and then to solve for the two directions dx/dz. After much manipulation, characteristic lines are obtained by:

$$\frac{dx}{dz} = \tan\left[\eta \pm \left(45 - \frac{\phi}{2}\right)\right] \tag{76}$$

where the negative sign represents α characteristic, and the positive sign represents β characteristic. Also, equation (74) goes to:

$$\frac{ds}{dz} = \pm 2s\tan\phi\frac{d\eta}{dz} + \gamma\left[1 \pm \tan\phi\frac{dx}{dz}\right] \tag{77}$$

where the positive sign represents α characteristic, and the negative sign represents β characteristic.

Therefore, we have four equations of (76) and (77) and four unknowns of x, z, η, and s. By moving along each of the two characteristic lines, the four unknowns can be solved at a new common point of the two characteristic lines.

Numerical Integration

To solve the four unknowns, it is necessary to numerically integrate equations (76) and (77). Two new variables, a and b are introduced to solve the equations for cohesionless soil. Let

$$a = \frac{\ln(s)}{2\tan\phi} - \eta \quad \text{with} \quad da = \frac{ds}{2s\tan\phi} - d\eta \tag{78}$$

$$b = \frac{\ln(s)}{2\tan\phi} + \eta \quad \text{with} \quad db = \frac{ds}{2s\tan\phi} + d\eta \tag{79}$$

Re-write equation (77) as:

$$ds = \pm 2s\tan\phi + \gamma\,[dz \pm \tan\phi dx]$$

For the α characteristic, we have:

$$\frac{ds}{2s\tan\phi} - d\eta = \frac{\gamma}{2s\tan\phi}[dz + \tan\phi dx] \tag{80}$$

For the β characteristic, we have:

$$\frac{ds}{2s\tan\phi} + d\eta = \frac{\gamma}{2s\tan\phi}[dz - \tan\phi dx] \tag{81}$$

From equations (78) to (79), we obtain new forms of da and db as:

$$da = \frac{\gamma}{2s\tan\phi}[dz + \tan\phi dx] \quad \text{validalong} \quad \frac{dx}{dz} = \tan[\eta - (45 - \frac{\phi}{2})] \tag{82}$$

$$db = \frac{\gamma}{2s\tan\phi}[dz - \tan\phi dx] \quad \text{validalong} \quad \frac{dx}{dz} = \tan[\eta + (45 - \frac{\phi}{2})] \tag{83}$$

Introducing finite differences to replace infinitesimal values of da, db, dx, and dz, we can re-write equations (82) and (83) as:

$$a - a_1 = \frac{\gamma}{(s + s_1)\tan\phi}[z - z_1 + \tan\phi(x - x_1)) \tag{84}$$

$$b - b_1 = \frac{\gamma}{(s + s_2)\tan\phi}[z - z_2 - \tan\phi(x - x_2)] \tag{85}$$

$$\frac{x - x_2}{z - z_2} = \tan[\frac{\eta + \eta_2}{2} - (45 - \frac{\phi}{2})) \tag{86}$$

$$\frac{x - x_1}{z - z_1} = \tan[\frac{\eta + \eta_1}{2} - (45 - \frac{\phi}{2})] \tag{87}$$

where $a_1 = \frac{\ln(s_1)}{2\tan\phi} - \eta_1 \quad b_1 = \frac{\ln(s_2)}{2\tan\phi} - \eta_2$. From equations (86) and (87) we obtain values of x and z at the new point as:

$$z = \frac{x_1 - x_2 - z_1\tan[\frac{\eta + \eta_1}{2} - (45 - \frac{\phi}{2})] + z_2\tan[\frac{\eta + \eta_2}{2} + (45 - \frac{\phi}{2})]}{\tan[\frac{\eta + \eta_2}{2} + (45 - \frac{\phi}{2})] - \tan[\frac{\eta + \eta_1}{2} - (45 - \frac{\phi}{2})]} \tag{88}$$

$$x = x_1 + (z - z_1)\tan[\frac{\eta + \eta_1}{2} - (45 - \frac{\phi}{2})] \tag{89}$$

so the expressions of a and b at the new point can be obtained from:

$$a = a_1 + \frac{\gamma}{(s+s_1)\tan\phi}[z-z_1+\tan\phi(x-x_1)] \tag{90}$$

$$b = b_2 + \frac{\gamma}{(s+s_2)\tan\phi}[z-z_2-\tan\phi(x-x_2)] \tag{91}$$

and values of η, s at the new point can be calculated by:

$$\eta = \frac{b+a}{2} \quad ; \quad s = \exp[(b+a)\tan\phi] \tag{92}$$

For a soil with cohesion and frictional angle (c, ϕ), we can derive that:

$$a_1 = \frac{\ln(s_1+\frac{c}{\tan\phi})}{2\tan\phi} - \eta_1 \ ; \ b_1 = \frac{\ln(s_2+\frac{c}{\tan\phi})}{2\tan\phi} + \eta_2 \tag{93}$$

For this case, the values of x and z at the new common point still can be obtained by equations (88) and (89), and the equations of a and b at the new point can be expressed as:

$$a = a_1 + \frac{\gamma}{(s+s_1)\tan\phi+2c}[z-z_1+\tan\phi(x-x_1)] \tag{94}$$

$$b = b_2 + \frac{\gamma}{(s+s_2)\tan\phi + 2c}[z - z_2 - \tan\phi(x - x_2)] \tag{95}$$

and

$$\eta = \frac{b-a}{2} \quad ; \quad s = \exp[(b+a)\tan\phi] - \frac{c}{\tan\phi} \tag{96}$$

The slip-line solution on ultimate bearing capacity of shallow strip footings

The typical failure area of bearing capacity problems of a strip footing can be considered a combination of three different zones as illustrated in Fig.30. Mathematically, these three zones can be solved by using different type solutions of characteristics, e.g. Goursat. zone I can be considered as Cauchy problem, zone II and zone III can be considered as Goursat and mixed problems respectively. The numerical integration may be directly applied to solve the Cauchy problem, where values of x, z, s,η are known on a given boundary. The procedure can be directly applied to give all points in the triangular field. For the Gousat problem we assume that s, η are known in the Prandtl singular point p and the geometry of the two characteristics A and B are given. From the geometry conditions η is know along both A and B and s then can be calculated for all points along A and B by the above integration procedure. It should note that, at the Prandtl singular point in this zone, β characteristic is a point, while all α characteristics pass through this point. If we treat that the Prandtl singular point is a infinitesimal β characteristic and

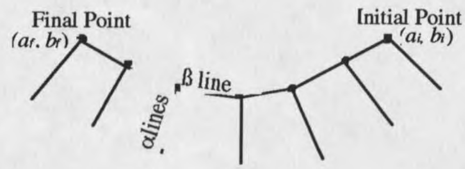

Figure 91 Pandtl singularity for Goursat solution

intersects into (n-1) increments by n α characteristics as shown in Fig.91. Since b represents value of the ß characteristic at a point, b is a constant at the Prandtl singularity. If we express b_i at the initial and b_f at the final point, we have

$$b_i = \frac{\ln(s_i + \frac{c}{\tan\phi})}{2\tan\phi} + \eta_i \;\; ; \;\; b_f = \frac{\ln(s_f + \frac{c}{\tan\phi})}{2\tan\phi} + \eta_f$$

From b_f - $b_i = 0$, we can obtain

$$s_f = (s_i + \frac{c}{\tan\phi})\exp[(\eta_i - \eta_f)2\tan\phi] - \frac{c}{\tan\phi} \tag{97}$$

where

$$s_i = \frac{\sigma_1 + \sigma_3}{2} = \frac{\sigma_3 \tan^2(45 + \frac{\phi}{2}) + 2c\tan(45 + \frac{\phi}{2}) + \sigma_3}{2}$$

As $\sigma = q_o$ (surcharge of the footing) s_i can be expressed as:

$$s_i = \frac{q[1+\tan^2(45+\frac{\phi}{2})]+2c\tan(45+\frac{\phi}{2})}{2} \tag{98}$$

and $\eta = \pi/2$, x and z at all points along the Prandtl singularity are zero. The value of η can be calculated by the following equation:

$$\eta_f = \eta_i - \Delta\eta = \frac{\pi}{2} - \frac{\pi}{2(n-1)}I \tag{99}$$

where n is the total number of the α characteristic passing through the Prandtl singularity, and I is the number of increments along the Prandtl singularity.

For the mixed zone, the values of s and η are known in one characteristics obtained from the integration of the second zone, and the direction of the principle stress is known in one boundary where η can be obtained from the roughness of footing bases. In our program, three different cases regarding roughness of footing bases are taken into account, perfect smooth footing base and partial rough footing base. These three footing base roughness cause different values of η at the boundary. As shown in Fig.92, for perfect smoothing footing base, the major principal stress σ_1 is vertical and η is zero for this case.For partial rough footing base, we assume that the direction of major principal stress changes from η =0 at the center of the footing to η =-(45+ϕ/2) at the end edge of the footing. For this case, expression of η at any point along the footing base can be defined as:

$$\eta_i = \frac{x_i}{B/2}(45+\frac{\phi}{2}) - (45+\frac{\phi}{2}) \tag{100}$$

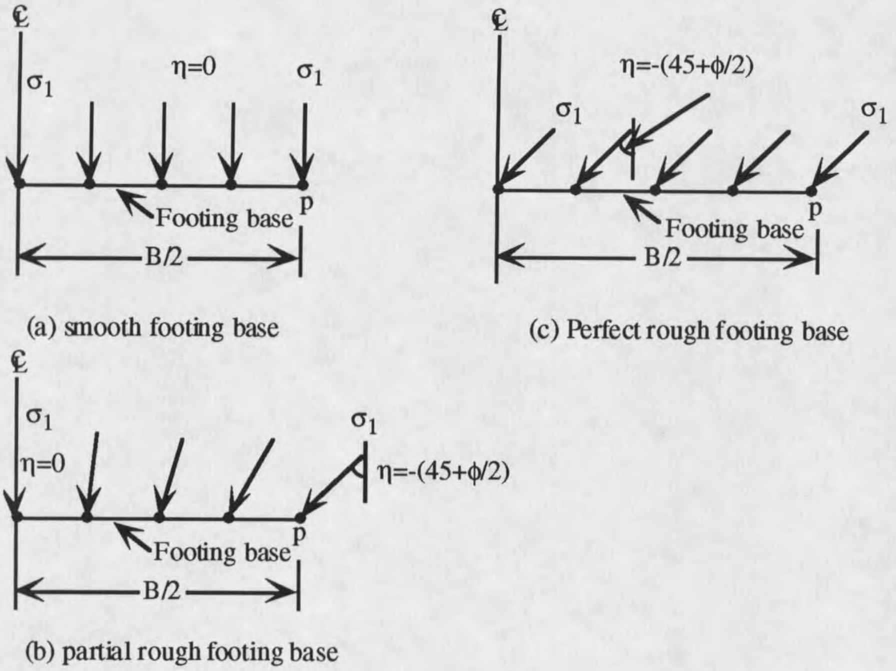

Figure 92 Direction of major principal stress for different roughness of footing bases

where x_i is the x coordinate of the ith point along the footing base, B is the footing width.

For perfect rough footing base, the direction of σ_1 is unchanged along the footing base and η =-(45+ϕ/2).

APPENDIX D

PROGRAMS OF THE SLIP - LINE METHOD

Program of Bearing Capacity Computation for Smooth Footing Base

```
*********************************************************************
*
* PROGRAM: CHARTS                                    *
* --------------                           *
* SOLUTION TO THE BEARING CAPACITY PROBLEM FOR A C, PHI, GAMMA *
* SOIL USING SLIP LINE FIELDS AND THE METHOD OF CHARACTERISTICS *
* DATA INPUT CONSISTS OF NUMBER OF INITIAL POINTS ALONG THE      *
* RANKINE PASSIVE ZONE, ITERATION TOLERANCE, FOOTING WIDTH, PHI*
* C AND GAMMA, AND SURCHARGE FOR THE FIRST RUN.  PROGRAM  *
* ITERATES BY INCREASING Q SUCH THAT THE NON-DIMENSIONAL  *
* WIDTH, BO, INCREASES BY 1 FOR EACH ITERATION.  THE *
* NON-DIMENSIONAL PRESSURE, QO, IS THEN CALCULATED.  PROGRAM *
* MUST BE RUN AGAIN FOR EACH  NEW  PHI.  PERFECTLY SMOOTH  *
* FOOTING BASE.
*
*********************************************************************
*
      REAL PI,PHI,C,GAMMA,Q,PXC(20,20),PZC(20,20),SC(20,20),
     +    ETAC(20,20),PXG(20,20),PZG(20,20),SG(20,20),ETAG(20,20),
     +    PXM(20,20),PZM(20,20),SM(20,20),ETAM(20,20),QULT,PT,
     +    X1,X2,Z1,Z2,A1,B2,ETANP,SNP,Z,X,A,B,ETANEW,SNEW,SIGMA1
      INTEGER NIP,I
      OPEN(4,FILE='INP.DAT',STATUS='OLD')
      OPEN(40,FILE='LOAD.OUT',STATUS='unknown')
      PI=3.14159264
*----------------------------------------------------------------+
*    Read In Data For Number of Initial Points and Material Parameters+
*    NIP=Number of initial points                    +
*    TOL=Iteration tolerance                       +
*    FB=Footing Width                            +
*    PHI=Friction Angle (degrees)                  +
*    C=Cohesion                               +
*    GAMMA=Soil Effective Weight                       +
*----------------------------------------------------------------+
      READ(4,*)NIP,TOL
      READ(4,*)FB
      READ(4,*)PHI,C,GAMMA
      FBI=FB
      FBN=FB
*----------------------------------------------------------------+
*----------------------------------------------------------------+
```

```
*    SOLUTION TO THE CAUCHY PROBLEM (RANKINE ZONE)                    +
*-----------------------------------------------------------------+
*-----------------------------------------------------------------+
*    Read in Data For Initial Points On The Free Boundary For the    +
*    Rankine (Cauchy) Zone:                                        +
*    Q=Uniform Vertical Surcharge On Rankine Boundary               +
*    PXC&PZC=Matricies of x and z coordinates for all points defining +
*         the intersection of characteristic lines within the      +
*         Cauchy region                                            +
*    SC=Matrix of mean normal stress at each point                 +
*    ETAC=Matrix of angles of orientation of Sigma_1 with vert. dir. +
*-----------------------------------------------------------------+
      DO 11 M=1,60
      Jcount=0
      Q=(FB*GAMMA/REAL(M)-C)/TAN(PHI*PI/180.0)
    1 RPL=FBN*1.5
      Jcount=Jcount+1
      IF (Jcount .ge. 500) THEN
        GOTO 11
      ENDIF
      DO 9 I=1,NIP
        PXC(1,I)=RPL/REAL(NIP-1)*REAL(I-1)
        PZC(1,I)=0.0
    9 CONTINUE
      DO 10 I=1,NIP
        SC(1,I)=(Q*(1.0+(TAN((45.0+PHI/2.0)*PI/180.0))**2.0)+
     +        2.0*C*TAN((45.0+PHI/2.0)*PI/180.0))/2.0
        ETAC(1,I)=90.0
   10 CONTINUE
*-----------------------------------------------------------------+
*    Set The Values for Data at the First Goursat Point Corresponding +
*    To the first Cauchy Point                                     +
*-----------------------------------------------------------------+
      PXG(1,1)=PXC(1,1)
      PZG(1,1)=PZC(1,1)
      SG(1,1)=SC(1,1)
      ETAG(1,1)=ETAC(1,1)
*-----------------------------------------------------------------+
*    Begin Calculating PXC, PZC, SC, ETAC For Each New Point On The  +
*    Next Row of Points From the Row Of Initial Points             +
*-----------------------------------------------------------------+
      DO 200 I=1,NIP-1
        DO 100 J=1,NIP-I
          K=1
```

```
      X1=PXC(I,J)
      Z1=PZC(I,J)
      X2=PXC(I,J+1)
      Z2=PZC(I,J+1)
      S1=SC(I,J)
      S2=SC(I,J+1)
      ETA1=ETAC(I,J)
      ETA2=ETAC(I,J+1)
      A1=ALOG(S1+C/TAN(PHI*PI/180.0))/(2*TAN(PHI*PI/180.0))-
     +   ETA1*PI/180.0
      B2=ALOG(S2+C/TAN(PHI*PI/180.0))/(2*TAN(PHI*PI/180.0))+
     +   ETA2*PI/180.0
      ETANP=(ETA1+ETA2)/2.0
      SNP=(S1+S2)/2.0
50     Z=(X1-X2-Z1*TAN(((ETANP+ETA1)/2.0-(45.0-PHI/2.0))*PI/180.0)+
     +   Z2*TAN(((ETANP+ETA2)/2.0+(45.0-PHI/2.0))*PI/180.0))/
     +   (TAN(((ETANP+ETA2)/2.0+(45.0-PHI/2.0))*PI/180.0)-
     +   TAN(((ETANP+ETA1)/2.0-(45.0-PHI/2.0))*PI/180.0))
      X=X1+(Z-Z1)*TAN(((ETANP+ETA1)/2.0-(45.0-PHI/2.0))*PI/180.0)
      A=A1+GAMMA/((SNP+S1)*TAN(PHI*PI/180.0)+2.0*C)*(Z-Z1+
     +   TAN(PHI*PI/180.0)*(X-X1))
      B=B2+GAMMA/((SNP+S2)*TAN(PHI*PI/180.0)+2.0*C)*(Z-Z2-
     +   TAN(PHI*PI/180.0)*(X-X2))
      ETANEW=(B-A)/2.0*180.0/PI
      SNEW=EXP((B+A)*TAN(PHI*PI/180.0))-C/TAN(PHI*PI/180.0)
      K=K+1
      IF (K .ge. 500) THEN
        GOTO 11
      ENDIF
      IF (ABS(SNEW-SNP) .GT. TOL .OR. ABS(ETANEW-ETANP) .GT.
     +   TOL) THEN
        SNP=SNEW
        ETANP=ETANEW
        GOTO 50
      ENDIF
*----------------------------------------------------------------+
*   Define The New Values For The New Row of Points              +
*   (where I is now taken as 1 for the initial row of points)    +
*----------------------------------------------------------------+
      PXC(I+1,J)=X
      PZC(I+1,J)=Z
      SC(I+1,J)=SNP
      ETAC(I+1,J)=ETANP
*----------------------------------------------------------------+
```

```
*    Record data for points lying on the boundary between the        +
*    Cauchy and Goursat zones                                        +
*--------------------------------------------------------------------+
          IF(J.EQ.1) THEN
            PXG(I+1,1)=PXC(I+1,J)
            PZG(I+1,1)=PZC(I+1,J)
            SG(I+1,1)=SC(I+1,J)
            ETAG(I+1,1)=ETAC(I+1,J)
          ENDIF
 100    CONTINUE
 200 CONTINUE
*--------------------------------------------------------------------+
*--------------------------------------------------------------------+
*    SOLUTION TO THE GOURSAT PROBLEM (LOG-SPIRAL ZONE)                +
*--------------------------------------------------------------------+
*--------------------------------------------------------------------+
*    Define Data Values Along the Beta Line Corresponding to the     +
*    Prandtl Singularity                                             +
*--------------------------------------------------------------------+
      DO 400 I=1,NIP-1
        PXG(1,I+1)=0.0
        PZG(1,I+1)=0.0
        ETAG(1,I+1)=PI/2.0-PI/2.0/REAL(NIP-1)*REAL(I)
        SG(1,I+1)=(SC(1,1)+C/TAN(PHI*PI/180.0))*EXP((PI/2.0-
     +        ETAG(1,I+1))*2.0*TAN(PHI*PI/180.0))-C/TAN(PHI*PI/180.0)
        ETAG(1,I+1)=ETAG(1,I+1)*180.0/PI
 400 CONTINUE
*--------------------------------------------------------------------+
*    Begin Calculating PXG, PZG, SG, ETAG For Each New Point On The  +
*    New Alpha Characteristic Line                                   +
*--------------------------------------------------------------------+
      DO 600 I=1,NIP-1
        DO 500 J=1,NIP-1
          K=1
          X1=PXG(J,I+1)
          Z1=PZG(J,I+1)
          X2=PXG(J+1,I)
          Z2=PZG(J+1,I)
          S1=SG(J,I+1)
          S2=SG(J+1,I)
          ETA1=ETAG(J,I+1)
          ETA2=ETAG(J+1,I)
          A1=ALOG(S1+C/TAN(PHI*PI/180.0))/(2*TAN(PHI*PI/180.0))-
     +       ETA1*PI/180.0
```

```
      B2=ALOG(S2+C/TAN(PHI*PI/180.0))/(2*TAN(PHI*PI/180.0))+
     +     ETA2*PI/180.0
      ETANP=(ETA1+ETA2)/2.0
      SNP=(S1+S2)/2.0
150     Z=(X1-X2-Z1*TAN(((ETANP+ETA1)/2.0-(45.0-PHI/2.0))*PI/180.0)+
     +    Z2*TAN(((ETANP+ETA2)/2.0+(45.0-PHI/2.0))*PI/180.0))/
     +    (TAN(((ETANP+ETA2)/2.0+(45.0-PHI/2.0))*PI/180.0)-
     +    TAN(((ETANP+ETA1)/2.0-(45.0-PHI/2.0))*PI/180.0))
      X=X1+(Z-Z1)*TAN(((ETANP+ETA1)/2.0-(45.0-PHI/2.0))*PI/180.0)
      A=A1+GAMMA/((SNP+S1)*TAN(PHI*PI/180.0)+2.0*C)*(Z-Z1+
     +    TAN(PHI*PI/180.0)*(X-X1))
      B=B2+GAMMA/((SNP+S2)*TAN(PHI*PI/180.0)+2.0*C)*(Z-Z2-
     +    TAN(PHI*PI/180.0)*(X-X2))
      ETANEW=(B-A)/2.0*180.0/PI
      SNEW=EXP((B+A)*TAN(PHI*PI/180.0))-C/TAN(PHI*PI/180.0)
      K=K+1
      IF (K .ge. 500) THEN
        GOTO 11
      ENDIF
      IF (ABS(SNEW-SNP) .GT. TOL .OR. ABS(ETANEW-ETANP) .GT.
     +     TOL) THEN
        SNP=SNEW
        ETANP=ETANEW
        GOTO 150
      ENDIF
*---------------------------------------------------------------+
*   Define The New Values For The New Set of Points On the Alpha Line+
*   (where I is now taken as 1 for the initial alpha line)          +
*---------------------------------------------------------------+
      PXG(J+1,I+1)=X
      PZG(J+1,I+1)=Z
      SG(J+1,I+1)=SNP
      ETAG(J+1,I+1)=ETANP
500   CONTINUE
600 CONTINUE
*---------------------------------------------------------------+
*---------------------------------------------------------------+
*   SOLUTION TO THE MIXED PROBLEM (RANKINE ACTIVE ZONE)            +
*---------------------------------------------------------------+
*---------------------------------------------------------------+
*   Register data for points lying on the boundary between the     +
*   Goursat and mixed zones                                         +
*---------------------------------------------------------------+
    DO 700 I=1,NIP
```

```
      PXM(I,1)=PXG(I,NIP)
      PZM(I,1)=PZG(I,NIP)
      SM(I,1)=SG(I,NIP)
      ETAM(I,1)=ETAG(I,NIP)
  700 CONTINUE
*-----------------------------------------------------------------+
*    Begin Calculating PXM, PZM, SM, ETAM For Each New Point On The  +
*    New Alpha Characteristic Line                              +
*-----------------------------------------------------------------+
    DO 900 I=1,NIP-1
      DO 800 J=1,NIP-1
       IF((I+J).LE.NIP) THEN
        IF (J.EQ.1) THEN
          X2=PXM(I+1,I)
          Z2=PZM(I+1,I)
          S2=SM(I+1,I)
          ETA2=ETAM(I+1,I)
          Z=0.0
          ETANP=0.0
          X=X2-Z2*TAN((ETANP/2.0+(45.0-PHI/2.0))*PI/180.0)
          SNP=(GAMMA*(Z-Z2-TAN(PHI*PI/180.0)*(X-X2))+
     +        S2*(1.0-TAN(PHI*PI/180.0)*(ETANP-ETA2)*PI/180.0))/
     +        (1.0+TAN(PHI*PI/180.0)*(ETANP-ETA2)*PI/180.0)
        ELSE
          K=1
          X1=PXM(I+J-1,I+1)
          Z1=PZM(I+J-1,I+1)
          X2=PXM(I+J,I)
          Z2=PZM(I+J,I)
          S1=SM(I+J-1,I+1)
          S2=SM(I+J,I)
          ETA1=ETAM(I+J-1,I+1)
          ETA2=ETAM(I+J,I)
          A1=ALOG(S1+C/TAN(PHI*PI/180.0))/(2*TAN(PHI*PI/180.0))-
     +       ETA1*PI/180.0
          B2=ALOG(S2+C/TAN(PHI*PI/180.0))/(2*TAN(PHI*PI/180.0))+
     +       ETA2*PI/180.0
          ETANP=(ETA1+ETA2)/2.0
          SNP=(S1+S2)/2.0
  250     Z=(X1-X2-Z1*TAN(((ETANP+ETA1)/2.0-(45.0-PHI/2.0))*PI/
     +      180.0)+Z2*TAN(((ETANP+ETA2)/2.0+(45.0-PHI/2.0))*PI/
     +      180.0))/(TAN(((ETANP+ETA2)/2.0+(45.0-PHI/2.0))*PI/
     +      180.0)-TAN(((ETANP+ETA1)/2.0-(45.0-PHI/2.0))*PI/
     +      180.0))
```

```
          X=X1+(Z-Z1)*TAN(((ETANP+ETA1)/2.0-(45.0-PHI/2.0))*PI/
     +      180.0)
          A=A1+GAMMA/((SNP+S1)*TAN(PHI*PI/180.0)+2.0*C)*(Z-Z1+
     +      TAN(PHI*PI/180.0)*(X-X1))
          B=B2+GAMMA/((SNP+S2)*TAN(PHI*PI/180.0)+2.0*C)*(Z-Z2-
     +      TAN(PHI*PI/180.0)*(X-X2))
          ETANEW=(B-A)/2.0*180.0/PI
          SNEW=EXP((B+A)*TAN(PHI*PI/180.0))-C/TAN(PHI*PI/180.0)
          K=K+1
          IF (K .ge. 500) THEN
            GOTO 11
          ENDIF
          IF (ABS(SNEW-SNP) .GT. TOL .OR. ABS(ETANEW-ETANP)
     +       .GT. TOL) THEN
            SNP=SNEW
            ETANP=ETANEW
            GOTO 250
          ENDIF
        ENDIF
*-----------------------------------------------------------------+
*   Define The New Values For The New Point On the Alpha Line     +
*   (where I is now taken as 1 for the initial alpha line)        +
*-----------------------------------------------------------------+
        PXM(I+J,I+1)=X
        PZM(I+J,I+1)=Z
        SM(I+J,I+1)=SNP
        ETAM(I+J,I+1)=ETANP
      ENDIF
 800  CONTINUE
 900 CONTINUE
*-----------------------------------------------------------------+
*   Determine the load per unit length along the footing          +
*-----------------------------------------------------------------+
    PT=0.0
    DO 999 I=1,NIP
      SIGMA1=(2.0*SM(I,I)+2.0*C*TAN((45.0-PHI/2.0)*PI/180.0))/
     +   (1.0+(TAN((45.0-PHI/2.0)*PI/180.0))**2.0)
      IF (I.EQ.1) THEN
        PVERT=ABS(PXM(I,I)-PXM(I+1,I+1))/2.0*SIGMA1
      ELSE
        IF (I.EQ.NIP) THEN
          PVERT=ABS(PXM(I,I)-PXM(I-1,I-1))/2.0*SIGMA1
        ELSE
          PVERT=(ABS(PXM(I+1,I+1)-PXM(I,I))/2.0+
```

```
+           ABS(PXM(I,I)-PXM(I-1,I-1)))/2.0)*SIGMA1
      ENDIF
    ENDIF
    PT=PT+PVERT
999 CONTINUE
*------------------------------------------------------------------+
*  Determine the calculated footing width and compare to FBI      +
*------------------------------------------------------------------+
   FB=2.0*abs(PXM(NIP,NIP))
   IF ((FBI-FB) .ge. 0.000001) THEN
     FBN=FBN+(FBI-FB)/2.0
     GOTO 1
   ENDIF
   IF ((FB-FBI) .GE. 0.000001) THEN
     FBN=FBN-(FB-FBI)/2.0
     GOTO 1
   ENDIF
*------------------------------------------------------------------+
*  Calculate output qunatities and print to file.                 +
*------------------------------------------------------------------+
   qult=PT/ABS(PXM(1,1)-PXM(NIP,NIP))
   BO=FB*GAMMA/TAN(PHI*PI/180.0)/(Q+C/TAN(PHI*PI/180.0))
   QQO=QULT/TAN(PHI*PI/180.0)/(Q+C/TAN(PHI*PI/180.0))
   WRITE(40,*)BO,QQO
   WRITE(6,*)BO,QQO
 11 CONTINUE
1000 STOP
   END
```

Program of Bearing Capacity Computation for Partial Rough Footing Base

```
*************************************************************************
*
* PROGRAM: CHARTPR                                  *
* ---------------                          *
* SOLUTION TO THE BEARING CAPACITY PROBLEM FOR A C, PHI, GAMMA *
* SOIL USING SLIP LINE FIELDS AND THE METHOD OF CHARACTERISTICS.*
* DATA INPUT CONSISTS OF NUMBER OF INITIAL POINTS ALONG THE     *
* RANKINE PASSIVE ZONE, ITERATION TOLERANCE, FOOTING WIDTH, PHI*
* C AND GAMMA, AND SURCHARGE FOR THE FIRST RUN.  PROGRAM  *
```

```
* ITERATES  BY INCREASING Q SUCH THAT THE NON-DIMENSIONAL     *
* WIDTH,  BO,  INCREASES BY 1 FOR EACH ITERATION. THE          *
* NON-DIMENSIONAL  PRESSURE, QO, IS THEN CALCULATED.  PROGRAM *
* MUST BE RUN AGAIN FOR EACH NEW PHI. PARTIALLY ROUGH FOOTING *
* BASE.                    *
*****************************************************************
*
      REAL PI,PHI,C,GAMMA,Q,PXC(20,20),PZC(20,20),SC(20,20),
     +    ETAC(20,20),PXG(20,20),PZG(20,20),SG(20,20),ETAG(20,20),
     +    PXM(20,20),PZM(20,20),SM(20,20),ETAM(20,20),QULT,PT,
     +    X1,X2,Z1,Z2,A1,B2,ETANP,SNP,Z,X,A,B,ETANEW,SNEW,SIGMAZ
      INTEGER NIP,I
      OPEN(4,FILE='INP.DAT',STATUS='OLD')
      OPEN(40,FILE='LOAD.OUT',STATUS='unknown')
      PI=3.14159264
*-----------------------------------------------------------------+
*    Read In Data For Number of Initial Points and Material Parameters+
*    NIP=Number of initial points                                  +
*    TOL=Iteration tolerance                                       +
*    FB=Footing Width                                              +
*    PHI=Friction Angle (degrees)                                  +
*    C=Cohesion                                                    +
*    GAMMA=Soil Effective Weight                                   +
*-----------------------------------------------------------------+
      READ(4,*)NIP,TOL
      READ(4,*)FB
      READ(4,*)PHI,C,GAMMA
      FBI=FB
      FBN=FB
*-----------------------------------------------------------------+
*-----------------------------------------------------------------+
*    SOLUTION TO THE CAUCHY PROBLEM (RANKINE ZONE)                 +
*-----------------------------------------------------------------+
*-----------------------------------------------------------------+
*    Read in Data For Initial Points On The Free Boundary For the  +
*    Rankine (Cauchy) Zone:                                        +
*    Q=Uniform Vertical Surcharge On Rankine Boundary              +
*    PXC&PZC=Matricies of x and z coordinates for all points defining +
*         the intersection of characteristic lines within the      +
*         Cauchy region                                            +
*    SC=Matrix of mean normal stress at each point                 +
*    ETAC=Matrix of angles of orientation of Sigma_1 with vert. dir. +
*-----------------------------------------------------------------+
      DO 11 M=1,60
```

```
      Jcount=0
      Q=(FB*GAMMA/REAL(M)-C)/TAN(PHI*PI/180.0)
    1 RPL=FBN*2.0
      Jcount=Jcount+1
      IF (Jcount .ge. 500) THEN
        GOTO 11
      ENDIF
      DO 9 I=1,NIP
        PXC(1,I)=RPL/REAL(NIP-1)*REAL(I-1)
        PZC(1,I)=0.0
    9 CONTINUE
      DO 10 I=1,NIP
        SC(1,I)=(Q*(1.0+(TAN((45.0+PHI/2.0)*PI/180.0))**2.0)+
     +        2.0*C*TAN((45.0+PHI/2.0)*PI/180.0))/2.0
        ETAC(1,I)=90.0
   10 CONTINUE
*-----------------------------------------------------------------+
*   Set The Values for Data at the First Goursat Point Corresponding +
*   To the first Cauchy Point                                    +
*-----------------------------------------------------------------+
      PXG(1,1)=PXC(1,1)
      PZG(1,1)=PZC(1,1)
      SG(1,1)=SC(1,1)
      ETAG(1,1)=ETAC(1,1)
*-----------------------------------------------------------------+
*   Begin Calculating PXC, PZC, SC, ETAC For Each New Point On The  +
*   Next Row of Points From the Row Of Initial Points            +
*-----------------------------------------------------------------+
      DO 200 I=1,NIP-1
        DO 100 J=1,NIP-I
          K=1
          X1=PXC(I,J)
          Z1=PZC(I,J)
          X2=PXC(I,J+1)
          Z2=PZC(I,J+1)
          S1=SC(I,J)
          S2=SC(I,J+1)
          ETA1=ETAC(I,J)
          ETA2=ETAC(I,J+1)
          A1=ALOG(S1+C/TAN(PHI*PI/180.0))/(2*TAN(PHI*PI/180.0))-
     +      ETA1*PI/180.0
          B2=ALOG(S2+C/TAN(PHI*PI/180.0))/(2*TAN(PHI*PI/180.0))+
     +      ETA2*PI/180.0
          ETANP=(ETA1+ETA2)/2.0
```

```
      SNP=(S1+S2)/2.0
 50    Z=(X1-X2-Z1*TAN(((ETANP+ETA1)/2.0-(45.0-PHI/2.0))*PI/180.0)+
  +     Z2*TAN(((ETANP+ETA2)/2.0+(45.0-PHI/2.0))*PI/180.0))/
  +     (TAN(((ETANP+ETA2)/2.0+(45.0-PHI/2.0))*PI/180.0)-
  +     TAN(((ETANP+ETA1)/2.0-(45.0-PHI/2.0))*PI/180.0))
      X=X1+(Z-Z1)*TAN(((ETANP+ETA1)/2.0-(45.0-PHI/2.0))*PI/180.0)
      A=A1+GAMMA/((SNP+S1)*TAN(PHI*PI/180.0)+2.0*C)*(Z-Z1+
  +     TAN(PHI*PI/180.0)*(X-X1))
      B=B2+GAMMA/((SNP+S2)*TAN(PHI*PI/180.0)+2.0*C)*(Z-Z2-
  +     TAN(PHI*PI/180.0)*(X-X2))
      ETANEW=(B-A)/2.0*180.0/PI
      SNEW=EXP((B+A)*TAN(PHI*PI/180.0))-C/TAN(PHI*PI/180.0)
      K=K+1
      IF (K .ge. 500) THEN
        GOTO 11
      ENDIF
      IF (ABS(SNEW-SNP) .GT. TOL .OR. ABS(ETANEW-ETANP) .GT.
  +      TOL) THEN
        SNP=SNEW
        ETANP=ETANEW
        GOTO 50
      ENDIF
*-----------------------------------------------------------------+
*   Define The New Values For The New Row of Points               +
*   (where I is now taken as 1 for the initial row of points)     +
*-----------------------------------------------------------------+
      PXC(I+1,J)=X
      PZC(I+1,J)=Z
      SC(I+1,J)=SNP
      ETAC(I+1,J)=ETANP
*-----------------------------------------------------------------+
*   Record data for points lying on the boundary between the      +
*   Cauchy and Goursat zones                                      +
*-----------------------------------------------------------------+
      IF(J.EQ.1) THEN
        PXG(I+1,1)=PXC(I+1,J)
        PZG(I+1,1)=PZC(I+1,J)
        SG(I+1,1)=SC(I+1,J)
        ETAG(I+1,1)=ETAC(I+1,J)
      ENDIF
 100  CONTINUE
 200 CONTINUE
*-----------------------------------------------------------------+
*-----------------------------------------------------------------+
```

```
*     SOLUTION TO THE GOURSAT PROBLEM (LOG-SPIRAL ZONE)          +
*-----------------------------------------------------------------+
*-----------------------------------------------------------------+
*     Define Data Values Along the Beta Line Corresponding to the  +
*     Prandtl Singularity                                          +
*-----------------------------------------------------------------+
      DO 400 I=1,NIP-1
        PXG(1,I+1)=0.0
        PZG(1,I+1)=0.0
        ETAG(1,I+1)=PI/2.0-(PI/2.0+PI/4.0+PHI/2.0*PI/180.0)*
     +            REAL(I)/REAL(NIP-1)
        SG(1,I+1)=(SC(1,1)+C/TAN(PHI*PI/180.0))*EXP((PI/2.0-
     +         ETAG(1,I+1))*2.0*TAN(PHI*PI/180.0))-C/TAN(PHI*PI/180.0)
        ETAG(1,I+1)=ETAG(1,I+1)*180.0/PI
  400 CONTINUE
*-----------------------------------------------------------------+
*     Begin Calculating PXG, PZG, SG, ETAG For Each New Point On The +
*     New Alpha Characteristic Line                                +
*-----------------------------------------------------------------+
      DO 600 I=1,NIP-1
        DO 500 J=1,NIP-1
          K=1
          X1=PXG(J,I+1)
          Z1=PZG(J,I+1)
          X2=PXG(J+1,I)
          Z2=PZG(J+1,I)
          S1=SG(J,I+1)
          S2=SG(J+1,I)
          ETA1=ETAG(J,I+1)
          ETA2=ETAG(J+1,I)
          A1=ALOG(S1+C/TAN(PHI*PI/180.0))/(2*TAN(PHI*PI/180.0))-
     +      ETA1*PI/180.0
          B2=ALOG(S2+C/TAN(PHI*PI/180.0))/(2*TAN(PHI*PI/180.0))+
     +      ETA2*PI/180.0
          ETANP=(ETA1+ETA2)/2.0
          SNP=(S1+S2)/2.0
  150     Z=(X1-X2-Z1*TAN(((ETANP+ETA1)/2.0-(45.0-PHI/2.0))*PI/180.0)+
     +      Z2*TAN(((ETANP+ETA2)/2.0+(45.0-PHI/2.0))*PI/180.0))/
     +      (TAN(((ETANP+ETA2)/2.0+(45.0-PHI/2.0))*PI/180.0)-
     +      TAN(((ETANP+ETA1)/2.0-(45.0-PHI/2.0))*PI/180.0))
          X=X1+(Z-Z1)*TAN(((ETANP+ETA1)/2.0-(45.0-PHI/2.0))*PI/180.0)
          A=A1+GAMMA/((SNP+S1)*TAN(PHI*PI/180.0)+2.0*C)*(Z-Z1+
     +      TAN(PHI*PI/180.0)*(X-X1))
          B=B2+GAMMA/((SNP+S2)*TAN(PHI*PI/180.0)+2.0*C)*(Z-Z2-
```

```
     +     TAN(PHI*PI/180.0)*(X-X2))
         ETANEW=(B-A)/2.0*180.0/PI
         SNEW=EXP((B+A)*TAN(PHI*PI/180.0))-C/TAN(PHI*PI/180.0)
         K=K+1
         IF (K .ge. 500) THEN
           GOTO 11
         ENDIF
         IF (ABS(SNEW-SNP) .GT. TOL .OR. ABS(ETANEW-ETANP) .GT.
     +     TOL) THEN
           SNP=SNEW
           ETANP=ETANEW
           GOTO 150
         ENDIF
*-----------------------------------------------------------------+
*   Define The New Values For The New Set of Points On the Alpha Line+
*   (where I is now taken as 1 for the initial alpha line)          +
*-----------------------------------------------------------------+
         PXG(J+1,I+1)=X
         PZG(J+1,I+1)=Z
         SG(J+1,I+1)=SNP
         ETAG(J+1,I+1)=ETANP
 500     CONTINUE
 600 CONTINUE
*-----------------------------------------------------------------+
*-----------------------------------------------------------------+
*   SOLUTION TO THE MIXED PROBLEM (RANKINE ACTIVE ZONE)              +
*-----------------------------------------------------------------+
*-----------------------------------------------------------------+
*   Register data for points lying on the boundary between the      +
*   Goursat and mixed zones                                          +
*-----------------------------------------------------------------+
     DO 700 I=1,NIP
       PXM(I,1)=PXG(I,NIP)
       PZM(I,1)=PZG(I,NIP)
       SM(I,1)=SG(I,NIP)
       ETAM(I,1)=ETAG(I,NIP)
 700 CONTINUE
*-----------------------------------------------------------------+
*   Begin Calculating PXM, PZM, SM, ETAM For Each New Point On The  +
*   New Alpha Characteristic Line                                    +
*-----------------------------------------------------------------+
     DO 2 I=1,NIP
       PXM(I,I)=REAL(I-1)/(NIP-1)*FB
   2 CONTINUE
```

```
      DO 900 I=1,NIP-1
        DO 800 J=1,NIP-1
         IF (I.EQ.J) THEN
         ETANP=PXM(I,J)/PXM(NIP,NIP)
     +       *(45.0+PHI/2.0)-(45.0+PHI/2.0)
         ENDIF
         IF((I+J).LE.NIP) THEN
          IF (J.EQ.1) THEN
           X2=PXM(I+1,I)
           Z2=PZM(I+1,I)
           S2=SM(I+1,I)
           ETA2=ETAM(I+1,I)
           Z=0.0
           ETANP=REAL(I)/REAL(NIP-1)*(45.0+PHI/2.0)-(45.0+PHI/2.0)
           X=X2-Z2*TAN((ETANP/2.0+(45.0-PHI/2.0))*PI/180.0)
           SNP=(GAMMA*(Z-Z2-TAN(PHI*PI/180.0)*(X-X2))+
     +        S2*(1.0-TAN(PHI*PI/180.0)*(ETANP-ETA2)*PI/180.0))/
     +        (1.0+TAN(PHI*PI/180.0)*(ETANP-ETA2)*PI/180.0)
          ELSE
           K=1
           X1=PXM(I+J-1,I+1)
           Z1=PZM(I+J-1,I+1)
           X2=PXM(I+J,I)
           Z2=PZM(I+J,I)
           S1=SM(I+J-1,I+1)
           S2=SM(I+J,I)
           ETA1=ETAM(I+J-1,I+1)
           ETA2=ETAM(I+J,I)
           A1=ALOG(S1+C/TAN(PHI*PI/180.0))/(2*TAN(PHI*PI/180.0))-
     +       ETA1*PI/180.0
           B2=ALOG(S2+C/TAN(PHI*PI/180.0))/(2*TAN(PHI*PI/180.0))+
     +       ETA2*PI/180.0
           ETANP=(ETA1+ETA2)/2.0
           SNP=(S1+S2)/2.0
250          Z=(X1-X2-Z1*TAN(((ETANP+ETA1)/2.0-(45.0-PHI/2.0))*PI/
     +       180.0)+Z2*TAN(((ETANP+ETA2)/2.0+(45.0-PHI/2.0))*PI/
     +       180.0))/(TAN(((ETANP+ETA2)/2.0+(45.0-PHI/2.0))*PI/
     +       180.0)-TAN(((ETANP+ETA1)/2.0-(45.0-PHI/2.0))*PI/
     +       180.0))
           X=X1+(Z-Z1)*TAN(((ETANP+ETA1)/2.0-(45.0-PHI/2.0))*PI/
     +       180.0)
           A=A1+GAMMA/((SNP+S1)*TAN(PHI*PI/180.0)+2.0*C)*(Z-Z1+
     +       TAN(PHI*PI/180.0)*(X-X1))
           B=B2+GAMMA/((SNP+S2)*TAN(PHI*PI/180.0)+2.0*C)*(Z-Z2-
```

```
+        TAN(PHI*PI/180.0)*(X-X2))
      ETANEW=(B-A)/2.0*180.0/PI
      SNEW=EXP((B+A)*TAN(PHI*PI/180.0))-C/TAN(PHI*PI/180.0)
      K=K+1
      IF (K .ge. 500) THEN
        GOTO 11
      ENDIF
      IF (ABS(SNEW-SNP) .GT. TOL .OR. ABS(ETANEW-ETANP)
+        .GT. TOL) THEN
        SNP=SNEW
        ETANP=ETANEW
        GOTO 250
      ENDIF
    ENDIF
*-----------------------------------------------------------------+
*   Define The New Values For The New Point On the Alpha Line      +
*   (where I is now taken as 1 for the initial alpha line)        +
*-----------------------------------------------------------------+
    PXM(I+J,I+1)=X
    PZM(I+J,I+1)=Z
    SM(I+J,I+1)=SNP
    ETAM(I+J,I+1)=ETANP
   ENDIF
 800    CONTINUE
 900 CONTINUE
*-----------------------------------------------------------------+
*   Determine the calculated footing width and compare to FBI      +
*-----------------------------------------------------------------+
   FB=2.0*abs(PXM(NIP,NIP))
   IF ((FBI-FB) .ge. 0.000001) THEN
     FBN=FBN+(FBI-FB)/2.0
     GOTO 1
   ENDIF
   IF ((FB-FBI) .GE. 0.000001) THEN
     FBN=FBN-(FB-FBI)/2.0
     GOTO 1
   ENDIF
*-----------------------------------------------------------------+
*   Determine the load per unit length along the footing          +
*-----------------------------------------------------------------+
   PT=0.0
   DO 999 I=1,NIP
     SIGMAZ=SM(I,I)*(1.0+SIN(PHI*PI/180.0)
+        *COS(-2.0*ETAM(I,I)*PI/180.0))+C*COS(PHI*PI/180.0)
```

```
+       *COS(-2.0*ETAM(I,I)*PI/180.0)
      IF (I.EQ.1) THEN
        PVERT=ABS(PXM(I,I)-PXM(I+1,I+1))/2.0*SIGMAZ
      ELSE
        IF (I.EQ.NIP) THEN
          PVERT=ABS(PXM(I,I)-PXM(I-1,I-1))/2.0*SIGMAZ
        ELSE
          PVERT=(ABS(PXM(I+1,I+1)-PXM(I,I))/2.0+
+               ABS(PXM(I,I)-PXM(I-1,I-1))/2.0)*SIGMAZ
        ENDIF
      ENDIF
      PT=PT+PVERT
 999 CONTINUE
*------------------------------------------------------------------+
*    Calculate output qunatities and print to file.                 +
*------------------------------------------------------------------+
      qult=PT/ABS(PXM(1,1)-PXM(NIP,NIP))
      BO=FB*GAMMA/TAN(PHI*PI/180.0)/(Q+C/TAN(PHI*PI/180.0))
      QQO=QULT/TAN(PHI*PI/180.0)/(Q+C/TAN(PHI*PI/180.0))
      WRITE(40,*)BO,QQO
      WRITE(6,*)BO,QQO
  11 CONTINUE
1000 STOP
      END
```